ISSN 2461-4254

EUREKA: PHYSICS AND ENGINEERING

- Chemical Engineering
- Chemistry
- Computer Science
- Earth and Planetary Sciences
- Energy
- Engineering
- Materials Science
- Mathematics
- Physics and Astronomy

Volume 1(8)
2017

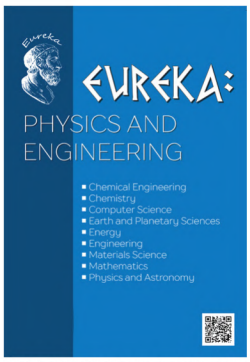

SCIENTIFIC JOURNAL

EUREKA: Physics and Engineering – scientific journal whose main aim is to publish materials allowed to see ***new discoveries at the intersection of sciences.***

- Chemical Engineering
- Chemistry
- Computer Science
- Earth and Planetary Sciences
- Energy
- Engineering
- Material Science
- Mathematics
- Physics and Astronomy
- Technology Transfer

EUREKA: Physics and Engineering
publishes
4 types of materials:
– review article,
– progress reports,
– original Research Article
– reports on research projects

PUBLISHER OÜ «Scientific Route»
European Union
Editorial office
«EUREKA: Physical Sciences and Engineering»
Narva mnt 7-634, Tallinn, Eesti
Harju maakond, 10117
Tel. + 372 602-7570
e-mail: info@eu-jr.eu
Website: http://eu-jr.eu

EDITORIAL BOARD

CONTENT

A METHOD FOR OPTIMIZING CHEMICAL COMPOSITION OF STEELS TO REDUCE RADICALLY THEIR ALLOY ELEMENTS AND INCREASE SERVICE LIFE OF MACHINE COMPONENTS

Nikolai Kobasko
Intensive Technologies Ltd
68/1 Peremohy ave., Kyiv, Ukraine, 03113
nkobasko@gmail.com

Abstract

A method for optimizing chemical composition of steel is proposed and a correlation is established to reduce cardinally alloy elements in existing steel grades that results in high compressive residual stresses at the surface of intensively quenched steel parts and increasing strength and ductility of material due to super-strengthening phenomenon. The algorithm of optimization consists in reducing alloy elements in existing alloy steel in 1.5–2 times and then lowering step-by-step content of steel, beginning from the most costly alloy element and ending the most cheaper one, until established correlation is satisfied. The range of reduction is minimal and during computer calculations can be chosen as 0,001 wt %. The proposed approach can save alloy elements, energy, increase service life of machine components and improve environmental condition. The method is a basis for development of the new low hardenability (LH) and optimal hardenability (OH) steels.

Keywords: steel chemistry, service life, reduced cost, carburizing elimination, natural gas savings.

DOI: 10.21303/2461-4262.2016.00253

1. Introduction

Author of the article has been developing a method for optimization of steel chemistry to reduce radically alloy elements, increase service of steel components and improve environment condition since 2005 [1–3]. In this article a summary of the investigations concerning optimization of chemical composition of steels is provided. Based on numerous experiments and FEM calculations of residual stresses, it was established a dimensionless correlation which is responsible for creation of optimal hardened layer that provides high compressive residual stresses at the surface of steel parts and allows getting super-strengthened material. For this purpose the Grossmann's classical experimental data were used concerning hardenability of steels and multiplying factors f_n which are the most accurate and widely used [4, 5].

The aim of developed method is providing methodology which allows engineers to develop the new low hardenability (LH) steels for elimination very costly carburizing processes. At present, in worldwide practice there is a tendency to switch from AISI 8620 carburized alloy steel to LH steel which should be intensively hardened in plain water. The matter is that carburizing process for big and complicated steel parts, like large gears, takes a long time, up to 60 hours and is rather costly and not environmental green. The LH steel with the proper optimal chemical composition can eliminate carburizing process completely and it takes only seconds or minutes for intensive hardening. The proposed method for optimizing chemical composition of LH steels can be successfully used for solving this very important for the worldwide practical and scientific problem.

2. Compressive residual stresses and super-strengthening phenomenon as a reason for cardinal decrease alloy elements in steels

Optimal hardenability of steels which provides optimal hardened martensitic surface layer with maximal compressive residual stresses in it and bainitic or pearlitic microstructure at the core after intensive quenching can be designed using established by author [1, 2] the similarity ratio (1):

$$\frac{DI}{D_{opt}} = 0.35 \pm 0.095, \quad (1)$$

here DI is critical diameter in m; D_{opt} is diameter of steel part to be quenched in m.

A procedure of its use is as follows:

1. A steel grade with certain chemical composition is chosen.
2. The ideal critical size for this steel is determined.
3. The ratio DI/D_{opt} for specific steel part is evaluated which must be in the range of 0.2–0.5.
4. The part is quenched in condition $0.8 \leq Kn \leq 1$ [6].
5. Intensive quenching is interrupted when optimal quenched layer is achieved with maximal compressive stresses at the surface [6].
6. The part is tempered at the temperature Ms or higher [6].

The history of such development started when Prof. Shepelyakovskii and his colleagues noticed that not through hardened but intensively quenched steel parts has much better service life as compared with through hardened steel parts [7–11]. As a result, steels with reduced content of Mn, Cr and Ni were recommended to use to increase service life of machine components (**Table 1**).

Table 1

Chemical composition of steels with reduced content of Mn recommended by Prof. Shepelyakovskii to use for through surface induction hardening of different machine components [10]

Alloy	Steel 1	Steel 2	Steel 3	Steel 4	Steel 5	Steel 6
C	0.55–0.63	0.44–0.51	0.95–1.05	0.42–0.48	0.53–0.60	1.10–1.20
Si	0.10–0.30	0.10–0.25	0.15–0.30	0.40–0.65	0.40–0.80	0.15–0.30
Mn	<0.20	0.95–1.25	0.15–0.30	0.17–0.32	0.21–0.35	0.40–0.60
Cr	<0.15	<0.25	0.35–0.50	<0.25	<0.25	<0.25
Ni	<0.25	<0.25	<0.30	<0.20	<0.20	<0.20
Cu	<0.30	<0.30	<0.25	<0.15	<0.20	<0.20
Ti	0	0.06–0.12	0	0	0	0.06–0.12
S	<0.04	>0.04	<0.027	<0.04	<0.04	<0.04
P	<0.04	>0.04	<0.02	<0.035	<0.04	<0.04
Area of use	Gears	Semi – axles and shafts	Leaf – springs	Common Springs	Crank – shafts	Hard working parts

To understand why such phenomenon occurs, authors [12–16] made numerous computer simulations to investigate current and residual stresses in cylindrical samples of 6, 20, 40, 50, 60, 80, 150, 200, and 300 mm. It was established that there is a similarity in stress distribution as shown in **Fig. 1.** The similarity means that a depth of optimal quenched layer should increase 10 times when switching from 6 mm cylindrical specimen to 60 mm specimen to get the same stress distribution. More information one can find in Refs. [17–22].

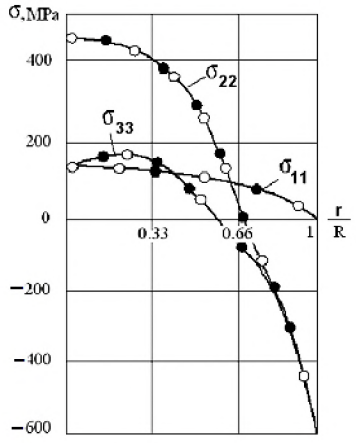

Fig. 1. Stress distribution through the section of two cylindrical specimens, one of diameter 6 mm (black data points) and the other of 60 mm (white data points), at the time of the achievement of maximum compressive stresses at the surface [12]: σ_{11} is radial stress; σ_{22} is axial stress, σ_{33} is tangential (hoop) stress

The established in 1983 [12] similarity in stress distribution has a great importance since it allows:

– transfer data, obtained from testing small specimens, to very large specimens or real steel parts;

– get similar stress distribution and hardened layer in complicated steel parts;

– create a basis for optimization of the chemical composition of steel to provide high compressive residual stresses at the surface of hardened steel parts;

– use previously experimental data to evaluate the ratio (1);

– make appropriate condition to get maximal benefit from super-strengthening processes.

The similar stress distribution when quenching through hardened cylindrical specimens in oil (**Fig. 2, *a***) and intensively quenched specimens with optimal hardened layer (**Fig. 2, *b***) are shown in **Fig. 2.** A scheme (**Fig. 3**) explains how one should understand the super-strengthening processes [23–25].

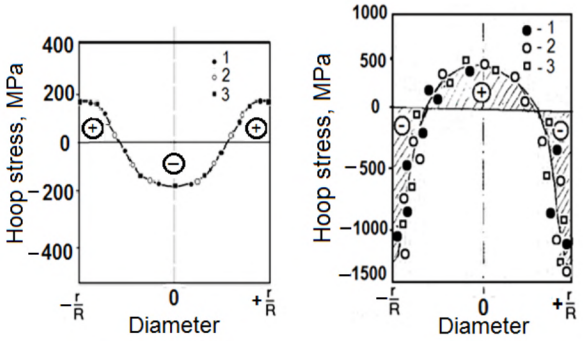

a *b*

Fig. 2. Residual stress distribution in cylindrical specimens when quenching slowly in oil and intensively in water flow: *a* – quenching in oil; *b* – intensive quenching in condition $0.8 \le \mathrm{Kn} \le 1$

Thus, along with the creation the surface compressive residual stresses, intensive quenching is a reason for super-strengthening of material (**Fig. 3, 4**) [24, 26].

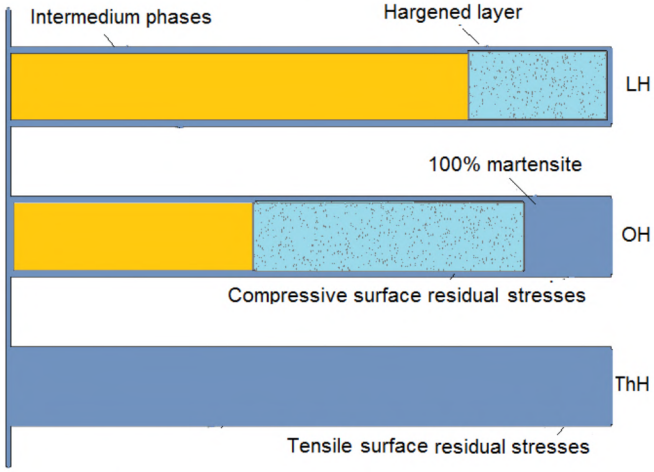

Fig. 3. Optimal depth of hardened layer corresponding to the maximum surface compressive residual stresses: LH, low hardenability steel; OH, optimal hardenability; ThH, through hardening

To understand the nature of super-strengthening, consider the scheme shown in **Fig. 4**. Imagine a superficial layer compressed to the limit (1,200–1,500 MPa) in which there are plates of martensite possessing a greater specific volume than the initial phase structure of supercooled austenite. The period of appearance of such plates is very short and less than 10^{-6} s. The plates of

martensite deform the supercooled austenite that is between them, as shown in **Fig. 4**. The hatched area indicates martensite, and the color area, the supercooled austenite. The higher the cooling rate is within the martensite range, the greater will be the extent to which the austenite is deformed, and the higher the dislocation density. Consequently, during rapid cooling, there is not enough time for the dislocations to accumulate in the grain boundaries and to form nuclei of future microcracks; they are frozen in the material. Thus, the superficial layer acts like a blacksmith: under conditions of high stress, the plates of martensite arise explosively, deforming the austenite and creating extremely high dislocation densities, which are frozen during rapid cooling. This process is analogous to low-temperature thermomechanical treatment (LTMT).

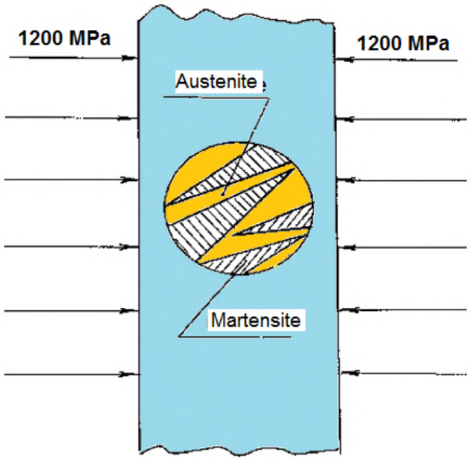

Fig. 4. The transformation scheme of austenite into martensite in the compressed layer, illustrating the effect of additional strengthening (super-strengthening) of the material

3. Verification of the idea in the production conditions

Author of a monograph published in 1980 [25] provided experimental data showing that semi-axles of track KrAZ (62 mm in diameter) made of plain carbon steel and intensively quenched work much better as compared with the axles made of AISI 4340 steel but quenched in oil (**Table 2, 3** and **Fig. 5**).

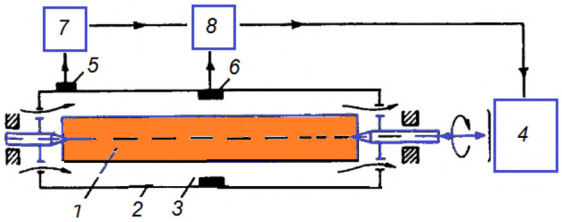

Fig. 5. Detailed scheme of quench chamber with automatic control [14, 28]: 1 – semi-axle; 2 – quench chamber; 3 – pressurized water flow; 4 – mechanical drive for semi-axles; 5 – sensor for analyzing the process of nucleate and film boiling; 6 – sensor for analyzing the portion of transformed structures by the changing ferromagnetic state; 7 – electronic device (amplifier and microprocessor); 8 – amplifier

Table 2

Chemical composition of steels AISI 4340H and 1040 used for manufacturing KrAZ track's semi-axles [27]

Steel grade	C	Mn	Si	Ni	Cr	Mo	P	S	DI, mm
AISI 4340H	0.37–0.44	0.65–0.85	0.15–0.35	1,65–2.00	0.65–0.95	0.20–0.30	0.025 max	0.040 max	131–269
1040	0.36–0.44	0.50–0.80	0.17–0.37	0.25 max	0.25 max	–	0.04 max	0.04 max	24–41

Table 3
Fatigue testing of KrAZ tracks semi-axles through quenched in oil (4340H steel) and intensively quenched for obtaining optimal quenched layer (1040 steel) [24–26]

Quenching method	Steel grade	Numbers of cycles to fracture	Notes
Oil	AISI/SAE 4340	$(3,8–4.6)\times10^5$	Semi-axles were destroyed
Intensive water spray cooling	AISI 1040	$(3,0–3.5)\times10^6$	No fracture observed

For plain carbon steel 1040 the main ratio (1) is equal:

$$\frac{DI}{D_{opt}} = \frac{24\ mm}{62\ mm} = 0.35 + 0.037$$

that perfectly fits the Eq. (1). Field testing showed that wear resistance of splines were three times higher as compared with 4340 steel. Note that plain carbon steel didn't contain Al, Ti and V.

Other good examples are rollers made of 35KhM steel (**Table 4** and **Fig. 6**)

Table 4
Chemical composition of steel 35KhM used for manufacturing rollers

Steel grade	C	Mn	Si	Cr	Ni	Mo	P	S	DI mm
35KhM	0.30–0.37	0.50–0.90	0.90–1.20	0.90–1.20	0.30 max	0.15–0.25	0.035 max	0.035 max	89–222
Average	0.335	0.70	1.05	1.05	0.15	0.20	–	–	153

Critical diameters in **Table 2**, **3** were calculated using Grossmann's Eq. (2) [4, 28, 29]:

$$DI = 25.4 f_{Fe} \times f_{Mn} \times f_{Si} \times f_{Cr} \times f_{Ni} \times f_{Mo} \times f_P \times f_S, \quad (2)$$

here f_{Fe}, f_{Mn}, f_{Si}, f_{Cr} …. are multiplying Grossmann's values depending on content of alloy in steel.

Average critical diameter is 153 mm and ratio (1) is satisfied for large diameter of roller, i. e.

$$\frac{DI}{D_{opt}} = \frac{153mm}{600mm} = 0.255 = 0.35 - 0.095;$$

$$\frac{DI}{D_{opt}} = \frac{153mm}{280mm} = 0.54 = 0.35 + 0.19.$$

To provide direct convection, heat transfer coefficients (HTCs) were calculated using Eq. (3) and Eq. (4) according to which HTC=1250 W/m^{2}K. It can be provided by agitation water salt solution of optimal concentration with 0.25 m/s.

According to patented technology [6], direct convection and uniform intensive quenching takes place when criterion (3) including (4) is satisfied:

$$Bi = \frac{2(\vartheta_0 - \vartheta_I)}{\vartheta_I + \vartheta_{uh}}, \quad (3)$$

$$\vartheta_I = \frac{1}{\beta}\left[\frac{2\lambda(\vartheta_0 - \vartheta_I)}{R}\right]^{0.3}, \quad (4)$$

where $\vartheta_0 = T_0 - T_S$; T_0 is initial austenitizing temperature; $\vartheta_I = T_I - T_S$, T_I is nucleate boiling start temperature; T_S is saturation temperature; $\vartheta_{uh} = T_S - T_m$; T_m is bath temperature; $\beta = 3.41$; λ is thermal conductivity of steel in W/mK; R is radius in m; Bi is conventional dimensionless Biot number.

Taken into account such approach, software has been developed for engineers to calculate cooling recipes when performing IQ-2 and IQ-3 processes [30–34]. The possibilities of governing the quenching processes are discusses in Refs [35–38].

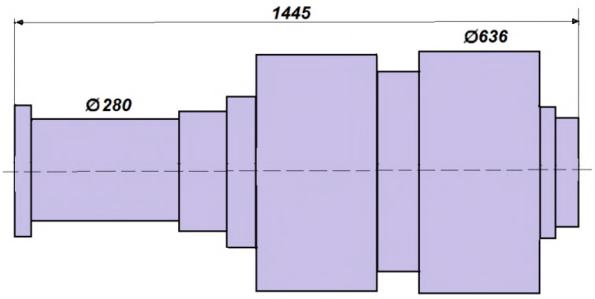

Fig. 6. The roller made of 35KhM steel and intensively quenched in agitated (0.3 m/s) water salt solution of optimal concentration

Cooling time of roller shown in **Fig. 6** was calculated using Eq. (5) [25] and existing computer program:

$$\frac{aKn}{K}\tau = \left(\frac{k_1 Bi_V}{2.095 + 3.873 Bi_V} + \ln\theta_o\right), \quad (5)$$

here a is thermal diffusivity in m^2/s; Kn is dimensionless Kondratjev number; K is Kondratjev form factor in m^2; τ is time in seconds; k_1 is 1, 2, 3 for plate, cylinder, and spherical like forms correspondently; Bi_V is generalized dimensionless Biot number; θ_o is dimensionless temperature.

Calculations provided cooling time for roller 48 minutes 15 seconds.

4. Low hardenability steel as an example of optimized chemical composition of material

Low hardenability (LH) steels are widely used in practice. For example, authors [7–11] used the first version of LH steels for manufacturing gears, shafts and bearing rings. The chemical composition of improved version of LH steel is provided in RU Patent № 2158320 [39]: 0.40–0.85 C; ≤0.20 Mn; ≤0.20 Si; ≤0.10 Cr; ≤0.10 Ni; ≤0.10 Cu; 0.03–0.10 Al; 0.06–0.12 Ti; ≤0.40 V. This LH steel was successfully used for manufacturing gears and different kinds of shafts if optimal quenched layer was provided [40, 41].

In 2010, a method for intense quenching of steel, containing 0.15–1.2 C; ≤1.8 Mn; ≤1.8Si; ≤1.8 Cr; ≤1.8 Ni; ≤0.5 Mo; ≤1.5 W; ≤0.007 B; ≤0.3 Cu; 0.03–0.1 Al; 0.4 Ti; 0.4 V; ≤0.1 N; ≤0.4 Zr; 0.03 Ca; ≤0.035 S; ≤0.035 P, in condition when HTC exceeds 40,000 W/m^2K was introduced by authors [42]. The equation for determining ideal critical diameter was modified by authors [42] and using nomograms related to cylinders, spheres and plates hardened layer of thickness (0.1–0.2) D was determined depending on critical diameter DI and size of real steel part. Self-tempering at the temperature 150–300 °C is provided during performing of this method. The notion has several disadvantages as compared with patented in 2002 in the USA similar intensive steel quenching technology and apparatus [6]. They are:

– heat transfer coefficients (HTCs) more than 40,000 W/m^2K are too high for medium and large steel parts and they should be evaluated using criterion (3) with condition (4) which is responsible for establishing direct convection;

– in the equation for DI calculation multiplying factors f_n are considered as linear functions of alloy concentrations for all interval up to 1.8 % that creates errors during DI calculations;

– at present time, tendency in metallurgy is to decrease alloy elements from 2 to 3 times due to possibilities of intensive quenching which creates high compressive residual stresses and provides super-strengthening of material [6, 38]. There is no sense to waste alloy elements and huge energy;

– authors [42] recommend to perform self-tempering at 150–300 °C after intensive quenching in condition HTC=40,000W/m^{2}K. However they don't provide interruption time to perform self-tempering. It can be done using Eq. (5). All of this was considered in detail in 2002 in US Patent [6]. Moreover, interruption and self- tempering should be done at optimal bainitic transformations [43];

– thickness 0.1D–0.2D is not optimal quenched layer, especially when using 0.1D. It can be calculated from Eq. (1). Moreover, even in through hardened steels at the surface of machine components the high compressive residual stresses are formed [44–46]. Thickness 0.1D–0.2D will not provide enough strength for hard working machine components;

– the main disadvantage of the elaboration is impossible to use technology for complicated steel parts configurations. It can be used only for cylinders, spheres and plates. Note that regular thermal condition theory of Kondratjev allows operating with any configuration of steel parts [47, 48];

– authors [42] use nomogram for prediction of hardened quench layer in classical forms by observing DI and size, however hardened layer cannot be correct if DI was calculated incorrectly.

In general, alloy elements in existing steels can be radically reduced due to high surface compressive residual stresses and super-strengthening of a material.

5. Discussion

At present time, alloy and high alloy steels are quenched in oil and optimal hardenability steels are intensively quenched in water flow or water sprays. LH steels, based on empirical and accurate metallurgical investigations, are suitable for small machine components like gears, shafts, crosses, bearing rings and rollers. LH steels combined with the intensive quenching produce high compressive residual stresses at the surface of steel parts and provide super-strengthening of material that increases their service life. Optimal chemical composition provides optimal quenched layer which in its turn provides optimal residual stress distribution in steel components. The optimal residual stress distribution means high (maximal) compressive residual stresses at the surface of steel parts which smoothly pass to low tensile stresses at their core. Due to soft core, the low tensile stresses cannot create cracks. And also, due to soft core, no swelling is observed in it and as a result the distortion is less. Empirical toleration the chemical composition of steel to size and configuration of machine component or tool takes a long time end is very expensive procedure. That is why in the paper the universal and simple method of chemical and residual stress optimization is developed and discussed. Such approach can be used when hardening irons [49]. The method was many times checked by FEM computer simulation and tested in field condition [12, 25]. Semi-axles of trucks and bearing rings were many times tested [25, 26]. The method of calculation can evaluate which steel fits the specific configuration and size of machine component. Based on developed method of calculation, it is possible to compose new grades of steels which can provide optimal residual stress distribution in the given steel component. Due to optimal residual stress distribution and intensive quenching the following benefits are achieved:

– high compressive residual stresses at the surface of steel parts are formed;

– the super strengthening phenomenon in surface layers takes place;

– mechanical properties of material at the core, especially impact strength, are significantly improved;

– crack formation decreases due to compressive residual stresses at the surface and low tensile residual stresses at the core where material is soft;

– distortion of steel parts decreases because core doesn't swell.

A tendency of reducing alloy elements in alloy and high alloy steels is very progressive and promising.

6. Conclusions

1. A similarity correlation concerning depth of hardened surface layer, which was established by author, is a reason for creation of high surface compressive residual stresses and is a basis for optimization of chemical composition of steel.

2. There is an opportunity to reduce all alloy elements in existing steel grades more than two times due to high compressive residual stresses and super-strengthening of material.

3. The similarity correlation allows predicting stress distribution in intensively quenched steel parts after intensive quenching.

4. If chemical composition of LH steel is proper optimized, it can eliminate carburizing processes for variety of large and complicated steel parts and provide the great benefits for industry.

References

[1] Kobasko, N. I. (2005). Quench Process Optimization for Receiving Super Strong Materials. Proceedings of the 5th WSEAS Int. Conference on simulation, modeling and optimization, 365–372.

[2] Kobasko, N. I. (2005). Quench Process Optimization, Proc. of 6th International Conference "Equipment and Technologies for Heat Treatment of Metals and Alloys. Part I", 88–96.

[3] Kobasko, N. I.; Bozo, S., Heimo, J., Vojteh, L. (Eds.) (2005). The main principles of intensive quenching of tools and dies, Proc. of the 1th International Conference on Heat Treatment and Surface Engineering of Tools and Dies, 39–44.

[4] Grossmann, M. A. (1964). Principles of Heat Treatment. Ohio: American Society for Metals, 302.

[5] Totten, G. E., Bates, C. E., Clinton, N. A. (1993). Handbook of quenchants and quenching technology. ASM international, 513.

[6] Kobasko, N. I. (2002). Patent US 6,364,974 B2. Quenching apparatus and method for hardening steel parts. Assignee: IQ Technologies, Inc. Appl. № 09/551,082. Filed 18.04.2000. Available at: http://patents.com/us-6364974.html

[7] Shepelyakovskii, K. Z. (1972). Strengthening of Machine Components by Induction Surface Hardening. Moscow: Mashinostroenie, 288.

[8] Shepelyakovskii, K. Z., Ushakov, B. K. (1990, December). Induction surface hardening-progressive technology of XX and XXI centuries. In Proc. 7th Int. Congress on Heat treatment and technology of surface coatings, 33–40.

[9] Ouchakov, B., Shepeljakovsky, K. (1998). New Steels and Methods for Induction Hardening of Bearing Rings and Rollers. Bearing Steels: Into the 21st Century, 307–307–14. doi: 10.1520/stp12136s

[10] Shepelyakovswkii, K. Z., Bezmenov, F. V. (1998). New Induction Hardening Technology. Advanced Materials & Processes, 154 (4), 225–227.

[11] Ushakov, B. K., Efremov, V. N., Kolodjagny, V. V., Skryagin, V. I., Dub, L. G. (1991). New Compositions of Bearing Steels of Controlled Hardenability. Stal', 10, 62–65.

[12] Kobasko, N. I., Morganyuk, V. S. (1983). Study of Thermal and Stress-Strain State at Heat Treatment of Machine Parts. Kyiv: Znanie, 16.

[13] Kobasko, N. I., Morganyuk, V. S. (1985). Numerical Study of Phase Changes, Current and Residual Stresses at Quenching Parts of Complex Configuration. Proceedings of the 4th International Congress of Heat Treatment Materials, 465–486.

[14] Kobasko, N. (2010). Intensive Steel Quenching Methods. Quenching Theory and Technology Second Edition. CRC Press, 510–568. doi: 10.1201/9781420009163-c15

[15] Morhuniuk, W. S., Ushakov, B. K., Kobasko, N. I. (2004). Design of Steel-Intensive Quench Processes. Handbook of Metallurgical Process Design. CRC Press, 733–764. doi: 10.1201/9780203970928.ch17

[16] Kobasko, N. I., Morganyuk, V. S., Dobrivecher, V. V. (2002). Control of Residual Stress Formation and Steel Deformation During Rapid Heating and Cooling. Handbook of Residual Stress and Deformation of Steel. Materials Park: ASM International, 312–330.

[17] Liscic, B., Tensi, H., Canale, L., Totten, G. (Eds.) (2010). Quenching Theory and Technology, Second Edition. CRC Press, 725. doi: 10.1201/9781420009163

[18] Xie, L., Funatani, K., Totten, G. (Eds.) (2004). Handbook of Metallurgical Process Design. CRC Press, 957. doi: 10.1201/9780203970928

[19] Neklyudov, I. M., Shulayev, V. M. (2005). Equipment and Technologies for Heat Treatment of Metals and Alloys. Proc. of 6th International Conference, 295.

[20] Sahay, S. S., Sarmiento, G. S. (Eds.) (2013). Special Issue on Thermal Process Modeling, Simulation and Optimization. ASTM International, W. Conshohocken, 459.

[21] Mastorakis, N., Mladenov, V., Bojkovic, Z. (Eds.) (2010). New Aspects of Fluid Mechanics, Heat Transfer & Environment. WSEAS Press, 385.

[22] Kobasko, N. (2012). Steels of optimal chemical composition combined with intensive quenching. International Heat Treatment and Surface Engineering, 6 (4), 153–159. doi: 10.1179/1749514812z.00000000032

[23] Kobasko, N. I. (2011). Correlation Between Chemical Composition of Steel, Optimal Hardened Layer, and Optimal Residual Stress Distribution. Film and Nucleate Boiling Processes, 81–102. doi: 10.1520/stp153420120005

[24] Kobasko, N. I. (2008). The steel superstrengthening phenomenon, part 2. International Journal of Microstructure and Materials Properties, 3 (4/5), 526–547. doi: 10.1504/ijmmp.2008.022034

[25] Kobasko, N. I. (1980). Steel Quenching in Liquid Media under Pressure. Kyiv: Naukova Dumka, 206.

[26] Liscic, B., Tensi, H. M., Luty, W. (Eds.) (1992). Theory and Technology of Quenching. Springer-Verlag Berlin Heidelberg, 484. doi:10.1007/978-3-662-01596-4

[27] Kim, T., Kobasko, N. I., Liu, Y., Nayar, A. (2006). Worldwide Guide to Equivalent Irons and Steels. Materials Park: ASM International, 1387.

[28] Dossett, J. L., Totten, G. E. (Eds.) (2013). Steel Heat Treating Fundamentals and Processes Vol. 4A. Materials Park: ASM International, 768.

[29] Powell, J. A. (2013). Basics of IQ Process, Presentation at Intensive Quenching Workshop, Cleveland, Ohio, USA.

[30] Kobasko, N. I. (2016). Improvement of IQ-3 processes to eliminate crack formation, decrease distortion, and maximize material strength, and ductility. Eureka: Physics and Engineering, 4, 3–10. doi: 10.21303/2461-4262.2016.000122

[31] Yu, W. (Ed.) (2009). Recent Advances in Intelligent Control Systems. London: Springer, 374. doi: 10.1007/978-1-84882-548-2

[32] Mastorakis, N., Demiralp, M., Mladenov, V. M., Zemliak, A. et al. (2011). Computers and Simulation in Modern Science. WSEAS Press, 238.

[33] Totten, G. E. (Ed.) (2002). Handbook of residual stress and deformation of steel. ASM international, 498.

[34] Totten, G. E. (2006). Steel Heat Treatment Handbook, Second Edition. CRC Press, 1077.

[35] Ravnik, F., Grum, J. (2011). Heat Transfer Stages Recognition by Boiling Acoustic During Quenching. Journal of ASTM International, 8 (1), 103386. doi: 10.1520/jai103386

[36] Grum, J., Bozic, S. (2003). Acoustic emission during quenching of 42 CrMo 4 steel. In 4 th International Conference on Quenching and Control of Distortion, 267–272.

[37] Kichigin, A. M., Kobasko, N. I., Povsten, S. G., Tyltin, A. A., Timchenko, N. P. (1990). Patent 4605186/31-02. Method for Control of Steel Parts Heat Treatment. Assignee: Bayer Materialscience Ag. Appl. № 621.785.79(088.8). Filed 14.11.1988. Available at: http://www.findpatent.ru/patent/159/1595928.html

[38] Kobasko, N., Aronov, M., Powell, J., Totten, G. (2010). Intensive Quenching Systems: Engineering and Design. ASTM International, 242. doi: 10.1520/mnl64-eb

[39] Shepeliakovskii, K. Z., Lobozov, V. P., Kuznetsov, A. A., Nikitin, S. I., Kamenskih, A. A., Karpov, A. A., Zelenov, V. N., Ezubchenko, V. N. (2000). Patent RF 2158320. Konstruktsionnaia STAL ponizhennoi prokalivaemosti. Assignee OAO "Chusovskoi metallurgicheskii zavod". Appl. № 99125102/02. Filed 29.11.1999. Available at: http://ru-patent.info/21/55-59/2158320.html

[40] Kobasko, N. I. (2010). Energy Efficient and Eco-friendly Intensively Quenched Limited Hardenability Low Alloy Steels. Advances in the State of the Art of Fire Testing, 644–644-18. doi: 10.1520/stp49177s

[41] Kobasko, N. (2007). Limited – Hardenability Steels and New Heat Treating Technologies. Material Science & Technology 2007 Conference and Exhibition (MS&T'07), 471–480.

[42] Munnig, J., Pennemann, B., Rausch, A. K. (2012). Patent RU 2450060. Method of thermal treatment of parts from structural steel of lower and regulated hardenability. Assignee: Scientific

and Production Company Technology Engineering and Space-surface hardening. Appl. 2010154543/02. B 13. Filed 31.12.2010.

[43] Bhadeshia, H. K. D. H. (2015). Bainite in Steels: Theory and Practice. 3rd edition. Money Publishing, 616.

[44] Rath, J., Lübben, T., Hunkel, M., Hoffmann, F., Zoch, H. W. (2009). Grundlegende Untersuchungen zur Erzeugung von Druckeigenspannungen durch Hochgeschwindigkeits-Abschrecken. HTM Journal of Heat Treatment and Materials, 64 (6), 338–350. doi: 10.3139/105.110037

[45] Rath, J., Lubben, T., Hoffmann, F., Zoch, H. W. (2010). Generation of compressive residual stresses by high speed water quenching. International Heat Treatment and Surface Engineering, 4 (4), 156–159. doi: 10.1179/174951410x12851626812970

[46] Zoch, H. W., Schneider, R., Luebben, T. (2014). Proc. of European Conference on Heat Treatment and 21st IFHTSE Congress. Munich (Germany), 566.

[47] Kondratjev, G. M. (1957). Teplovye Izmereniya [Thermal Measurements]. Moscow: Mashgiz, 8.

[48] Lykov, A. V. (1967). Teoriya Teploprovodnosti [Theory of Heat Conductivity]. Moscow: Vysshaya Shkola, 600.

[49] Aronov, A., Kobasko, N. I., Powell, J., Kim, H., O'Rourke, B., Andreski, B. (2015). Application of Intensive Quenching Process for Steel Mill Rolls Made of Ductile Iron. The MS&T, Material Science & Technology Conference and Exhibition, 4–8.

A STUDY OF THE FLOCCULS STRENGTH OF POLYDISPERSE COAL SUSPENSIONS TO MECHANICAL INFLUENCES

Andrii Shkop
Department of Chemical Technique and Industrial Ecology
National Technical University «Kharkiv Polytechnic Institute»
21 Bahaliya str., Kharkiv, Ukraine, 61002
shkop_ecomass@ukr.net

Musii Tseitlin
Department of Chemical Technique and Industrial Ecology
National Technical University «Kharkiv Polytechnic Institute»
21 Bahaliya str., Kharkiv, Ukraine, 61002
mzeit@i.ua

Oleksii Shestopalov
Department of Chemical Technique and Industrial Ecology
National Technical University «Kharkiv Polytechnic Institute»
21 Bahaliya str., Kharkiv, Ukraine, 61002
shestopalov.it@khpi.edu.ua

Valentina Raiko
Department of Chemical Technique and Industrial Ecology
National Technical University «Kharkiv Polytechnic Institute»
21 Bahaliya str., Kharkiv, Ukraine, 61002
raiko.ntu@yandex.ua

Abstract

The effect of the concentration and disperse composition on the flocculation strength to mechanical influence is investigated. It is found that the residual rate of floccules sedimentation after the mechanical influence at a constant rate of flocculant has a maximum value at a concentration of solids in the slime in the range of 7–30 g/dm^3. The best results are obtained in all the experiments at a solids concentration of 10 g/l. It is found that at a concentration up to 7 g/l and more than 30 g/l, the floccules is formed. They have the lowest residual rate after mechanical influences. With increasing content of the solid fraction of 40–100 microns over 15 %, the strength of floccules increases. They retain their shape and relatively high sedimentation rate even after mechanical influence. The obtained data allow to recommend correction of the slime composition before flocculant injection both the concentration close to the optimum, and the content of size fraction of 40–100 mm more than 15 %.

Keywords: flocculation, polydisperse slime, floccules destruction, floccules strength, residual sedimentation rate.

DOI: 10.21303/2461-4262.2017.00268

1. Introduction

Coal slime is formed during coal mining and processing. It is a fine product with high ash content. The solid phase of slime of coal preparation plants is often a valuable mineral raw materials, and the liquid phase should be used in a closed system of water recycling. Local cleaning system of chemically contaminated waste water in order have been developed and implemented in modern coal preparation plants to create closed water and slime system [1]. An efficiency of enrichment operations and reduce of water losses for a plant depend on the quality of suspension separation in the thickener. Therefore, a closed cycle, used in coal preparation, presents particular requirements to the quality of solid-liquid separation in the thickener. In modern conditions one of the pressing problems in the practice of coal preparation is to improve the technics and technology of dewatering of coal polydisperse suspensions of small classes (fine silt, slime, flotation concentrate and others classes with a particle size 0–0.5 mm), formed at the preparation plants [2].

Intensification of clarification processes of the liquid phase due to the use of polymer flocculants is carried out at all stages of slime thickening and dewatering [3]. As a result of the destruction of already formed floccules during slime transportation from thickening to dewatering equipment in modern water and slime schemes reflocculation is carried out before each apparatus. Therefore, an important aspect of improving the economic performance of thickening process is to reduce the consumption of expensive flocculant used for intensification of water clarification process. This leads to the need to establish optimal conditions for flocculation that provide a strong enough aggregates that do not require reflocculation after transportation.

Flocculation efficiency for coal slime depends on many factors that affect the formation of aggregates. To clean coal slime containing fine mineral impurities of clay particles nonionogenic [4], ionigenic (cationogenic and anionogenic) flocculants [5], their combination with each other [6] with coagulants [3] or mineral salts [7] are used. General recommendations for the use of flocculants are reduced to the selection of the type and concentration of flocculant for purification of a particular type of slime with a certain concentration and disperse composition. At the same time still insufficiently studied issues such as the impact of concentration and dispersion composition on the structure of polydisperse slime floccules. It is poorly understood changes of the floccules after mechanical influence, their strength characteristics and strength retention mechanism. According to the theory, destruction of the floccules occurs when the shear stress of the order of 1–10 Pa, with the strength of aggregates increased with increasing dose of flocculant [8]. It is found that slime of coal flotation concentrate without the use of flocculants according to the nature of the flow are near Newtonian liquids, and nucleation does not occur in the slime [9]. Suspension becomes pseudoplastic properties when a flocculant supply [10, 11], and the general guidelines for reduce destruction of the floccules are reduced to reduce the shear deformation [12].

Research results that are described in [13] showed that the sedimentation rate of the floccules at the same flow rate of the flocculant has the highest value at the solids concentration in the slime below 30 g/dm^3. Criterion for evaluating formation of solid aggregates has been proposed, which may be a residual flocculation sedimentation rate after mechanical influence, characterizing the size and structure of the aggregates. These data require further experimental verification of the strength of aggregates that formed at lower concentrations.

Thus, despite considerable study of coal slime flocculation, structure and strength characteristics of the floccules of polydisperse suspensions are enough studied. Knowledge of the laws of the formation of strong aggregates, depending on the concentration and disperse composition of suspension will optimize the flocculation process, as well as to predict the possibility of their transportation, ensuring minimal degradation of the floccules.

2. Materials and Methods

Research of polydisperse slime flocculation is carried out using model slimes with controlled parameters of concentration and disperse phase, which are synthesized as follows. Real slime, taken on one of the existing coal preparation plants, passed through a sieve with a size of 40, 60, 80 and 100 microns and coarse fractions were separated. Slime less than 40 microns fraction was thickened by settling and then diluted by clarified liquid to a concentration of 3 to 100 g/dm^3 required to examine the effect of solids concentration on the flocculation process.

For the subsequent series of experiments to study the effect of disperse slime composition was synthesized with solids content from 3 to 100 g/dm^3 and adding medium-sized particles of 40–100 microns in an amount from 5 to 30 %.

The fraction more than 100 microns was not of interest for further research, because such particles are efficiently sedimented without the use of flocculants. The density of the solid phase of the slime was 1.7 kg/dm^3.

Measurement of flocculants sedimentation kinetics in the mode of free (unconstrained) sedimentation was conducted in a laboratory graduated cylinder of 50 mm diameter and 500 mm height.

Flocculant type and concentration were selected before experiment. Combination of nonionogenic production (20 % of total amount) and anionogenic (80 % of the total amount) of flocculants were used for this slime. Dosage amounts of flocculant before each experiment recalculated so that

the flocculant consumption per weight unit of the solid phase was constant at 200 g/t. This flow provides effective formation of the floccules and flow consistency excludes the effect of flocculant dose of the strength of the floccules at various concentrations of solids in the slime.

3. Experimental procedures

To assess the strength of the floccules to mechanical influences we used the following technological test. In the measuring cylinder (**Fig. 1, *a***) with slime of certain solids concentration slime (from 3 to 100 g/l) and size distribution (from 0 to 30 % of fraction content of 40–100 microns) nonionogenic flocculant was added in an amount of 40 g/t. Anionogenic flocculant after stirring was injected in an amount of 160 g/m by cylinder tilting and was stirred again. After formation of the floccules and their sedimentation, flocculed slime was stirred with a stirrer with a speed at the blade tip about 2 m/s for 40 seconds in a rectangular container 120×70 mm (**Fig. 1, *b***). In our opinion, such mechanical effect simulates the movement of flocculed slime through a pipeline from thickening apparatus to dehydration apparatus. The residual rate of sedimentation after a mechanical influence characterizes the size of the aggregates and, thus, the flocculation strength to mechanical influence.

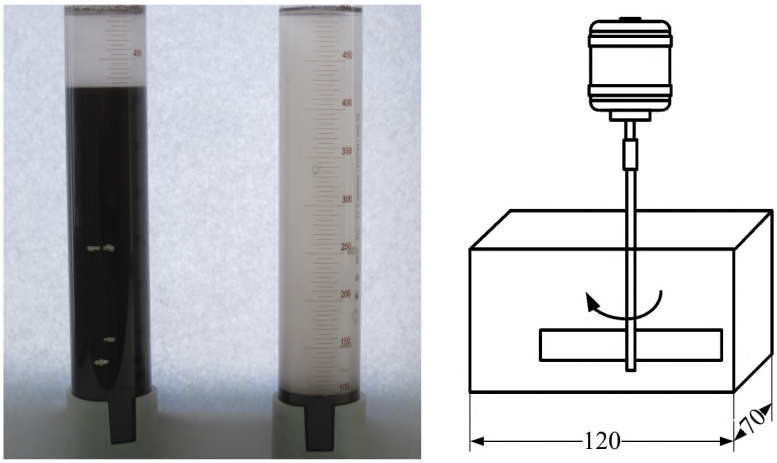

a *b*

Fig. 1. Laboratory equipment for the experiments: *a* – measuring cylinders for investigation of the slime sedimentation rate; *b* – rectangular container with a stirrer for mechanical impact on the floccules

Then the content was poured into a measuring cylinder and determined the sedimentation rate of suspended particles in the sample after mechanical impact. The sedimentation rate of the floccules was calculated using the following formula:

$$V = \frac{0,4H}{t_i}, \quad (1)$$

where H – height of the clarified layer, mm; t_i – free sedimentation time of the floccules (0.4 of the height), s.

Flocculed sediments were sampled after mechanical influence. These samples were studied under the microscope.

4. Results

The study revealed that for the same flocculant concentration residual sedimentation rate of the floccules after mechanical influence depends on the initial concentration and composition of disperse composition of the slime (**Fig. 2**). In the solids concentration range of 3–10 g/l (**Fig. 2, *a***) in all cases of the content of medium-sized class (more than 40 micron) there is an exponential

increase of the rate with increasing concentration, with a maximum content at 10 g/l. In the concentration range of 10–50 g/l (**Fig. 2, *b***) in all cases of the content of medium-sized class there is a decrease of residual flocculation rate, having a character close to the line. In the concentration range of 50–100 g/l (**Fig. 2, *c***) in all cases of the content of medium-sized class there is a sharp exponential decrease of the rate.

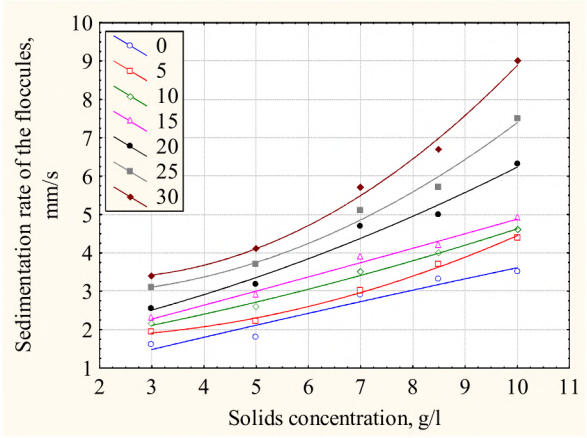

a

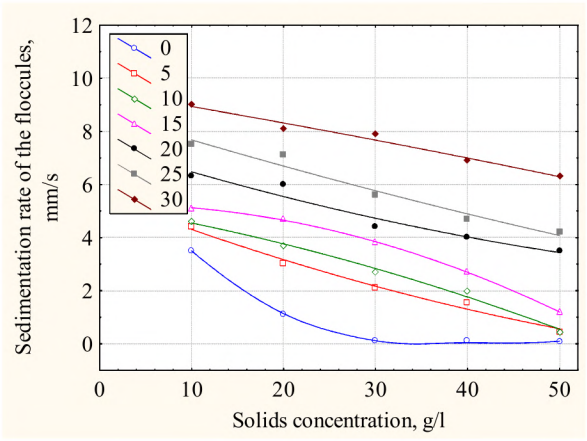

b

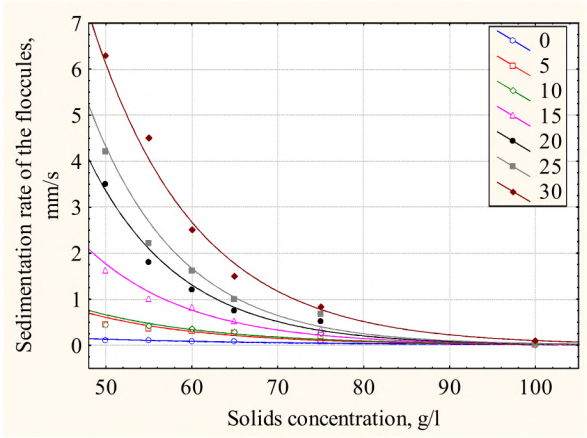

c

Fig. 2. Dependence of sedimentation rate of the floccules undergoing mechanical influence on the concentration (*a* – 3–10 g/l, *b* – 10–50 g/l, *c* – 50–100 g/l) and disperse composition of solids in the slime: the points on the chart – the results of laboratory tests; the lines on the chart – the smoothed line of scatter of experimental values; refer on the lines – the proportion of solids more than 40 micron, %

Investigation of the effect of the disperse composition on the sedimentation rate of the floccules after mechanical influence shown (**Fig. 3**) that with increasing content of the medium-sized class (40–100 microns) the sedimentation rate at all concentrations increases. This is the result of increasing the strength of floccules. Sedimentation rate is reduced with increasing concentration of the solids in the slime and at a concentration more than 50 g/l it is a minimal. At concentrations 75 and 100 g/l sedimentation rate of the slime after mechanical influence is virtually constant, indicating the almost complete destruction of the formed aggregates of the floccules.

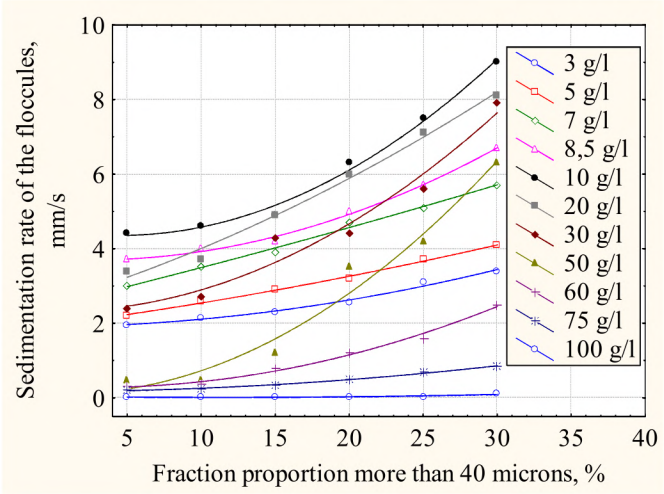

Fig. 3. Dependence of sedimentation rate of the floccules undergoing mechanical influence at different concentrations on the content of fraction proportion of 40–100 microns of the solids in the slime

For content of fraction proportion of 40–100 microns up to 15 % there is a slight increase of the residual rate, and more than 15 % – an increase of the rate becomes significant, particularly in the concentration range of solids in the slime of 7–30 g/l (more than 1 mm/s for every 5 %).

5. Discussion

Research results, presented in **Fig. 2, 3**, show that the concentration and disperse composition of the slime have a significant impact on preserving the strength of floccules to mechanical influences. It is interesting that at low concentrations of solids (up to 7 g/l, **Fig. 2, *a***) and high (more than 50 g/l, **Fig. 2, *c***) there is formation of floccules unstable to mechanical influences. Mechanical influences lead to the destruction of the floccules and a sharp reduction of the residual sedimentation rate. This is confirmed by photos of the floccules shown in **Fig. 4**. At a concentration close to 10 g/l (**Fig. 4, *c***) after mechanical influence floccules are stored with clear contours at a low (**Fig. 4, *a, b***) and high (**Fig. 4, *d, e, f***) concentrations aggregates are visible. They are divided into microfloccules.

Analyzing the obtained data, we can recommend to conduct the slime flocculation at a concentration of the solids close to 10 g/l (the optimal concentration) or in the concentration range of 7–30 g/l (conditions close to optimal). The most resistant to mechanical stress floccules are formed in these concentrations. They retain a sufficiently high sedimentation rate.

Growth of the coarse particles content in the slime (fractions more than 40 microns) leads to the formation of more stable flocculation structures under all concentrations. Moreover, for slimes at a concentration of solids in the range of 7–30 g/l (upper curves in **Fig. 3**) fraction share growth more than 40 microns has significant influence, when a for low (less than 7 g/l) and high (more than 30 g/l) solids concentration there is a slight increase of the residual rate. Floccules hardening increases significantly (by a residual rate) at a fraction proportion of 40–100 microns in the slime more than 15 %. This is clearly seen in the photos of the floccules and presented in **Fig. 5**. Sufficiently coarse floccules are formed with a clear outline and transparent liquid phase at a fraction proportion of 40–100 microns in the slime more than 15 % (**Fig. 5, *d, e, f***), then with the less content of medium-sized particles (**Fig. 5, *a, b, c***).

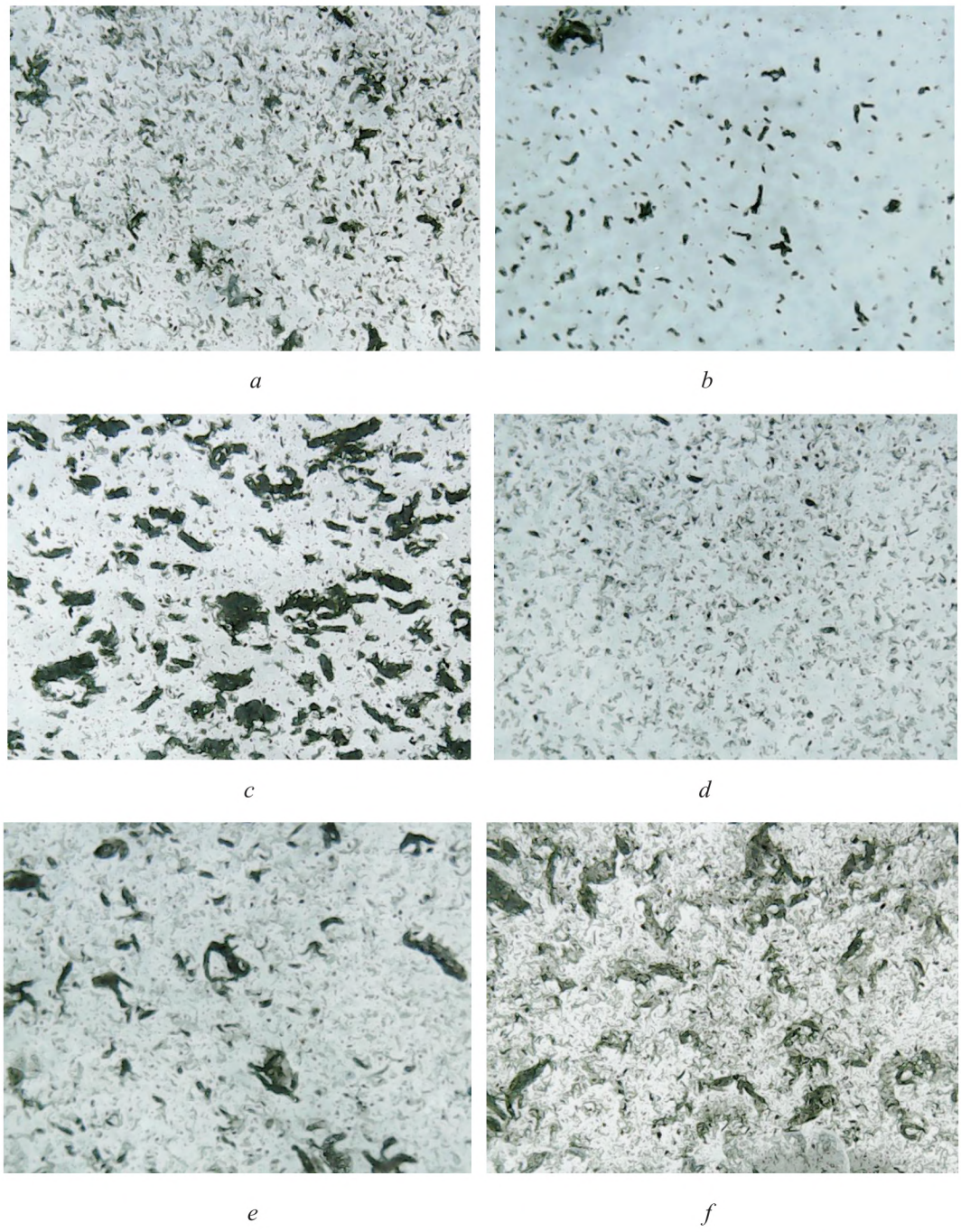

Fig. 4. Photos of the floccules after mechanical influence at solids concentrations in finely divided (less than 40 microns) slime, g/l: *a* – 3, *b* – 5, *c* – 8.5, *d* – 50, *e* – 75, *f* – 100

An ability of the slime correction has a practical interest to achieve the most favorable conditions for the formation of strong aggregates of the floccules. For example, by dilution or thickening of the slime it can adjust the solids concentration in the range of the best values (7–30 g/l). The second way of the intensification of strong aggregates formation can be adding of coarse slime particles more than 40 microns. Compliance with the optimum ratio of the concentration and disperse composition of the slime at the stage of aggregate formation (slime flocculation) provides to obtain fairly strong floccules that are resistant to mechanical influences, and to minimize the destruction of the floccules during transportation and dehydration.

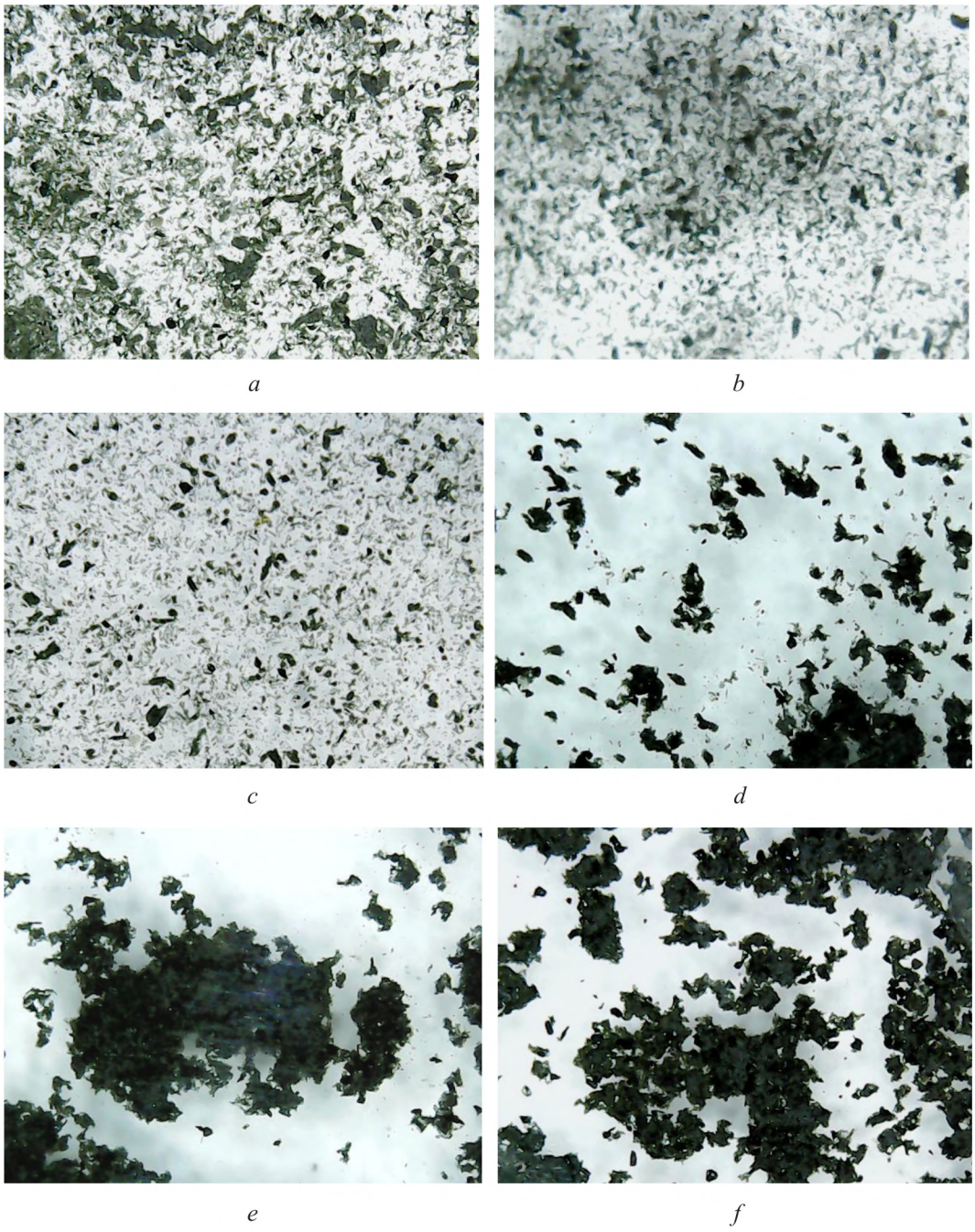

a *b*

c *d*

e *f*

Fig. 5. Photos of the floccules after mechanical influence at a concentration of 10 g/l and the content of the medium-sized fraction in the slime, %: *a* – 5, *b* – 10, *c* – 15, *d* – 20, *e* – 25, *f* – 30

6. Conclusions

The studies allow to formulate the following conclusions:

1. Investigation of the influence of solids concentrations show that the most stable to mechanical stress aggregates formed when the concentration of solids in the slime of 7–30 g/dm^3 (the best conditions for flocculant adsorption).

2. Investigation of the influence of content of the medium-sized class (particle size 40–100 microns) showed that stronger aggregates form in the presence of the fraction of 40–100 microns in the slime more than 15 %.

The results allow to control the process of formation of solid aggregates by correction of the concentration and composition of the slime by dilution or adding of fraction of the solid phase before flocculant injection.

The resulting experimental dependencies can be used to optimize the process of flocculation and getting aggregates resistant to mechanical influences. This will control the slime treatment process with minimal degradation of the floccules, and hence saving flocculant consumption at the stage of dehydration.

Acknowledgments

The authors express their gratitude to LLC "NTC "Ecomash" in the name of technical director G. Troshin for help and full cooperation in the course of carrying out laboratory tests.

References

[1] Zhang, Y., Gong, G., Wu, G. (2014). Research of slime water treatment methods. Clean Coal Technology, 20 (3), 1–4.

[2] Shkop, A. A. (2015). Dewatering coal polydisperse suspensions. Eastern–European Journal of Enterprise Technologies, 2 (6 (74)), 44–49. doi: 10.15587/1729-4061.2015.40557

[3] Sun, Y. Y., Xu, C. Y., Nie, R. C., Zheng, J. H. (2013). Application of Flocculant and Coagulant to Coal Slime Water. Advanced Materials Research, 781–784, 2170–2173. doi: 10.4028/www.scientific.net/amr.781-784.2170

[4] Sabah, E., Erkan, Z. E. (2006). Interaction mechanism of flocculants with coal waste slurry. Fuel, 85 (3), 350–359. doi: 10.1016/j.fuel.2005.06.005

[5] Ofori, P., Nguyen, A. V., Firth, B., McNally, C., Ozdemir, O. (2011). Shear-induced floc structure changes for enhanced dewatering of coal preparation plant tailings. Chemical Engineering Journal, 172 (2-3), 914–923. doi: 10.1016/j.cej.2011.06.082

[6] Sabah, E., Yuzer, H., Çelik, M. S. (2004). Characterization and dewatering of fine coal tailings by dual-flocculant systems. International Journal of Mineral Processing, 74 (1-4), 303–315. doi: 10.1016/j.minpro.2004.03.001

[7] Wang, W. D., Wang, H. F., Sun, J. T., Sun, Y. Y. (2013). Experimental study on slime water flocculation sediment based on the montmorillonite hydration expansion inhibition. Journal of Coal Science and Engineering, 19 (4), 530–534. doi: 10.1007/s12404-013-0414-y

[8] Golberg, G. Yu., Lavrinenko A. A. (2015). Education, the existence and destruction flocculation structures. Mining informational and analytical bulletins, 11, 47–54.

[9] Konovalova, T. A., Veksler, G. B., Lavrinenko, A. A., Golberg, G. Ju. (2014). Primenenie flokuljantov dlja povyshenija jekologicheskoj bezopasnosti vodno-shlamovyh shem ugleobogatitel'nyh fabric. Izvestija MGTU, 3 (1 (19)), 5–10.

[10] Il'in, S. O., Malkin, A. Y., Korobko, E. V., Novikova, Z. A., Zhuravskii, N. A. (2011). Rheological properties of high-concentration suspensions used for obtaining electrorheological media. Journal of Engineering Physics and Thermophysics, 84 (5), 1016–1025. doi: 10.1007/s10891-011-0562-0

[11] Heller, H., Keren, R. (2002). Anionic Polyacrylamide Polymers Effect on Rheological Behavior of Sodium–Montmorillonite Suspensions // Soil Science Society of America Journal, 66 (1), 19–25. doi: 10.2136/sssaj2002.0019

[12] Evmenova, G. L. (2008). Influence of deformation of a medium on flocculation of coal dispersions. Journal of Mining Science, 44 (3), 298–301. doi:10.1007/s10913-008-0020-3

[13] Shkop, A., Tseitlin, M., Shestopalov, O. (2016). Exploring the ways to intensify the dewatering process of polydisperse suspensions. Eastern-European Journal of Enterprise Technologies, 6 (10 (84)), 35–40. doi: 10.15587/1729-4061.2016.86085

DEVELOPMENT OF THE INTEGRATED MODEL OF THE AUTOMOTIVE PRODUCT QUALITY ASSESSMENT

Hadi Amineh
Department of Aviation Devices and Measuring
N. E. Zhukovsky National Aerospace University "Kharkiv Aviation Institute"
17 Chkalov str., Kharkiv, Ukraine, 61070
hadiamineh@hotmail.com

Nataliya Kosach
Department of Aviation Devices and Measuring
N. E. Zhukovsky National Aerospace University "Kharkiv Aviation Institute"
17 Chkalov str., Kharkiv, Ukraine, 61070
nataliya.kosch@khai.edu

Abstract

Issues on building an integrated model of the automotive product quality assessment are studied herein basing on widely applicable methods and models of the quality assessment. A conceptual model of the automotive product quality system meeting customer requirements has been developed. Typical characteristics of modern industrial production are an increase in the production dynamism that determines the product properties; a continuous increase in the volume of information required for decision-making, an increased role of knowledge and high technologies implementing absolutely new scientific and technical ideas. To solve the problem of increasing the automotive product quality, a conceptual structural and hierarchical model is offered to ensure its quality as a closed system with feedback between the regulatory, manufacturing, and information modules, responsible for formation of the product quality at all stages of its life cycle. The three module model of the system of the industrial product quality assurance is considered to be universal and to give the opportunity to explore processes of any complexity while solving theoretical and practical problems of the quality assessment and prediction for products for various purposes, including automotive.

Keywords: model development, automotive product quality, technical control, automotive products, customer requirements, product quality improvement, high-quality products.

DOI: 10.21303/2461-4262.2017.00269

1. Introduction

International recognition of the country and its credibility depend on the quality of manufactured products. Therefore, all great world manufacturers pay great attention to the product quality and, in particular, to the automotive product quality, decisively affecting formation of consumers' preferences and competitiveness both of multinationals automobile corporations, automakers, and automobile sales centers and service stations. Therefore, the quality management system (QMS) of the automotive products at appropriate companies is believed to be strategically important aspect of their operation, allowing to adapt to rapidly changing requirements of consumers and the external market, to improve their competitiveness. So formation of effective, meeting the current requirements of the product QMS become urgent these days.

Currently Ukrainian product quality often seems to be unsatisfactory for some reasons, in particular, due to the low level of the QMS implementation, directly affecting the product quality.

Therefore, in order to release competitive products, effective management systems and quality control over released products should be developed and implemented at enterprises based on domestic and foreign experience, which may ensure a proper level and determine the level of development of the country's economy in this economic sector in the world market.

As we know, issues of the product quality assessment within technical control of industrial plants are considered to be a top priority in most countries and, in particular, the UK, Germany, USA, and Japan [1–12].

Quality management in the stream production like the automotive industry is considered to be complicated because of the following reasons [1]:

– all processes at the automotive company are mandatory, since they are involved into achievement of the main purpose of production to meet customers' requirements (demands);

– in the production process, a product is manufactured which tangibly complete material streams of the main logistics object, for creation of which material support is required;

– material flows always pass through transformation processes, required to meet consumers, from their creation location to the point of final use;

– necessity to control the quality of production operations binding supply (inbound logistics) and distribution (outbound logistics).

It should be noted that solutions in the production are characterized by strategic nature, since they are associated with significant investments and cannot be quickly reversed. Therefore taken decisions in production largely predetermine restrictions on decisions regarding supply and distribution, as well as the entire supply chain.

All production operations are defined as a transformational process that uses resources: buildings, machinery and equipment, financial resources, materials, human and information resources, knowledge, and other, and with certain technologies, converts them into products. During transformation, product qualities (properties) that meet consumers' expectations are achieved.

2. Materials and Methods

To assess the product quality, two approaches are used, namely the quality assessment according to standards applied at an automobile enterprise, and qualimetry methods. The first approach is based on experience, certain historical traditions in the industry, reflected in the relevant government and industry standards for a certain type of product. The second approach is based on modern qualimetry methods for evaluation of the product quality based on the corresponding generalized (integrated) indicator [1].

While designing the product quality, the quality function deployment methodology is accepted as a basis using the concurrent engineering principles, where cross-function commands are used at all stages of the product development. Each stage of the Quality Function Deployment (QFD*)* process uses control stages or matrix from the initial planning stage to the production end, representing a specific set of requirements for the product [2].

3. Experimental procedures for development of the automotive product quality assurance system

Stage 1 – Product planning: development of the quality passport – the customer's documented requirements to the product, its warranty, competitive advantages, taking into account the results of the study of competing cars, as well as the manufacturer's technical capabilities to meet the customers' requirements; the product unified quality indicators (UQI) are formed, etc. Thus the customer's requirements are considered to be crucial.

Stage 2 – Product projecting and designing: product development designing – a creative approach and innovative ideas are required when developing specifications, which are considered the most important to satisfy the consumers' requirements during planning.

Stage 3 – Development of production processes and technological parameters (or target indicators): their indicators are documented, the quality target indicators of the whole system by released products are fixed basing on the selected reference sample or an "ideal" planning model.

Stage 4 – Production process management: indicators, developed for production process control, are used, technical maintenance and operators' trainings are scheduled, decisions on processes of the greatest risks and on defect prevention are made.

For example, the developments of research companies Hui Zhou and YiQiu Human Factors Research Unit allow to plan a comfortable driving basing on the mathematical model of the car dynamic system that can be a very useful tool for the developers involved into the car design at stage 2 of its conceptual design. Also, as a result of the own researches, this company has developed a simple mathematical model to determine the vibration influence on the car and driving quality that is believed to be crucial to its performance characteristics and consumer properties [3].

Another very important problem of the automotive industry is to reveal and eliminate defects because "ignoring defects may result in serious consequences for the business organization" [4–8]. It is currently quite difficult to take into consideration complexity, time and cost of surveillance and prediction of the car quality. To meet the high quality and reliability requirements, the car manufacturers put considerable efforts aimed at software development for its verification and validation. Testing with software is an important part of ensuring proper functioning and reliability of all car systems. At the same time, such testing is also considered to be resource-intensive activity, accounting for 50 % of the total costs of the appropriate verification and validation [9], to have a good test strategy with the proper software is essential for any industry.

The algorithm of the product designing meet customers' requirements is given in **Fig. 1.**

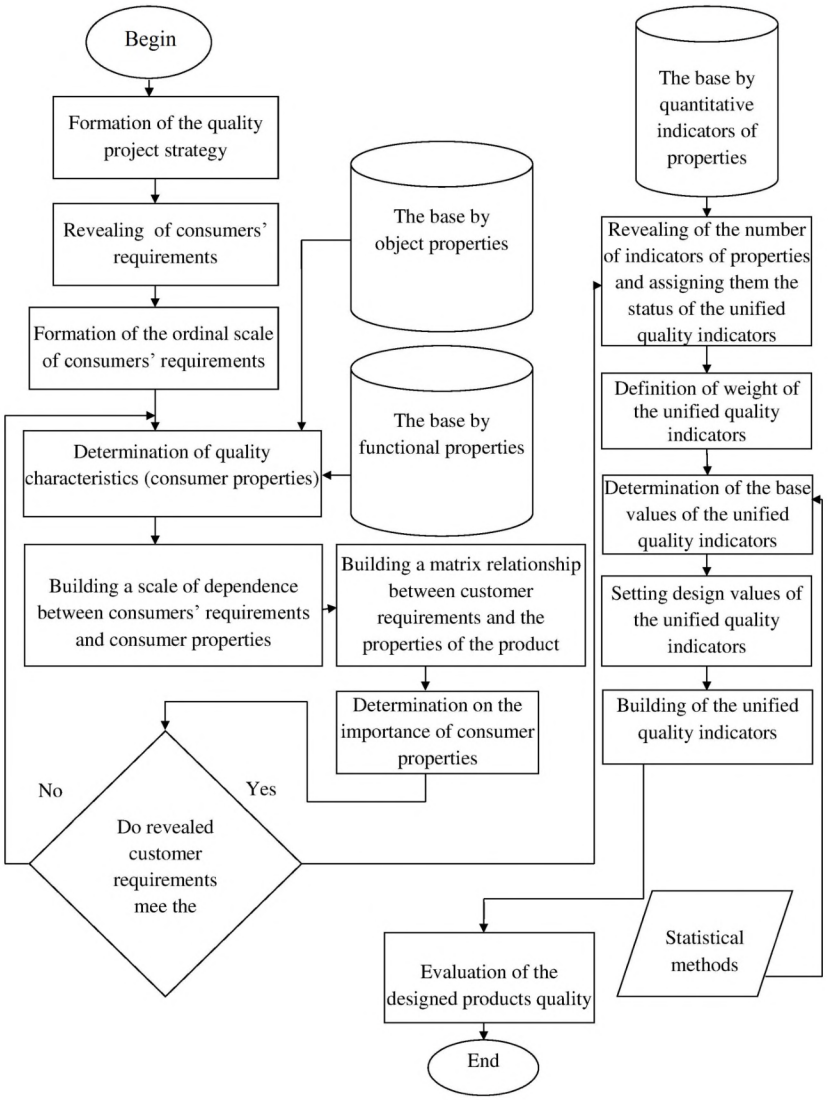

Fig. 1. Algorithm of the product designing meet customers' requirements

In accordance with the algorithm, first, requirements to the test product quality, expressed freely by consumers, are determined. Then, these requirements are transformed into qualitative characteristics (properties). Later most informative quantitative indicators (physical quantities) are selected by each property by assigning them the appropriate status.

In order to increase the product quality, the following principles should be considered [10]:

– focus upon demands of consumers of its market segment, studying of automotive products consumers' preferences via the Internet, including by 24 hour online opinion polls;

– continuous improvement of the production and activity associated with quality;
– continuous improvement of the competence of the organization's personnel;
– quality assurance at all stages of the product life cycle;
– involvement of all personnel into solving quality problems.

Upon analyzing previous researches in this area, we can point at several aspects of the product quality assurance [11]:

1. Quality control – in some quality control systems, manufactured products are checked and tested by random sampling and all rejected samples are reported.

2. Quality assurance – includes both quality control and high performance, provided mainly by high-quality tools and equipment.

A control chart is used as a statistical control over the production process, which allows to see whether the production process runs according to the plan or the executed work quality does not meet the standards. At the same time, concern for the quality is embodied in the concept of the quality management as a whole – a kind of philosophy of management that puts quality at the center of the company operation being an existence point [12].

An increase in the production process dynamism is considered to be typical features of the modern industrial production determining the product properties; a continuous increase in the volume of information required for decision-making, an increase in the role of knowledge and high technologies implementing absolutely new scientific and technical ideas.

The modern industrial production is characterized by multi-functionality, hierarchy and complexity of the internal structure, resulting in growth of intellectualization of production processes, the need for information and integrative approaches to establish relationships between the individual processes of the quality management systems at different stages of the product life cycle. Under these circumstances, the role of the information support to ensure product quality grows, efficiency of production processes and management increases by ordering and synchronization of information flows between the enterprise's structural and functional elements. Information support of production processes solves issues on document circulation, harmonization and acceleration of cooperation of enterprise's divisions and partners, selection and systematization of enterprise's performance to determine corrective actions aimed at elimination and prevention of inconsistencies, and as a result, leads to increased competitiveness.

Modern requirements for information support at all stages of the product life cycle necessitate to apply intelligent decision support systems (IDSS).

Considering the complexity and multiparametricity of products and processes of the modern industrial production, the intelligent decision support systems should meet the following system requirements:

– openness and adaptability;
– hierarchy and ordering at each level;
– intellectualization (ability to select an appropriate algorithm for operation and information processing according to the change in management tasks, incoming effects and resources available);
– use of modern means of measuring technique, which provide simultaneous execution of measuring and processing of multidimensional information;
– providing analysis of incomplete, inaccurate and contradictory information; ability to analyze indicators of certain characteristics of products and processes (spot estimation) and their aggregates; compression (aggregation) of multi-dimensional information for the transition from a large number of parameters to their generalized estimation; diagnostics, control, recognition of different parameters considering their changes over time and in a multidimensional space of different scales; registration, conversion, and interpretation of large amounts of information;
– ability to solve insufficiently formalized, unstructured problems in incomplete and unclear criteria for decision-making.

4. Results of the research of the automotive product quality assurance

To solve the problems of increasing the automotive products quality, the conceptual structural and hierarchical model of quality assurance system is offered as a closed system of feedback

between the regulatory, production, and information modules, responsible for the product quality at all stages of its life cycle. The scheme of this model is shown in **Fig. 2.**

The regulatory module includes documents of the quality management system regulating organizational and managerial procedures. Thus, each quality level is linked to the production module and appropriate levels of the information module by feedback through information flows, creating an information three-level model of an industrial enterprise.

The production module is a functional unit of transformation of incoming resources into outputs, regulating processes of formation of product quality at the stage of their manufacture.

The information module consists of three levels of intelligent systems of decision support that form hierarchical relationship of the information systems, namely:

1st level – collection, analysis, storage, transfer and presentation of the information at all stages of the life cycle;

2nd level – support of project and management decisions by analytical procedures to obtain forecasts and scenarios of the production processes development, optimization of production parameters with technologies and tools, data analysis;

3rd level – decision making – the highest level of process control by the enterprise's top management according to the set goals and QMS policy.

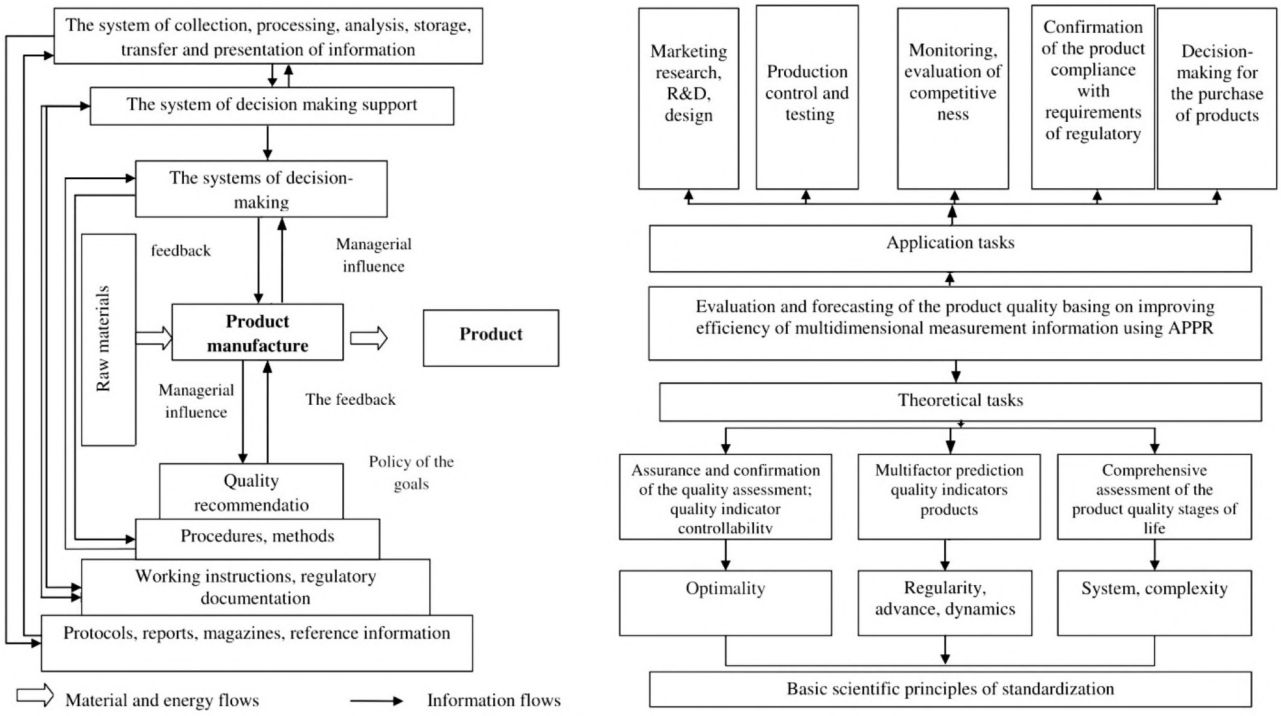

Fig. 2. Scheme of quality assurance for the automotive product

At the same time, the information module provides the organizational and technical system functioning associated with the necessity of operational analysis of large volumes of quantitative and qualitative information in solving unstructured problems that require computer and software tools of modeling, forecasting, and systematization of information on the basis of applied statistical methods, CALS technology, fuzzy logic, neural networks, Data Mining techniques [13].

These technologies and tools make a basis for intelligent decision support systems and are used to assess and predict the product quality, to improve the efficiency of multi-dimensional information processing during preventive and corrective actions in the quality management system.

The three modular model of the industrial product quality assurance system is universal and gives the opportunity to study processes of any complexity in solving theoretical and practical problems of assessment and prediction of the product quality for various purposes, including automotive one.

Automobile enterprises' operation represents a complex of interrelated factors – people, technique, technology, acting as a single unit with the effective functioning of the technical services. The term "technology" refers to combination of experience, knowledge, skills, materials, machines, tools and equipment, used in production. The developed scheme of interaction between technical, social, and environment of the automobile enterprise is given in **Fig. 3.**

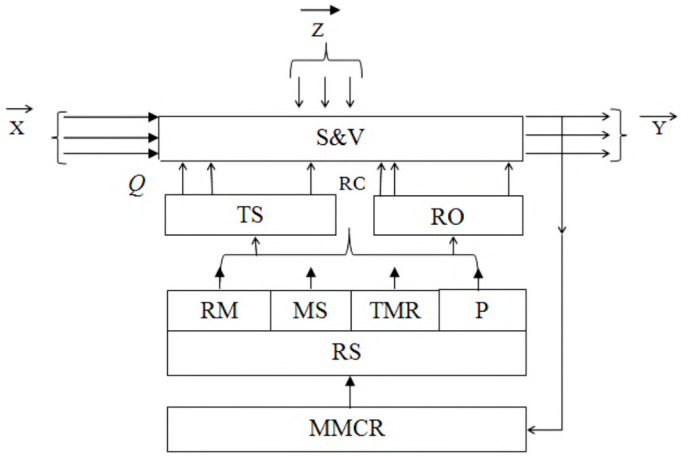

Fig. 3. System of interaction of human-machine-environment of the automobile enterprise: S&V – system and vehicles (cars) at service centers; X – factors providing operation (manpower, fuel, oil); Z – factors characterizing the reliability indicators (operating conditions, service personnel qualification, and so on); Q – factors, characterizing the internal state; Y – technical condition of the equipment and basic characteristics of their reliability indicators; MMCR – management methods, level of the car reliability; RS – repair system; RM – repairing materials; TMR – technical maintenance and repair; MS – maintenance supply; P – personnel; TS – technical support; RO – repair operations

Physical and natural resources are limited in any production activity. So, they should be used to provide base for long-term development (almost endless). This means ensuring inexhaustible sources in the development process at planning its intensity growth.

While the product quality is planned to be improved, the enterprise should be considered to have sustainable economic development. This is associated with certain expenses for the product quality different for each industry and enterprise depending on their level.

We would like to present the updated production model of economic subjects, adapted to automotive enterprises, associated with modern concepts of the sustainable economic development. It differs from existing [14] by adding new components (D, A, S) in the cost price:

$$\xi = C + V + D + E + A + P + O + S, \tag{1}$$

where ξ – indicator of the market price for products or services; C – cost of material resources, V – cost of labor, D – value of energy resources, E – cost of waste and emission disposal, A – value of assets, P – profit, O – taxes and charges, S – social protection at the enterprise.

The index of the enterprise's sustainable development, consisting of various economic entities subject to the enterprise's general policy, but with own operational independence, can be determined by the following formula:

$$Iesd = \frac{1}{m} \Sigma \psi j KE, \tag{2}$$

where j = 1, 2,..., m, m – the number of economic entities in one enterprise;

$$K_E = \frac{1}{n}\sum \frac{(Et_i - Eb_i)}{Ec_i},$$

the average coefficient of growth /progress for each subject; i=1, 2,...n, n – the number of indicators of the subject, Et_i – the current index of the i subject, Eb_i – the benchmark for the i subject, Ec_i – the target indicator of the i subject, Ψj – coefficients wt (actual model error) for the subjects.

Proceeding from sustainable enterprise's development, and importance of the product quality, we have the following relation

$$\Sigma\psi j = \psi 1 + \psi 2 + \ldots\ldots + \psi m = 1. \quad (3)$$

For the practical model realization, MS Excel 2010 spreadsheets have been developed, with specific values for individual components of the formula (1): ξ, C, V, D, A, E, O, S.

Tables for "ACCO Motors", with filled values for individual input components, are listed below. "ACCO Motors" is an official "Mazda" dealer. The company is involved into sales of new cars, warranty and maintenance of cars, sale of original spare parts, accessories, car care. **Table 1** shows the calculations.

Table 1

MS Excel spreadsheet for data input to assess "ACCO Motors" contains approximate component values

N	Expenses	Optimization direction	Base indicator Eb	Objective indicator Ec	Current indicator Et
		Economic indicator Ei			
1	The cost of material resources	decrease	18000	15000	16000
2	The cost of labor invested	decrease	14000	10000	13400
3	The cost of fuel and energy resources	decrease	5000	2000	4000
	Environmental indicator Ei				
4	The cost of waste disposal and emissions	decrease	5000	2500	4000
5	The cost of the assets	decrease	3000	2000	2000
	Social indicator Si				
6	The cost of taxes and fees	decrease	15000	10000	10000
7	The cost of expenses for social protection of the society	increase	6000	8000	7000

An algorithm of estimation of changes in stability indicators was obtained basing on MS Excel. It covers two hierarchical levels:

Ist level – assessment of progress in sustainable development of the enterprise as a whole;

IInd level – assessment of progress in sustainable development of individual entities (divisions) of the enterprise.

To evaluate changes in sustainable development of the enterprise as a whole (Ist level), the changes in its individual subjects should be evaluated first. Assessment is based on general category expenses – "economic", "environmental" and "social" (shopping area of each subject obtained for certain time period, the category contains n number of indicators to be assessed).

Correction coefficient K_{EJ} by each indicator is defined as the difference between the current indicator and its base indicator. Base expenses Eb may differ from indicators of target expenses Ec. Each type of expense Ec should be indicated desired (expected) target indicator ("decrease" or "increase") regarding its baseline value (Eb).

Depending on the ratio of the planned values for this indicator, the following assessment may imply:

– E_i>0 – positive change in the indicator regarding the base cost;

– KE_i=0 – the indicator amendment regarding the base cost is not taken into account;

– KE_i<0 – negative change in the indicator regarding the base cost;

Since the assessment of the progress of individual car sales centers and large auto corporations is a process recurrent in time, using the MS VBA capabilities, macro is designed, integrated in the tables of Ist and IInd level of MS Excel.

Through it, a new "Worksheet" created as a copy of the previous estimation is added in a "Workbook" for each object of each next period of estimations.

For each subsequent estimation (Worksheet), indicators of current expenses (Ec_i) are to be set as the base costs (Eb) for the next period. In the early period, the estimation team represent new target indicators for expenses (Et_i), and at the end, the actual expenses (Ec) for the previous period are to be set; numeric data estimations and graphic data representation in the chart are automatically updated.

Thus, the accumulated data for individual subjects, and for the whole enterprise make it possible to monitor change rates, stability and profit indicators, formed at its divisions and at the enterprise for long prior periods, as well as to predict their behavior in future.

Continuous evolution of changes at the automobile enterprise leads to effective solutions both at the strategic and tactical, and operational levels [15, 16].

5. Discussion of the investigated issue

The introduction of new models of organization of maintenance and repair, compliance with car manufacturers' policy and customers' requirements creates the need in the information system for processing large amounts of information in a short time.

The practical use of the model at the information level provides a solution to quality assessment problems during development, production control and product testing, evaluation of competitiveness and confirmation of the product compliance with quality requirements, development of the QMS and control systems of metrological reliability. Thus, the model takes into account the need for the design and development of theoretical approaches regarding the provision of guaranteed quality assessment and multivariate prediction of quality indicators, comprehensive assessment of the product quality at all stages of the life cycle, considering the basic scientific principles of standardization – optimality, flexibility, regularity, dynamics, system, and complexity.

The conceptual model of the quality assurance system for automotive products is implemented for structural and functional modeling of the quality management system. The developed model is an as-is model. It reflects the existing structure and interconnections of the quality assurance system at the life-cycle stages, and according to the principles of the structural analysis and hierarchical ordering determines the order of the system research, which begins with its general description (formalization), then detailing (decomposition), acquiring a hierarchical structure with a large number of levels. This makes it possible to improve the system by various criteria by building simulation to-be models and to determine ways of rationalization of the structures of the quality management system processes, and relationships between them [17–20].

The model determines the structure of the material and information flows between functional blocks of the management system considering constraints of available resources and regulatory documentation. The built model of the quality management system can be used for solution of analytical and prognostic problems of project and management decisions during the product development, manufacture, and operation at all stages of the life cycle.

6. Conclusions

Production of high quality products provides great advantages and prospects, in particular in reducing production costs, expenses at working with reclamations, defects elimination, and, net income growth, domestic market expansion and entry into the international market. Therefore, until entrepreneurs understand the urgent need to ensure the quality of their products, they will keep losing their potential income and market share.

Namely, the state and enterprises' top-management together with the shareholders should create all necessary conditions to increase the quality and competitiveness of the national products, sustainable economic development, to improve conditions and living standards, and others.

The developed integrated scheme of evaluation of the information support, quality automotive products as a closed loop with feedback between the regulatory, manufacturing, and informa-

tion modules of the production makes it possible to improve the product quality while reducing economic expenses. The practical use of this model provides the scientific principles of standardization in solving problems of the product quality control using intelligent systems of decision support.

The conceptual scheme of automotive product quality assurance is implemented for structural and functional modeling of the quality management system. Based on the SADT methodology and IDEF0 standards, taking into account the principles of the system, the process approaches, structural analysis, system model is developed that can be used to solve analytical and prognostic problems of project and management decisions in the design, manufacture and operation of automotive products at all stages of their life cycle.

Thus, this research can be used for assessment of the automotive product quality. The author is planning to develop a method of the automotive product quality assessment.

References

[1] Zhou, H., Qiu, Y. (2015). A simple mathematical model of a vehicle with seat and occupant for studying the effect of vehicle dynamic parameters on ride comfort. 50th UK Conference on Human Responses to Vibration. Available at: https://pdfs.semanticscholar.org/eb75/506ba9c84ca2a2bbf45572d7879da44b2204.pdf

[2] Ebert, C., Jones, C. (2009). Embedded Software: Facts, Figures, and Future. Computer, 42 (4), 42–52. doi:10.1109/mc.2009.118

[3] Jones, E. L. (2001). Integrating testing into the curriculum – arsenic in small doses. ACM SIGCSE Bulletin, 33 (1), 337–341. doi: 10.1145/366413.364617

[4] Broy, M. (2006). Challenges in automotive software engineering. Proceeding of the 28th International Conference on Software Engineering, 33–42. doi: 10.1145/1134285.1134292

[5] Furst, S. (2010). Challenges in the design of automotive software. 2010 Design, Automation & Test in Europe Conference & Exhibition, 256–258. doi: 10.1109/date.2010.5457201

[6] Eklund, U., Gustavsson, H. (2013). Architecting automotive product lines: Industrial practice. Science of Computer Programming, 78 (12), 2347–2359. doi: 10.1016/j.scico.2012.06.008

[7] Mellegard, N. (2013). Improving Defect Management in Automotive Software Development. Chalmers University of Technology, 247.

[8] Grady, R. B. (1996). Software failure analysis for high-return process improvement decisions. Hewlett Packard Journal, 47, 15–24.

[9] Yevdokimova, L. I. (2015). Complex assessment of dynamics of an enterprise's operation effectiveness as a tool for the analytical activity activation at an industrial enterprise. Moscow: Academic International Institute, 150.

[10] Zakharov, M. G. (1999). System quality is the enterprise of self-preservation tool in times of crisis. Standards and quality, 2, 33–34.

[11] Zekunov, A. G., Ivanov, V. N., Mishin, V. M., Pazyuk, Yu. V., Vlasova, T. I. (2015). Quality management. Moscow: Yurait Publishing house, 475.

[12] Medunetsky, V. M. (2013). Fundamentals of quality assurance and certification of industrial products. Saint Petersburg: ITMO, 61.

[13] Huang, E. (2010). Quality Products and Methods of their Evaluation in an Industrial Enterprise. Problems of modern science and practice, 10-12 (31), 248–264.

[14] Hadi, A. (2016). The product quality: characteristics, essence, evolution of approaches. Economy. Management. Modern problems and prospects of development, 4, 64–72.

[15] Kosach, N. I., Siroklyn, V. P., Hadi, A. (2016). The quality of the system engineering company Iran Khodro management. All-Ukraine Scientific and Technic Conference of Young Scientists in Metrology, 1-5, 82–96.

[16] Hadi, A., Kosach, N. (2016). Assessment of Consumers' Satisfaction with the Automotive Product Quality. International Journal of Environmental & Science Education, 11 (16), 8726–8739.

[17] Stroganov, V. I. (2012). Results and prospects of development of electro mobiles and hybrid vehicles. Electronics and electrical transport, 2.

[18] Vitovtova, A. A. (2016). Analysis and evaluation of quality competitiveness. Kuban State University, 12.

[19] Leonov, O. A., Temasova, G. N. (2015). Economics of quality. Saarbruken, 305.

[20] Leonov, O. A., Temasova, G. N., Vergazova, Y. G. (2015). Quality management. Moscow: Publishing house RGAU – MSHA, 180.

DEVELOPMENT OF ECOLOGICALLY SAFE TECHNOLOGY OF WASTE MYCELIA RECYCLING

Oksana Yegorova
Department of General Ecology, Pedagogy and Psychology
Cherkasy State Technological University
460 Shevchenko str., Cherkasy, Ukraine, 18006
yegorova.ok@gmail.com

Abstract

Chitosan is a cationic polymer derived by deacetylation of chitin obtained from crustaceans. Biodegradable and mucoadhesion properties of chitosan have recently led to increasing the interest. Chitosan can be used as raw material for the manufacture of films, membranes and fibers, in such branches as medicine, agriculture, veterinary medicine, biotechnology, cosmetics and pulp, and paper industry. Previously it was investigated that in Aspergillus Niger cell wall constituents, chitin comprises of 42 % and also researchers confirmed that the chitosan content of fungi depends on fungal strains, mycelial age, cultivation medium and conditions [1]. In the paper the results of the study of physical and chemical properties of obtained samples of chitosan are shown. The influence of initial parameters of the process on the quality of chitosan is investigated. Use of the biomass to produce chitosan on the basis of the developed methodology is shown. It is found that the resulting chitosan is characterized by low values of ash content, moisture content and the value is within 75–82 %. A further development of the scientific basis for the creation of an efficient, competitive and environmentally safe technologies for utilization mycelial biomass of the fungus Aspergillus Niger with the production of a valuable product is chitosan, which is in contrast to the known allows to reduce production costs by 10–80 % (by using not concentrated solutions of chemicals and low temperature process. This leads to reducing the cost of reagents and electricity. The calculation was performed on indicators such as net present value, internal rate of return and payback period.) The use of the developed technological schemes in practice allows utilization of mycelial waste with the aim of obtaining from them valuable product of chitosan, and to ensure the improvement of ecological situation in the region.

Keywords: chitosan, filamentous waste, processing technology, recycling, Aspergillus Niger.

DOI: 10.21303/2461-4262.2017.00264

1. Introduction

Environmental studies that were conducted in the last decades in many countries and in Ukraine showed that the increasing devastating impact of anthropogenic factors on the environment leads to the brink of crisis [2–4] Among the various components of the environmental crisis (depletion of raw material resources, lack of clean fresh water, possible climate catastrophe) is the most threatening, took the problem of pollution of irreplaceable natural resources – air, water and soil waste management industry. Waste water is generated in the production process, which differs in their physical properties, chemical composition and degree of contamination, and environmentally hazardous wastes that are stored in the fields of filtration and adversely affect the ecological safety of the regions.

Academic interest to chitin, chitosan and chitin-containing compounds increased last years. Chitosan is mainly obtained by deacetylation of chitin (poly-β-(1,4) acetylglucosamine) obtained from wastes of the sea-food industry (crab and shrimp shells and squid pens) and presents all the advantages of a low-cost renewable raw material. Chitosan is an effective sorbent for metal species. Chitosan can be used as raw material for the manufacture of films, membranes and fibers in such fields as medicine, agriculture, veterinary medicine, biotechnology, cosmetics and pulp and paper industry [5–8]. According to the analysis of literary sources revealed that one of the cheapest sources of chitin can be the mycelium of mold fungus Aspergillus Niger. Currently existing methods of removal of chitin and chitosan from waste mycelia of the fungus Aspergillus Niger based on the use of concentrated solutions of acids and alkalis (30–50 %) and a large amount of solvents [9–13]. In this regard, the actual problem is a modification of known methods for the isolation of mycelial chitosan from waste using available and inexpensive reagents.

2. Materials and Methods

The first appropriate step was to conduct physical and chemical studies of the mycelial biomass of fungus Aspergillus Niger – waste biotechnological production of citric acid. For experimental studies with the purpose of properties comparison, samples of biomass were taken from different fermentors after a complete cycle of fermentation. The cultivation of biomass was carried out by submerged fermentation on beet molasses under virtually the same conditions. Obtained experimental data are given in **Table 1**, further confirmed the already known fact that the chemical composition of biomass and its characteristics are significantly influenced by the conditions of fermentation of the fungus Aspergillus Niger.

Table 1

Characteristics of mycelial waste of the fungus Aspergillus Niger

Sample of biomass*	Ash content, %	Humidity, %	Content, %				pH
			Fats	Proteins	ChCS**	AOM***	
1	10,5	70	1,65	18,5	22,5	58,4	3,6
2	10,0	70	1,64	18,2	23,0	58,2	3,6
3	9,0	74	1,62	18,7	22,0	57,7	3,4
4	8,2	72	2,34	14,6	19,5	61,6	3,7
5	8,6	72	2,35	14,4	20,8	62,5	3,6
6	8,0	75	2,30	15,0	20,0	62,7	3,6

*Note: * – samples of biomass were selected from different fermentors; ** – chitin-containing complexes; *** – accompanying organic matter*

It is established that the biomass, which were obtained in strict compliance with technology of deep fermentation of the fungus Aspergillus Niger on beet molasses (biomass № 4–6), in its composition contain about 20 % of chitin in the form chitin-containing complexes. For biomass, selected from fermentor, a breach of the conditions of the technological regime, that is, when there is insufficient aeration, low temperature, poor quality of the underlying molasses (samples № 1–3 respectively), characterized by the increase in the number of chitin to 22 %.

The increase of the amount of chitin complexes in biomass can be regarded as a response of the fungus to adverse environmental conditions and protects cells from their actions with these sustainable complex biopolymers. A consequence of the low quality of the source beet molasses, which is the presence in its composition of a significant amount of mineral salts, there are higher values of ash content of the mycelial waste. Partial extraction of soluble salts from the biomass and reduce of its ash content contributes to pre-washed thoroughly with water (biomass № 4, 6). An important task that was set when the method of producing chitosan, was the choice of optimal conditions of processing mycelial waste with the aim of obtaining a product with a stable chemical composition regardless of the quality of waste mycelia of the fungus Aspergillus Niger.

Method for isolation of chitosan from waste Aspergillus Niger consists of the following steps:

1. Diacetylguanine chitosan 37 % solution of NaOH at t=110 °C for 7 hours.

2. Cooling the mix and a thorough rinsing with distilled water to pH=12,5, filtering the mixture.

3. Extraction of chitosan from the precipitate by acetate acid.

4. The deposition of chitosan solution of NaOH, rinsing the precipitate with distilled water followed by filtration and drying the precipitate.

During the study of physicochemical characteristics of chitosan it is determined (test setup of the physical and chemical characteristics was determined empirically):

1. The product yield according to the formula:

$$W = \frac{m}{m_o} \cdot 100\ \%, \tag{1}$$

where m – the weight of chitosan, g; m_0 – the weight of the portion of the original biomass, g.

2. Ash content – combustion of the sample of chitosan for 2 hours at t=800 °C.

3. The moisture content of chitosan was determined according to the difference of the masses of the original sample (1 g) and dried for one hour at t=110 °C.

4. The calculations were carried out according to the formula:

$$W_{H_2O} = \frac{g_1 - g_2}{g_1} \cdot 100\ \%, \tag{2}$$

where g_1, g_2 – the mass of wet and dried chitosan, accordingly, g.

5. The pH of the aqueous extract was determined after three minute boil chitosan sample weighing 5 g in 50 of distilled water followed by filtration of the suspension through a paper filter and cooled. The pH measurements were carried out on a universal odometer «Ecotest-2000» (Russia).

6. The degree of swelling were determined by soaking 4 g of chitosan in distilled water during the day with fixing the initial and final volumes. The calculation was performed according to the formula:

$$S_n = \frac{V_n - V_o}{m}, \tag{3}$$

where S_n – the degree of swelling, ml/g; V_0 та V_n – volumes of dry and swollen sample, accordingly, cm^3; m – the dry weight of the sample, g.

7. Water holding capacity was determined by soaking the sample chitosan weight of 2 g in distilled water for 20 hours, followed by filtration and centrifugation for 10 minute at a speed of 4000 rpm. The chitosan was dried to constant weight at 105 °C. The calculation was performed according to the formula:

$$WHC = \frac{(m_1 - m_0)}{m_1} \cdot 100\ \%, \tag{4}$$

where WHC – water holding capacity, %; m_1 and m_0 – the mass of the sample before and after drying.

8. Diacetylguanine degree (DD), which characterizes the degree of conversion of chitin to chitosan, was determined by several methods: photocolorimetric, potentiometric and IR spectroscopy.

The photocolorimetric method is based on the interaction of chitosan amino groups with a pigment ninhydrin. To construct the calibration curve, solutions of result standardized chitosan with DD=40 % acetic acid were prepared with the addition of a phosphate buffer mixture and ninhydrin. The optical density was measured on photocolorimeter KFK-2 MP (Russia) at a wavelength of 400 nm. Degree diacetylguanine calculated by the formula:

$$DD = \frac{m_x}{m \cdot 10^3} \cdot 100\ \%. \tag{5}$$

Potentiometric method consists on the construction of titration curves. Titration curves were obtained by titration with alkali solution of chitosan with chloride acid. Weighed 0,2 g of chitosan was dissolved under stirring on a magnetic stirrer (MM-5, Russia) for 1 hour. The resulting solution

was titrated with 0,03 N solution of sodium hydroxide to a pH of about 11. On the calibration chart, the first leap on the titration curve corresponds to an excess of hydrochloric acid, and the second – concentration of amino groups in chitosan Nawaz.

For spectral studies, the samples of chitosan were tableted by compacting highly dispersed sample with KBr with a ratio of 1 mg:70 mg. Tablets are pressed under the pressure of 10 MPa. Preparation of thus samples gave the opportunity to obtain spectra in the region 4000–400 cm^{-1}. IR spectra were recorded by using a Fourier spectrometer Perkin Elmer Spectrum One (USA).

3. The results and analysis of waste mycelia and chitosan

An important task that was set when the method of producing chitosan, was the choice of optimal conditions of processing mycelial waste with the aim of obtaining a product with a stable chemical composition regardless of the quality of waste mycelia of the fungus Aspergillus Niger.

Samples of chitosan were obtained by changing conditions of the technological process (**Table 2**). In **Table 3** presents the physico-chemical characteristics of produced chitosan.

Table 2

The conditions of the production process

№	W(NaOH), %	Temperature, °C	The duration of the process, hours	The amount extractions of chitosan	The duration of each extraction, min
1	37	110	7	3	30
2	37	110	3	3	30
3	40	110	7	3	10
4	45	110	7	1	100
5	**37**	**110**	**7**	**1**	**80**
6	45	110	7	1	80
7	42	120	7	1,5	100
8	40	110	7	1	100

Table 3

Physico-chemical characteristics of obtained chitosan

№	Ash content, %	The moisture content, %	pH	The degree of swelling, ml/g	WHC, %	The product yield, %	DD, %
1	2,585	75	5,2	0,68	76	3,00	23,0
2	2,585	80	5,2	0,60	80	4,97	67,4
3	2,585	82	5,2	0,54	82	26,25	51,3
4	2,585	88	5,2	0,48	86	12,50	71,6
5	**2,585**	**75**	**5,2**	**0,676**	**72**	**4,35**	**82,0**
6	2,585	75	5,2	0,60	70	3,45	75,0
7	2,585	80	5,2	0,61	82	3,00	78,6
8	2,585	82	5,2	0,546	85	5,80	69,6

Analysis of the data given in **Table 2**, **3** showed that all the samples of chitosan are characterized by a low value of ash content and humidity value is in the range of 75–82 %. The yield of chitosan is not stable, and in our opinion, its value is affected by the process temperature and the concentration of NaOH used for reaction diacetylguanine. DD of chitosan ranges from 23 % to

80 %. In our opinion, the most favorable condition for obtaining chitosan in the production process is number 5 (**Table 2**), which allows to obtain chitosan with high value of degree diacetylguanine – 82 % (**Table 3**).

An important parameter for chitosan, which determines its physico-chemical properties, is DD, which reflects the degree of substitution of acetyl groups on the amino group in the molecule aminopolysaccharide. Classical methods for determining the DD of chitosan in the solution is photometry and conductometry – conductometric direct titration of acids, however, for chitosan, in most cases, using back titration with alkali, as the direct titration of chitosan is longer. The content of chitosan by the photometric method was determined by calibration line, and the corresponding formula calculates the degree diacetylguanine for the studied samples (**Fig. 1**).

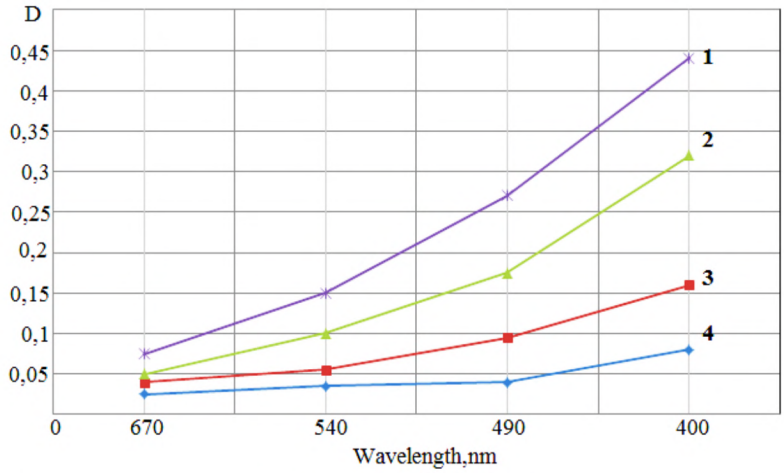

Fig. 1. Absorption spectrum of chitosan solutions. The mass of chitosan in the solution: 1 – 20 mg; 2 – 15 mg; 3 – 10 mg; 4 – 5 mg

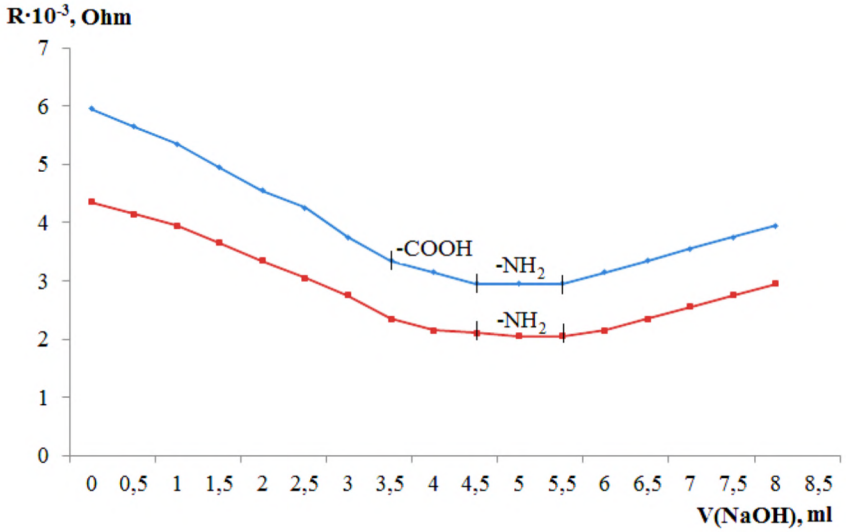

Fig. 2. The curves of conductometric titration of chitin-containing complexes (1) and chitosan (2)

When conductometric titration according to the obtained data, the curves of conductometric titration were built (**Fig. 2**). The calculations were carried out according to prescribed formulas. The results of the calculations are given in **Table 4**.

The degree of conversion of chitin to chitosan in the cell wall of the fungus Aspergillus Niger (sample № 5) was measured by method of IR-spectroscopy.

As can be seen from **Fig. 3,** the spectrum of the chitosan sample obtained in accordance with the flowcharts (if use the solution of NaOH for processing mycelial waste) in the region 1500–1700 cm^{-1}

manifested intense absorption bands characteristic of chitin with highs 1540 cm^{-1} (amide II), 1640 and 1620 cm^{-1} (amide I). The group of absorption bands of medium intensity in the region 1000–1200 cm^{-1} can be assigned to vibrations of C-O bonds in ether groups. An intense absorption band at 1320 cm^{-1} corresponds to the vibration of C-H groups. The broad absorption band from 2800 to 3600 cm^{-1} with a maximum of 3450 cm^{-1} indicates the presence of a valence O-H vibration, excited by hydrogen bonds.

Table 4

The results determine the degree of diacetylguanine (DD) solution of chitosan photometric and conductometric methods

Samples of chitosan	DD, %	
	photometric methods	conductometric methods
1	24,0	25,2
2	67,5	67,3
3	51,9	52,5
4	72,0	73,2
5	**82,0**	**81,8**
6	75,4	76,6
7	77,8	79,0
8	70,1	70,5

According to the literature data, absorption bands in the region 2800–3100 cm^{-1} with maxima 2830 and 2920 cm^{-1} characterize the stretching symmetric and asymmetric vibrations of C-H groups, and a maximum of 3050 cm^{-1} corresponds to the vibration of N-H. In the region 500–900 cm^{-1} observed group of bands that can reliably be attributed to the skeletal vibrations of polysaccharide cycles [14].

When comparing the properties of the obtained samples of chitosan obtained according to the proposed method, it was found that in the IR spectra of all samples of differences practically is not observed. The main difference in the spectra is the decrease in the intensity and halfwidth of the band of C-H stretching vibrations in the region of 2920 cm^{-1} with increasing concentration of alkaline solutions.

Such change, in our opinion, is due to the increase of order and decrease of branching of the polysaccharide molecules. The increase in branching of the molecules leads to the additional formation of hydrogen bonds with an energy that causes additional spreading of the strip. It might increase and the intensity of the band due to Fermi resonance, which is characteristic for oxygen-containing molecules.

Thus, the analysis of the IR spectra of chitosan further confirmed that when the concentration of the alkaline solutions, which are used for processing mycelial waste, there is a tendency to increase of ordering in the structure that might disrupt its fibrous structure and have a negative impact on sorption properties.

As can be seen from **Fig. 3**, the intensity of characteristic bands 1640 and 1620 cm^{-1} increases, which is a proof of the high degree deacetylase complexes. We also made sure that the formation of chitosan into the structure of the complexes when the reaction is carried out, diacetylguanine is characterized by spectral changes in the region 1500–1700 cm^{-1}.

Technological scheme of chitosan production from waste mycelia (**Fig. 4**) was proposed on the basis of the methods of disposal of the waste. A preformed solution of sodium hydroxide with the reagent plant supplied to the mixer 1, which is also in the pipeline, is mycelia biomass. This mixer is heated with saturated steam to a temperature of 115 °C. Concentration of the mixture in the apparatus should be 40 %. The mixing process is carried out for 7 hours. Thereafter, the resulting slurry is fed to a drum vacuum filter 2, where the separation of the alkaline solution and the

precipitate. The pressure in the apparatus is about 0,085 MPa. After filtering the alkaline solution is given for recycling, and obtained sludge is supplied to the mixer 3, where a solution of acetic acid is supplied over pipeline from reagent production unit. Here is extraction of chitosan from the resulting precipitate within a specified time, after which the mixture is fed to the drum vacuum filter 4, where the separation of the precipitate from the filtrate. The resulting precipitate going to disposal and the filtrate is supplied to the mixer 5, where in the pipeline is a sodium hydroxide solution to precipitate the chitosan. After deposition of chitosan, the suspension flows into the sump 6. Clarified water is recycled, and the resulting precipitate was fed to the centrifuge 7 dewatering, after which it is sent to the mixer 8 where it is washed with distilled water to pH close to neutral. Then re-centrifugations had done in the apparatus 9. Drying of the precipitate (chitosan) occurs in a drum dryer 10, and the resulting chitosan enters the container.

The cost of the project will depend on production capacity (tones/year), the selected technological scheme, technological equipment, buildings, communications, etc.

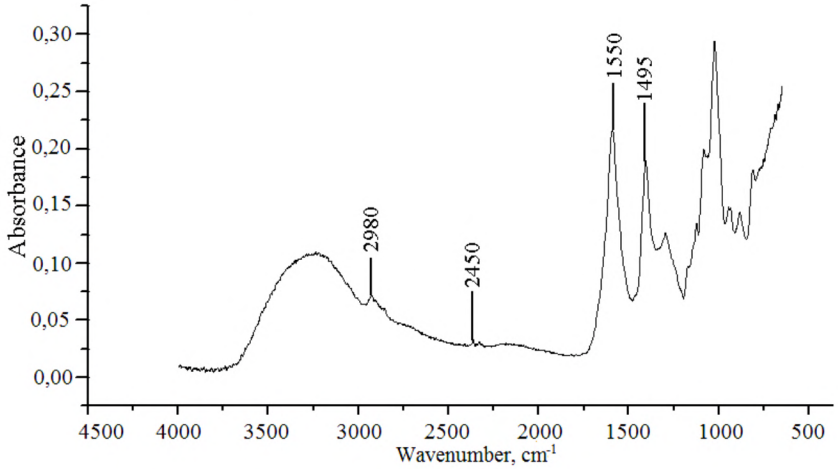

Fig. 3. IR spectra of chitosan obtained by the extraction method (V example)

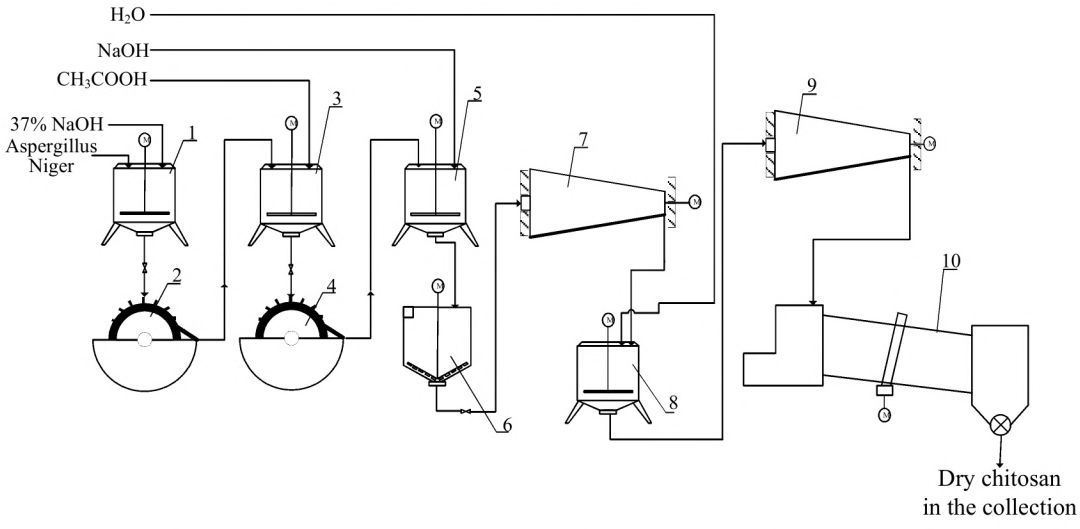

Fig. 4. Technological scheme of production of chitosan from mycelial biomass: 1 – contact apparatus; 2, 4 – drum vacuum filter; 3, 5, 8 – mixer; 6 – sump; 7, 9 –centrifuge; 10 – drum dryer

4. Conclusions

The possibility of recycling and secondary use of large mycelial biomass of the fungus Aspergillus Niger in various consumer goods to minimize its negative impact on the environment is theoretically substantiated and experimentally proved.

Using technology developed by the scheme in practice will recycling mycelial biomass of the fungus Aspergillus Niger, industrial reduce pressure on the environment, ensure improvement of ecological situation in the region and will provide a valuable product – chitosan.

The resulting secondary raw materials – chitosan – can be used for the production of films, membranes and fibers in areas such as medicine, agriculture, veterinary science, biotechnology, food, perfumes and cosmetics, pulp and paper industry.

Energy-saving process of obtaining valuable aminopolysaccharide-chitosan from biomass of fungus is developed Aspergillus Niger – waste of production of citric acid including the process of chemical treatment with alkali solution followed by heat treatment and extraction. The technological scheme of obtaining chitosan from mycelial biomass was created. Analysis of experimental samples showed that the quality is not inferior to chitosan obtained according to the classical scheme, but for DD, even surpasses them.

Studied impact of processes of alkaline processing of mycelial waste on the morphological structure of chitosan is shown that use of alkaline solutions with a high concentration of the product is characterized by a low value of the purity of the product.

It is planned to continue research towards chitosan and zeolite-based sorbents for sewage treatment from ions of heavy metals.

References

[1] Pochanavanich, P., Suntornsuk, W. (2002). Fungal chitosan production and its characterization. Letters in Applied Microbiology, 35 (1), 17–21. doi: 10.1046/j.1472-765x.2002.01118.x

[2] Hutsuliak, H. D. (2004). Ekoloho-ekonomichni problemy v Ukraini i napriamy yikh vyrishennia. Naukovyi visnyk NLTU Ukrainy, 14.3, 207–214.

[3] Zbirnyk naukovykh statei II-i vseukrainskyi zizd ekolohiv z mizhnarodnoiu uchastiu (2009). Vinnytsia: FOP Danyljuk, 603.

[4] Monin, A. S., Shishkov, N. A. (1991). Globalnye ekologicheskie problemy. Nauki o Zemle. Znanie, 136.

[5] Krasavtsev, V. E. (1999). Krill as promising raw material for the production of chitin in Europe. International conference of the Chitin Society, 1–3.

[6] Kennedy, J., Paterson, M. (1994). Chitin Enzymology. Carbohydrate Polymers, 25 (1), 61–61. doi: 10.1016/0144-8617(94)90165-1

[7] Rane, K. D., Hoover, D. G. (1993). Production of Chitosan by fungi. Food Biotechnology, 7 (1), 11–33. doi: 10.1080/08905439309549843

[8] White, S. A., Farina, P. R., Fulton, I. (1979). Production and isolation of chitosan from Mucor rouxii. Appl Environ Microbiol, 38 (2), 323–328.

[9] Nudga, L., Ganicheva, S., Petrova, V., Bystrova, E., Lvova, E., Galkin, A., Petropavlovsky, G. (1997). Sorption of ions of Cr(III) chitin-glycanova complex isolated from mycelium of the fungus Aspergillus Niger, cultured in different conditions. Journal of applied chemistry, 70 (2), 242–246.

[10] Kogan, G., Machoval, E., Chorvatovicova, D., Slovakova, L. (1997). Chitin-glucan complex of Aspergillus Niger and its derivatives: antimutagenic and antiinfective activity. Proc. of the third Asia-Pacific chitin and chitosan Symposium, Taiwan, 372–379.

[11] Starostina, I. V., Ovcharova, I. V. (2012). Obtaining foam slurry of waste containing protein in a high-frequency electromagnetic field. Modern problems of science and education, 6. Available at: https://www.science-education.ru/pdf/2012/6/647.pdf

[12] Kapoor, A., Viraraghavan, T. (1998). Application of immobilizedaspergillus niger, biomass in the removal of heavy metals from an industrial wastewater. Journal of Environmental Science and Health, Part A, 33 (7), 1507–1514. doi: 10.1080/10934529809376801

[13] Zhao, Z. P., Wang, Z., Wang, S. C. (2003). Formation, charged characteristic and BSA adsorption behavior of carboxymethyl chitosan/PES composite MF membrane. Journal of Membrane Science, 217 (1-2), 151–158. doi: 10.1016/s0376-7388(03)00105-4

[14] Tereshina, V., Memorskaya, A., Feofilova, E., Nemtsev, D., Kozlov, V. (1997). Isolation of polysaccharide complexes from mycelial fungi and determination of their deacetylation degree. Microbiology, 66 (1), 70–75.

MATHEMATICAL MODELING OF HORIZONTAL DISPLACEMENT OF ABOVE-GROUND GAS PIPELINES

Denys Kukhtar
Department of Land Management and Cadastre
Ivano-Frankivsk National Technical University of Oil and Gas
15 Carpathian str., Ivano-Frankivsk, Ukraine, 76019
mailden@meta.ua

Abstract

The modern geodetic equipment allows observations as soon as possible, providing high accuracy and productivity. Achieving high accuracy of measurement is impossible without taking into account external factors that create influence on an observation object. Therefore, in order to evaluate an influence of thermal displacement on the results of geodetic monitoring a mathematical model of horizontal displacement of above-ground pipelines was theoretically grounded and built. In this paper we used data of experimental studies on the existing pipelines "Soyuz" and "Urengoy-Pomary-Uzhgorod". Above-ground pipeline was considered as a dynamic system "building-environment". Based on the characteristics of dynamic systems the correlation between the factors of thermal influence and horizontal displacement of the pipeline axis was defined.

Establishing patterns between input factors and output response of the object can be useful not only for geodetic control, but also for their consideration in the design of new objects. It was investigated that the greatest influence on the accuracy of geodetic observations can create dispersion of high-frequency oscillations caused by daily thermal displacement. The magnitude of displacement exceeds actual measurement error.

The article presents the results of calculation of high-frequency oscillations of above-ground gas pipeline.

The result made it possible to substantiate the accuracy and methodology of geodetic observations of the horizontal displacement of pipeline axes taking into account an influence of cyclical thermal displacement.

Research results were recommended for use in practice for enterprises that serve the main gas pipelines and successfully tested by specialists of PJSC "Ukrtransgaz" (Kharkiv, Ukraine) during the technical state control of aerial pipeline crossing in Ukraine and also can be used to form the relevant regulations.

Keywords: above-ground pipeline, thermal displacement, dynamic model, geodetic control.

DOI: 10.21303/2461-4262.2017.00274

1. Introduction

Among the most important scientific and technical problems of the XXI century [1] is the problem of evaluation of the technical condition and the continuation of safe operation of potentially dangerous objects. Among them there are main gas pipelines, most of which worked more than half of their life project. According to the "Rules of technical operation of main gas pipelines" [2], observation complex of above-ground pipelines (**Fig. 1**) includes the works to determine the spatial position of the pipeline axis by geodetic methods. Stress-strain state and evaluation of the bearing capacity of the pipeline are calculated on this basis.

Fig. 1. Aerial "Urengoy-Pomary-Uzhgorod" gas pipeline crossing above Bystrytsia Solotvynska River (Ukraine)

One of the main tasks of geodetic science and practice during the construction of buildings, installation of process equipment and control of the technical condition of the objects in the operation is to establish the required measurement accuracy [3, 4]. The required accuracy is the amount of acceptable error in determining displacement relating to stable point, which is considered as the original. To select the optimal methods of control of above-ground pipeline location and equipment for these works we must fulfill a priori accuracy calculation of geodetic observations.

The results of geodetic observations of deformations of any buildings integrate the patterns of complex interaction of "building-environment." The establishment of such patterns may be useful not only for geodetic control, but also for their consideration in the design of new buildings. "Environment" subsystem includes short-time loads of non-load influence factors. These include: changes in ambient temperature, atmospheric and soil moisture, solar radiation. The processes of changing temperatures and horizontal pipeline displacement have a harmonious character. High-frequency daily oscillations and the main harmonic, which is seasonal, are occurred.

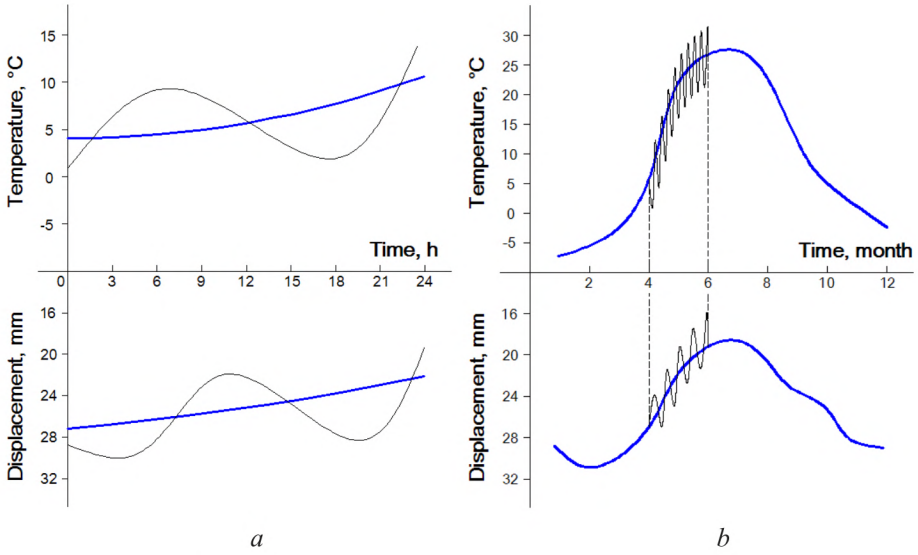

a *b*

Fig. 2. Schematic representation of pipeline displacement under changing temperature conditions: *a* – daily harmonic; *b* – seasonal harmonic

The main influence on the accuracy of observations will create dispersion of high-frequency oscillations that can exceed actual measurement errors.

Ukrainian and foreign regulations [2, 5] lack any requirements for appointment of observational accuracy for planned and high-altitude displacements of above-ground pipelines. Therefore, the line-maintenance services, serving the main gas pipelines, require to determine the plan position of the pipeline axes with maximum accuracy. The problem of observation accuracy justification of high-altitude displacement is discussed in detail in [6].

The aim is to develop a mathematical model of horizontal displacement of above-ground pipeline axis to evaluate the influence of high-frequency oscillations on the results of geodetic observations. To achieve this aim it is necessary to solve the following problems:

1. To set the ratio between input factors (factors of thermal influence) and initial reaction of the building (horizontal displacement of the pipeline) based on the characteristics of dynamic systems.

2. To prove the methodology and accuracy of observation of horizontal displacements of above-ground pipelines in view of high-frequency oscillations caused by thermal influence factors.

2. Materials and methods of research

High accuracy of observations of the horizontal displacement of pipeline axes is impossible without the influence of cyclic thermal displacement. Depending on changes in air temperature, position of the pipeline axis, during the day, varies 10 mm or more [7]. The difference between

the surface temperature of the pipe on the sunny and shady sides creates additional tension in the pipeline [8, 9], the result of which is also a horizontal shift of the pipes.

The author's experimental researches of cyclic thermal displacement on operating pipelines "Soyuz" and "Urengoy-Pomary-Uzhgorod" confirm the effect of ambient temperature on the pipeline. Period of maximum amplitude of daily changes in air temperature was chosen. In the foothills of the Carpathian Mountains (Western Ukraine) this period is in June. During observations were recorded: air temperature t, the temperature difference of solar and shadow sides of the pipe ΔT within the reference section and horizontal displacement S. Diameter of investigated area – 1420 mm. The temperature of the pipe was determined using a portable pyrometer with an accuracy within 0,1 °C. Within 13 hours there were 41 series of observations. The temperature was ranged from 13 to 37 °C.

Graphic results in [10] clearly trace the pattern of pipeline displacement during the observation period. The greatest value of thermal displacement of pipeline axis corresponds to the period of maximal air temperature, confirming the lack of inertial delay of building reaction.

A similar trend is observed in [11], where the largest displacement amplitude of the bridge corresponds to the period of maximum cooling of the metal from which it is made.

Based on the correlation analysis [12] it is found that 62 % of the daily thermal displacement of above-ground pipeline depends on the air temperature and the uneven side heat of the pipe by solar rays.

3. Development of a dynamic model of horizontal displacement of above-ground pipeline

3. 1. Model development

The theory of dynamical systems, arising from automatic control theory, is successfully used in various fields of science and technology, using mathematical modeling techniques to solve the tasks. One of the advantages of mathematical models of dynamic systems is taking into account the inertial delay of the building when displaying natural properties of convert of the input data into the system reaction [13].

Let's consider a system of "building-environment" as a dynamic system. Previously it was found that the main factors affecting the horizontal displacement of the pipeline are air temperature and uneven side heat of the pipe by solar rays. These factors are input factors of the dynamic system. The responses of the system, or output variables, are pipeline displacement.

The dynamic model of deformation has three main components [14]. The first component reflects the dynamic properties of the system "building-environment"; the second – the fate of the movements that occur under the influence of the main input actions; the third component – includes displacement arising as a result of unaccounted factors (noise component).

Differential and recurrence equations establish a correspondence between the input and output variables. Let's introduce the designation of these processes:

S_k – horizontal displacement of the pipeline;

t_k – air temperature;

ΔT_k – pipe surface temperature gradient between sunny and shady sides;

k – number of series of observations.

It is known that when inertial delay of the building response doesn't exceed 1/4 of the basic harmonic for modeling of the investigated process should be used the first order differential equations [13]. Above-ground pipeline is an open metal structure. Therefore, the processes of heat transfer in the system "building-environment" are no time delay.

Taking into account designation and the fact of the absence of inertial delay, let's write the model of horizontal displacement of the pipeline S_k in the recurrent form based on first order equations [13]

$$S_k = \varphi S_{k-1} + \beta_1 t_k + \beta_2 \Delta T_k, \quad (1)$$

where φ – dynamic factor, β_1, β_2 – factors reflecting the impact of input factors on pipeline displacement.

Initial data for model development:

– the results of observations of the horizontal displacement of the reference section S_k of aerial "Urengoy-Pomary-Uzhgorod" gas pipeline crossing (pipe diameter 1420 mm) made using geodetic methods;

– the results of measurements of air temperature t_k;

– the results of determination of the temperature difference between the surface of the pipeline on the sunny and shady sides within the reference section.

Methods of observations and the results are detailed written in [12]. Reference section was selected for modeling, because values of its displacement had the largest amplitude. The observations were carried out in the period of maximum change in temperature during the day (June).

An evaluation of model parameters describing displacement of one point (reference section of the pipeline) should start with the expectation approximation. Conditional expectation of equation (1) is:

$$M\left\{S_k / S_{k-1}, t_k, \Delta T_k\right\} = \hat{S}_{k/k-1} = \hat{\varphi} S_{k-1} + \hat{\beta}_1 t_k + \hat{\beta}_2 \Delta T_k. \quad (2)$$

Model development is beginning to evaluate the parameters φ, β_1, β_2 on the basis of daily observations of the input t_k, ΔT_k and output S_k. To do this, let's find the minimum of the function [15]

$$F(\varphi, \beta_1, \beta_2) = \sum_{k=2}^{N} (S_k - \hat{S}_{k/k-1})^2, \quad (3)$$

$$\left.\begin{aligned} \frac{\partial F}{\partial \varphi} &= -2\sum_{k=2}^{N} (S_k - \hat{\varphi} S_{k-1} - \hat{\beta}_1 t_k - \hat{\beta}_2 \Delta T_k) \cdot S_{k-1} = 0, \\ \frac{\partial F}{\partial \beta_1} &= -2\sum_{k=2}^{N} (S_k - \hat{\varphi} S_{k-1} - \hat{\beta}_1 t_k - \hat{\beta}_2 \Delta T_k) \cdot t_k = 0, \\ \frac{\partial F}{\partial \beta_2} &= -2\sum_{k=2}^{N} (S_k - \hat{\varphi} S_{k-1} - \hat{\beta}_1 t_k - \hat{\beta}_2 \Delta T_k) \cdot \Delta T_k = 0, \end{aligned}\right\} \quad (4)$$

This gives the system of normal equations to calculate parameters φ, β_1, β_2:

$$\begin{cases} \hat{\varphi}\sum_{k=2}^{N} S_{k-1}^2 + \hat{\beta}_1 \sum_{k=1}^{N} S_{k-1} t_k + \hat{\beta}_2 \sum_{k=1}^{N} S_{k-1} \Delta T_k - \sum_{k=1}^{N} S_k S_{k-1} = 0, \\ \hat{\varphi}\sum_{k=2}^{N} S_{k-1} t_k + \hat{\beta}_1 \sum_{k=1}^{N} t_k^2 + \hat{\beta}_2 \sum_{k=1}^{N} t_k \Delta T_k - \sum_{k=1}^{N} S_k t_k = 0, \\ \hat{\varphi}\sum_{k=2}^{N} S_{k-1} \Delta T_k + \hat{\beta}_1 \sum_{k=1}^{N} t_k \Delta T_k + \hat{\beta}_2 \sum_{k=1}^{N} \Delta T_k^2 - \sum_{k=1}^{N} S_k \Delta T_k = 0. \end{cases} \quad (5)$$

Evaluation of unknown parameters in this system of normal equations should perform according to centered input and output values. This does not alter the structure of the system of normal equations and replace S_k, t_k, ΔT_k by their centered values:

$$\overset{o}{S}_k = S_k - \overline{S}, \ \overset{o}{t}_k = t_k - \overline{t}, \ \overset{o}{\Delta T}_k = \Delta T_k - \Delta \overline{T}, \quad (6)$$

where $\overline{S}, \overline{t}, \Delta \overline{T}$ – arithmetic average. Solving the system of equations, and substituting the unknown parameters in (1), we obtain short-period nature model of horizontal displacement process of the pipeline:

$$S_k = 0.04 S_{k-1} + 0.38 t_k + 0.15 \Delta T_k. \quad (7)$$

The graphs of pipeline axis displacements derived from empirical data and modeling results are presented in **Fig. 3**.

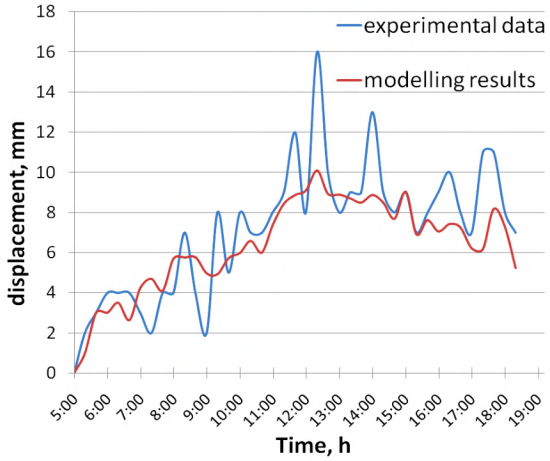

Fig. 3. The results of modeling short-period horizontal displacement of above-ground pipeline

After completing the accuracy evaluation of the calculated parameters, the following values are obtained: $m_{\varphi} = 0.01$; $m_{\beta 1} = 0.01$; $m_{\beta 2} = 0.02$.

3. 2. Evaluation of the influence of high-frequency oscillations on the accuracy of the horizontal displacement of the pipeline

In order to correct organization of geodetic observations we must ensure the conditions:

$$m_{xy0} \le m_{xy}, \tag{8}$$

where m_{xy} – mean square error of geodetic observations of the planned position of the pipeline axis; m_{xy0} – mean square error, which describes the range of possible high-frequency oscillations.

In [13], based on the tools of frequency characteristics of dynamic systems, an equation is obtained that establishes a connection between the average square error of input and output for dynamic systems. Let's write the equation due to our case (two input parameters):

$$m_{xy0} = \sqrt{\frac{\beta_1^2 m_t^2 + \beta_2^2 m_{\Delta T}^2}{1 + 2\varphi \cos \omega\tau + \varphi^2}}, \tag{9}$$

where the parameters φ, β_1, β_2 are obtained according to modeling results (7); m_t, $m_{\Delta T}$ – mean square errors of amplitude changes in air temperature and surface temperature gradient of the pipe; $\omega\tau = \frac{\pi}{12} \cdot 0.3 = 4.5°$ because a half of high-frequency daily fluctuation harmonic is used for prediction (12 hours of observations); sampling interval is 20 minutes (0.333 hours) – time between observation cycles.

Errors m_t, $m_{\Delta T}$ are calculated using the formulas

$$m_t = \sqrt{\sigma_t^2 + m_{tcalc}^2}, \quad m_{\Delta T} = \sqrt{\sigma_{\Delta T}^2 + m_{\Delta Tcalc}^2}, \tag{10}$$

where $\sigma_t^2, \sigma_{\Delta T}^2$ – dispersions of temperature fluctuations; $m_{tcalc} = \pm 1\,°C$ – measurement error of air temperature; $m_{\Delta Tcalc} = \pm 0.1°C$ – measurement error of surface temperature of the pipe using a portable pyrometer

Substituting in the formula (9) the parameters of the model (7), and the calculated errors m_t and $m_{\Delta T}$, as a result, we get:

$$m_{xy0} = \sqrt{\frac{\beta_1^2 m_t^2 + \beta_2^2 m_{\Delta T}^2}{1 + 2\varphi \cos \omega\tau + \varphi^2}} = \sqrt{\frac{0.38^2 \cdot 42.5 + 0.15^2 \cdot 1.11}{1 + 2 \cdot 0.04 \cdot \cos 4.5° + 0.04^2}} = \sqrt{\frac{6.16}{1.081}} = 2.4 \text{ mm}. \tag{11}$$

This result indicates that the horizontal displacement of the pipeline axis, the value of which is determined in the geodetic control, is exposed to high-frequency temperature fluctuations.

Where there is a need to assign the highest possible accuracy of geodetic observations according to planned displacement of the pipeline axis, which is characterized by the mean square error m_{xy}, enforcement of conditions $m_{xy}>m_{xy0}=2.4$ mm will allow neglect dispersion of high-frequency oscillations, which are caused by temperature deformations.

4. Discussion of research results

Beam above-ground gas pipelines (**Fig. 1**) are the most common in Ukraine. Therefore, experimental research was carried out on buildings of this type. The results are typical for aerial crossing of 1420 mm beam above-ground gas pipelines.

We believe that the correct method during the geodetic control of the position of the pipeline axis is to carry observations in the same periods of the day. High-frequency oscillations will be fixed at the same level of their amplitude, or in one of the culminations (period of maximum cooling or heating of the pipes).

However, it can choose the method of random selection of observation points in relation to high-frequency oscillations. It must ensure the conditions (8) – observation accuracy of horizontal displacement of above-ground pipeline will not exceed the mean square error of high-frequency oscillations. Therefore, it is recommended that the observation accuracy of horizontal displacement of above-ground pipeline axes is not higher than 2.4 mm.

Appointment of accuracy on this principle can be performed only if the value of the error $m_{xy}=2.4$ mm does not create a significant influence on the evaluation of the object.

It should be noted that the value of the mean square error of high-frequency oscillations of above-ground gas pipelines is not constant. It will vary depending on the air temperature conditions for certain areas, and the amount of solar radiation, which depends on the geographical latitude.

5. Conclusions

1. Selection justification of mathematical model of horizontal displacement of above-ground pipeline axis is done.

2. Value $m_{xy0}=2.4$ mm, which describes the range of possible high-frequency oscillations of beam above-ground pipelines (D=1420 mm) caused by daily thermal displacement, is calculated.

3. An accuracy of geodetic observations of the horizontal displacement of the pipeline axes is proved taking into account the impact of cyclical thermal displacement.

4. Research results are recommended for use in practice for enterprises that serve the main gas pipelines and successfully tested during the technical state control of aerial pipeline crossing in Ukraine

We believe that further studies related to the implementation and development of automated systems for monitoring oil and gas facilities are promising.

References

[1] Makhutov, N. A., Gadenin, M. M., Chernyavskiy, A. O., Shatov, M. M. (2012). Analysis of the risk of failures in the functioning of potentially dangerous objects. Problems of risk analysis, 9 (3), 8–21.

[2] SOU 49.5-30019801-115:2014 Pravyla tekhnichnoi ekspluatatsii mahistralnykh gazoprovodiv (2014). Kyiv: Ukrtransgaz, 67.

[3] Huliaiev, Yu. (2007). Analiz podkhodov k obosnovaniyu tochnosti geodezicheskikh nabliudenii za deformatsionnyimi protsessami. Geodeziia i kartografiia, 8, 11–15.

[4] Chybiriakov, V. K., Starovierov, V. S., Nikitenko, K. O. (2011). Zahalnyi pidkhid do modeliuvannia tochnosti geodezichnikh robit pry provedenni monitorinhu liniinykh sporud. Inzhenerna geodeziia, 57, 68–80.

[5] VSN 39-1.10-003-2000 Polozhenie po tekhnicheskomu obsledovaniiu i kontroliu za sostoianiem nadzemnykh perekhodov mahistralnykh gazoprovodov (2000). Moscow: Gazprom, 50.

[6] Trevoho, I. S., Ilkiv, Ye. Yu., Kukhtar, D. V. (2013). Tochnost geodezicheskikh rabot dlia opredeleniia vertikalnikh smeshchenii opor deformirovannykh uchastkov nadzemnykh truboprovodov. Geodeziia i kartografiia, 7, 5–7.

[7] Subbotin, I. Ye. (1987). Inzhenerno-geodezicheskie raboty pri proektirovanii, stroitelstve i ekspluatatsii magistralnykh neftegazoprovodov. Moscow: Nedra, 140.

[8] Oliinyk, A. P., Ivasiv, O. Ya. (2005). Matematychne modeliuvannia teplofizychnykh protsesiv v truboprovodakh z urakhuvanniam neodnoridnosti materialu pry konvektyvno-promenevomu teploobmini. Shtuchnyi intelekt, 3, 194–200.

[9] Mandryk, O., Olijnyk, A., Moroz, A. (2016). Application Of Mathematical Methods For Condition Monitoring Of Oil And Gas Facilities. Journal of Applied Computer Science & Mathematics, 10 (1), 42–45. doi: 10.4316/jacsm.201601007

[10] Trevoho, I. S., Ilkiv, Ye. Yu., Kukhtar, D. V. (2011). Metodyka kontroliu temperaturnykh deformatsii nadzemnykh perekhodiv mahistralnykh hazoprovodiv. Visnyk geodezii ta kartografii, 6, 6–9.

[11] Herasymov, V., Lobazov, V., Reznik, B. (2010). Kontseptsyia geodezicheskoho monitorinha deformatsyonnykh protsessov v usloviiakh zapoliaria. Geoprofi, 1, 17–21.

[12] Trevoho, I. S., Ilkiv, Ye. Yu., Kukhtar, D. V. (2013). Doslidzhennia temperaturnykh deformatsii nadzemnykh truboprovodiv metodom koreliatsiinoho analizu. Visnyk geodezii ta kartografii, 2, 12–15.

[13] Huliaiev, Yu. (2008). Prohnozirovaniie deformatsyi sooruzhenii na osnove rezultatov geodezicheskikh nabliudenii. Novosibirsk: SHGA, 256.

[14] Rekomendatsyi po prohnozyrovaniiu deformatsyi sooruzhenii hydrouzlov na osnove rezultatov geodezicheskikh nabliudenyi (1991). Leningrad: VNIIG, 57.

[15] Fan, H. (2010). Theory of Errors and Least Squares Adjustment. Stockholm: Royal Institute of Technology, 226.

CONSTRUCTION AND RESEARCH OF FULL BALANCE ENERGY OF VARIATIONAL PROBLEM MOTION SURFACE AND GROUNDWATER FLOWS

Petro Venherskyi
Department of Applied Mathematics and Informatics
Franko National University of Lviv
1 Universytetska str., Lviv, Ukraine, 79001
petro.vengersky@gmail.com

Abstract

Based on the laws of conservation of mass and momentum the basic equations of motion with unknown quantities velocity and piezometric pressure are written. These equations are supplemented with boundary and initial conditions describing the motion of compatible flows. Based on the laws of motion continuum, received conditions contact on the common border interaction of surface and groundwater flows. Variational problems formulated compatible flow. Energy norms of basic components of variational problem are analyzed. Correctness of constructing variational problem arising from construction of the energy system of equations that allow to investigate properties of the problem solution, its uniqueness, stability, dependence on initial data and more. Energy equation of motion of surface and groundwater flows are derived and investigated. It is shown that the total energy compatible flow depends on sources that are located inside the domain or on its border.

Keywords: surface flow, groundwater flow, watershed, incompressible fluid, velocity fluid and hydrostatic and piezometric pressure, energy equation, bilinear form, Initial and boundary conditions, interface conditions, coupling flow.

DOI: 10.21303/2461-4262.2017.00270

1. Introduction

An important role in studying the water cycle plays hydrological system. In general, research integrity of the system, taking into account all impacts, are complex and not always feasible problem for the study because only investigated some of the area involved in the water cycle [1–3] Highly likely part of the territory may be a watershed area (**Fig. 1**), which is characterized by similar climatic conditions and is influenced by such factors that affect the water movement.

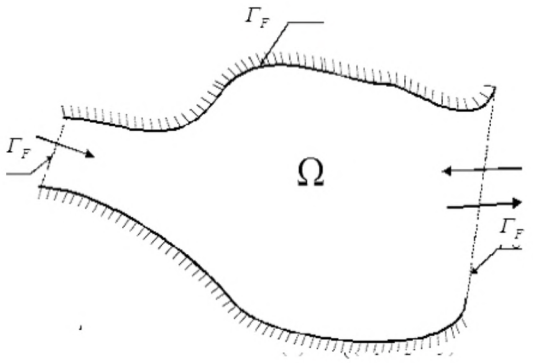

Fig. 1. Two-dimensional projection watershed on the plane X_1OX_2

At the watershed may be an interaction between flow and located above and below water-bearing layers. Models of different dimensions are used in each layer to describe the water movement and their solutions are connected by boundary conditions [4–6].

We select in solid medium (liquid) moving surface layer $F(t) \in R^3$ (**Fig. 2**) of such a structure

$$\Omega_F(t) := \left\{(x_1, x_2, x_3) \in R^3, \quad \eta(x) < x_3 < \nu(x,t) \quad \forall x = (x_1, x_2) \in \Omega(t)\right\}. \tag{1}$$

Let's denote projection of its lower

$$\Omega(t):=\left\{(x_1,x_2,x_3)\in R^3 \;\middle|\; x_3=\eta(x),\ \forall x=(x_1,x_2)\in\Omega(t)\right\} \tag{2}$$

and upper

$$\Lambda_F(t):=\left\{(x_1,x_2,x_3)\in R^3 \;\middle|\; x_3=\nu(x,t)\ \ \forall x=(x_1,x_2)\in\Omega(t)\right\} \tag{3}$$

bases on the plane $0x_1x_2$. The rest of the surface layer

$$\Gamma_F(t):=\left\{(x_1,x_2,x_3)\in R^3,\ \ \eta(x)<x_3<\nu(x,t)\ \ \forall x=(x_1,x_2)\in\Omega(t)\right\} \tag{4}$$

will be called the lateral surface layer $F(t)$.

Similarly denote part of fluid that moves in the soil, so

$$\Omega_P(t):=\left\{(x_1,x_2,x_3)\in R^3,\ \ h(x)<x_3<\eta(x),\ \ \forall x=(x_1,x_2)\in\Omega(t)\right\} \tag{5}$$

the projection of the lower part will be written as

$$\Lambda_P(t):=\left\{(x_1,x_2,x_3)\in R^3 \;\middle|\; x_3=h(x),\ \forall x=(x_1,x_2)\in\Omega(t)\right\}. \tag{6}$$

Then, a layer of ground water

$$\Gamma_P(t):=\left\{(x_1,x_2,x_3)\in R^3,\ \ h(x)<x_3<\eta(x)\ \ \forall x\in\Gamma_P(t)\right\}. \tag{7}$$

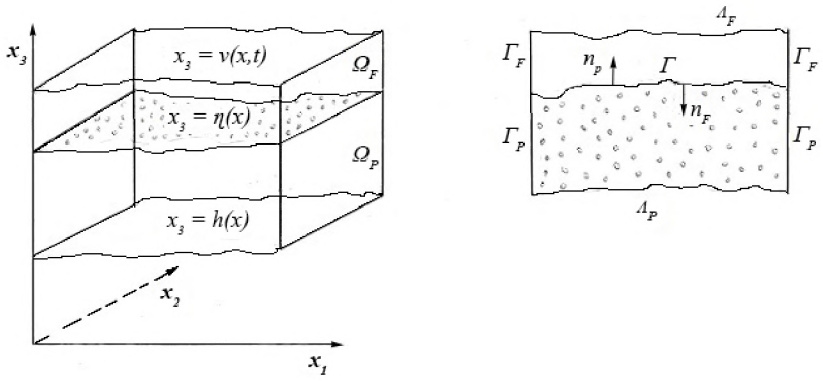

Fig. 2. General view of the model of flows and their cross-section

2. Materials and Methods

2. 1. Initial boundary value problem of interaction of water flows

We formulate initial boundary problem of motion of surface and groundwater flows on the surface watershed considering boundary and initial conditions [7–9].

Find unknown quantities $\{u,p,\varphi\}$ *such that satisfy the following system of equations:*

$$\frac{\partial}{\partial t}(\rho u_i)+\sum_{k=1}^{3}\frac{\partial}{\partial x_k}(\rho\, u_i u_k)-\rho\, f_i-\sum_{k=1}^{3}\frac{\partial\sigma_{ik}}{\partial x_k}=0, \tag{8}$$

$$\sigma_{ij}=-p_F\delta_{ij}+\tau_{ij},$$

$$\tau_{ij}=2\mu\, e_{ij}, i,j=1,2,3,$$

$$e_{ij}=\frac{1}{2}\left(\frac{\partial u_i}{\partial x_j}+\frac{\partial u_j}{\partial x_i}\right),$$

$$\frac{\partial \rho}{\partial t}+\sum_{k=1}^{3}\frac{\partial\left(\rho\ u_k\right)}{\partial x_k}=0,\ \text{in}\quad \Omega_F\times(0,T], \tag{9}$$

$$m\frac{\partial \varphi}{\partial t}=\sum_{j=1}^{3}\frac{\partial}{\partial x_j}\left(k\frac{\partial \varphi}{\partial x_j}\right)+\varepsilon\ \text{in}\quad \Omega_P\times(0;T], \tag{10}$$

where $\{u_i(x,t)\}^3_{i=1}$ and $p_{F_3}=p_F(x,t)$ – sought velocity vector of fluid and hydrostatic pressure, respectively; $F=\left\{g\ f_i(x)\right\}_{i=1}^3$ – mass forces; $\rho=\rho(x,t)>0$ – density of the mass water flow; $\mu=\mu(x)>0$ – viscosity coefficient; $\left\{e_{ij}\right\}_{i,j=1}^3$, $\left\{\sigma_{ij}\right\}_{i,j=1}^3$ – tensors of velocities of deformation and stress of the liquid at the point x in time t; δ_{ij} – Kronecker symbol; $k=k(x,t)$ – filtration coefficient; $m=m(x,t)$ – coefficient of specific water loss; $\varepsilon=\varepsilon(x,t)$ – known function of sources of water influx;

$$\varphi=x_3+\frac{p_p}{\rho g} \tag{11}$$

piezometric pressure;

$$q=-k\nabla\varphi \tag{12}$$

flow (flow separation); $\upsilon=\upsilon(x,t)$ – velocity vector of fluid in the ground; $\upsilon=\frac{q}{\omega}$, ω – volume porosity; $\overrightarrow{n_F}=-\overrightarrow{n_P}$ – vectors normal to the boundary area Ω_F and Ω_P in accordance;

$$\overline{\Omega}=\overline{\Omega_F}\cup\overline{\Omega_P},\Omega_F\cap\Omega_P=\{\varnothing\},\overline{\Omega_F}\cap\overline{\Omega_P}=\Gamma,$$

$$\partial\Omega_F=\Gamma_F\cup\Lambda_F\cup\Gamma;\partial\Omega_P=\Gamma_P\cup\Lambda_P\cup\Gamma.$$

Boundary conditions [10, 11]:

$$\vec{u}_i=0\ \text{ on }\ \Gamma_F,\ i=1,2,3, \tag{13}$$

$$\sigma_{n\tau}=\overline{\sigma},\ \text{on}\ \Lambda_F, \tag{14}$$

$$u_3+R=\frac{\partial \nu}{\partial t}+u_1^0\frac{\partial \nu}{\partial x_1}+u_2^0\frac{\partial \nu}{\partial x_2}\ \text{ in }\ \Omega_F\times(0,\ T], \tag{15}$$

where R – velocity of falling rain drops, u_1^0, u_2^0 – horizontal components of velocity on the free surface $\nu(x.t)$ (Λ_F);

$$\upsilon_{\bullet}\ n_p=\overline{\upsilon}\quad\text{on}\quad\Gamma_P; \tag{16}$$

$$\upsilon_1=\upsilon_2=0\quad\text{on}\quad\Lambda_P, \tag{17}$$

$$\upsilon_3=-I\ \text{ on }\quad\Lambda_P, \tag{18}$$

where I – known function that describes the velocity of fluid flow through the surface Λ_P.

Initial conditions:

$$\begin{aligned} u|_{t=0}&=u_0,\\ p|_{t=0}&=p_0,\ \text{in}\ \Omega.\\ \varphi|_{t=0}&=\varphi_0, \end{aligned} \tag{19}$$

Contact flow conditions on a common boundary Γ [4–6, 8]:

$$\sigma_{nn}(u,p_F)=p_p,$$

$$\sigma_{\tau n}=0, \tag{20}$$

$$u_n=-\upsilon_n.$$

2. 2. Variational formulation of the problem of interaction of water flows

We introduce the following bilinear forms:

$$M_v(r;w,q)=\int_v\sum_{i=1}^{3} rw_iq_ids,\ N_v(w;u,q)=\int_v\sum_{k=1}^{3}\sum_{i=1}^{3}\rho w_k\frac{\partial u_i}{\partial x_k}q_ids,$$

$$C_v(w,q)=\int_v 2\mu\ e(w):e(q)ds,$$

$$A_v(w,q)=-\int_v wdivqds,\quad Y_v(w,q)=-\int_v wq_nd\gamma,\quad B_v(p,w)=-\int_v\sum_{i=1}^{3} p.\nabla wds.$$

Introduce spaces:

$$H_F:=\left\{\xi\in(H^1(\Omega_F))^3\mid\xi=0\ \ \text{on}\ \ \Gamma\right\},$$

$$H_p:=\left\{\psi\in H^1(\Omega_p)\mid\psi=0\ \ \text{on}\ \ \Gamma\right\},\quad W:=H_F\times H_P,\ \Im_j:W\to R,j=\overline{1,3},$$

$$\left\langle\Im_1,\xi\right\rangle=\sum_{i=1}^{3}\int_{\Omega_F}\rho f_i\xi_ids+\int_{\Lambda_F}(\xi_np_a+\xi_\tau\cdot\hat{\sigma})d\gamma,$$

$$\left\langle\Im_2,\theta\right\rangle=-\int_{\partial\Lambda_F}u_n^0\theta d\gamma,\ \left\langle\Im_3,\psi\right\rangle=\int_{\Omega_P}\frac{\varepsilon(x,t)\rho g\psi}{\omega}dp-\int_{\partial\Lambda_P}\overline{\upsilon}\psi\rho gd\gamma.$$

Let's denote

$$\tilde{\psi}=\psi\rho g,\quad\tilde{m}=\frac{m}{\omega},$$

Then, let's write the following variational problem [1–2, 10, 11]:

$$\begin{gathered}\text{Find}\left\{u,p,\varphi\right\}\in V\times Q\times W,\\ M_{\Omega_F}(\rho;u',\xi)+N_{\Omega_F}(u;u,\xi)+A_{\Omega_F}(p,\xi)+C_{\Omega_F}(u,\xi)+\\ +Y_\Gamma(u,\xi)=\left\langle\Im_1,\xi\right\rangle,\forall\xi\in V,\end{gathered}\tag{21}$$

$$B_{\Omega_F}(u,\theta)+Y_\Gamma(\theta,u)=\left\langle\Im_2,\theta\right\rangle,\forall\theta\in Q,\tag{22}$$

$$M_{\Omega_p}(\tilde{m};\varphi',\tilde{\psi})+A_{\Omega_p}(\tilde{\psi},\upsilon)+Y_\Gamma(\tilde{\psi},\upsilon)=\left\langle\Im_3,\tilde{\psi}\right\rangle,\forall\psi\in W\tag{23}$$

with initial conditions

$$M_{\Omega_F}(u'(0)-u_0,\xi)=0,\tag{24}$$

$$B_{\Omega_F}(p(0)-p_0,\theta)=0;\tag{25}$$

$$M_{\Omega_p}(\varphi'(0)-\varphi_0,\tilde{\psi})=0.\tag{26}$$

Let's calculate, considering initial conditions (24)–(26) and boundary conditions (13)–(18), values of variables u and p with relations (21) and (22). Then on the basis of coupling flow conditions (interface conditions) (20) and boundary condition (11) the value of the variable φ is calculated from (23).

2. 3. The properties of the components and norms of variational problem interaction water flows.

It should be noted that trilinear form

$$N_v(w;u,q)=\int_v \sum_{k=1}^{3}\sum_{i=1}^{3} \rho w_k \frac{\partial u_i}{\partial x_k} q_i ds, \tag{27}$$

is continuous and bilinear form

$$C_v(w,q)=\int_v 2\mu e(w):e(q)\,ds \tag{28}$$

continuous and symmetrical.

It is a scalar product in the space H_F and creates a norm

$$\left\|w\right\|_{H_F}=\sqrt{C_v(w,w)}, \forall w \in H_F.$$

Then, let's write the scalar function φ bilinear forms

$$D_v(\varphi,\psi)=\int_v k(x,t)\nabla\varphi\cdot\nabla\psi\ dp. \tag{29}$$

which is continuous and integral in the space of admissible functions H_p. It is also symmetrical and forms a semi-norm

$$\left|\varphi\right|_{H_p}=\sqrt{D_v(\varphi,\varphi)}, \forall\varphi \in H^1(\Omega_p). \tag{30}$$

Let's consider the properties of bilinear forms

$$A_v(w,q)=\int_v divwdivqds. \tag{31}$$

In space H_F, it is continuous, integral and symmetrical, and also forms the norm

$$\left|\left|\left|q\right|\right|\right|_{H_F}=\sqrt{A_v(q,q)}, \forall q \in H_F. \tag{32}$$

3. Results of research

3. 1. Equation balance energy of coupling water flow

Let's write variational equations for momentum

$$\begin{aligned} &M_{\Omega_F}(\rho;u',u)+N_{\Omega_F}(u;u,u)+C_{\Omega_F}(\mu;u,u)= \\ &=\left\langle\varphi_1,u\right\rangle-Y_{\Omega_F}(p,u)-A_{\Omega_F}(p,u). \end{aligned} \tag{33}$$

Let's write left side of the equation:

$$\begin{aligned} &\int_{\Omega_F}\sum_{i=1}^{3}\rho_i u_i' u_i ds+\int_{\Omega_F}\sum_{k=1}^{3}\sum_{i=1}^{3}\rho u_k\frac{\partial u_i}{\partial x_k}u_i ds-\int_{\Omega_F}\sum_{k=1}^{3}\frac{\partial\sigma_{ik}}{\partial x_k}u_k ds=\int_{\Omega_F}\sum_{i=1}^{3}\rho_i u_i' u_i ds+ \\ &+\int_{\Omega_F}\sum_{k=1}^{3}\sum_{i=1}^{3}\rho u_k\frac{\partial u_i}{\partial x_k}u_i ds+\int_{\Omega_F}\sum_{k=1}^{3}\sigma_{ik}\frac{\partial u_i}{\partial x_k}ds-\int_{\partial\Omega_F}u_i\sum_{k=1}^{3}\sigma_{ik}n_{F_k}d\gamma. \end{aligned} \tag{34}$$

Given that

$$\sigma_{ik} = -p\delta_{ik} + 2\mu e_{ik}$$

rewrite (34) in the following form

$$\int_{\Omega_F} \sum_{i=1}^{3} \rho_i u_i' u_i ds + \int_{\Omega_F} \sum_{k=1}^{3}\sum_{i=1}^{3} \rho u_k \frac{\partial u_i}{\partial x_k} u_i ds - \int_{\partial\Omega_F} p\ u_n d\gamma +$$
$$+ \int_{\Omega_F} u\ \nabla p ds + \int_{\Omega_F} 2\mu\, e(u) : e(u)\, ds - \int_{\partial\Omega_F} u_i \sum_{k=1}^{3} \sigma_{ik} n_{F_k} d\gamma. \quad (35)$$

Let's write left side of variational equations for the law of conservation of mass flow

$$\int_{\Gamma} u.n_F p d\gamma - \int_{\Omega_F} u.\nabla p ds = 0. \quad (36)$$

Substituting (23) in place of ψ the function φ will be

$$\int_{\Omega_p} m \frac{\partial \varphi}{\partial t} \varphi \frac{\rho g}{\omega} dp - \int_{\partial\Omega_p} k \frac{\partial \varphi}{\partial n_p} \varphi d\gamma +$$
$$+ \int_{\Omega_p} \sum_{j=1}^{3} m \frac{\partial \varphi}{\partial x_j} \frac{\partial \varphi}{\partial x_j} dp - \int_{\Omega_p} \varepsilon \varphi dp = 0. \quad (37)$$

Let's multiply (37) on the expression $\frac{\rho g}{\omega}$, then

$$\frac{1}{2} \int_{\Omega_p} m \frac{\partial \varphi^2}{\partial t} \frac{\rho g}{\omega} dp - \int_{\partial\Omega_p} \sum_{j=1}^{3} \frac{k(x,t)}{\omega} \frac{\partial \varphi}{\partial \bar{n}} \varphi\ \rho g d\gamma +$$
$$+ \int_{\Omega_p} \sum_{j=1}^{3} \frac{k(x,t)}{\omega} \frac{\partial \varphi}{\partial x_j} \frac{\partial \varphi}{\partial x_j}\ \rho g\ dp - \int_{\Omega_p} \frac{\rho g}{\omega} \varepsilon \varphi dp = 0. \quad (38)$$

Let's estimate the term in (38) on the boundary Ω_p

$$-\int_{\partial\Omega_p} \frac{k}{\omega} \frac{\partial \varphi}{\partial n_p} \varphi \rho g d\gamma = -\int_{\Gamma_p} \frac{k}{\omega} \frac{\partial \varphi}{\partial n_p} \varphi \rho g d\gamma - \int_{\Gamma} \frac{k}{\omega} \frac{\partial \varphi}{\partial n_p} \varphi \rho g d\gamma - \int_{\Lambda_p} \frac{k}{\omega} \frac{\partial \varphi}{\partial n_p} \varphi \rho g d\gamma =$$
$$= -\int_{\Gamma} k \varphi \rho g \frac{\nabla \varphi n_p}{\omega} d\gamma - \int_{\Gamma_p} k \frac{\nabla \varphi n_p}{\omega} \varphi \rho g d\gamma =$$
$$= \int_{\Gamma} p_p \upsilon_{n_p} d\gamma - \int_{\Gamma_p} \bar{\upsilon}\ \varphi \rho g d\gamma. \quad (39)$$

Simplifying a term on the border Ω_F in the form (35), we obtain

$$-\int_{\partial\Omega_F} u_i \sum_{k=1}^{3} \sigma_{ik} n_{F_k} d\gamma = -\int_{\Lambda_F} (u_n \sigma_{nn} + u_\tau \sigma_{n\tau}) d\gamma -$$
$$-\int_{\Gamma_F} (u_n \sigma_{nn} + u_\tau \sigma_{n\tau}) d\gamma - \int_{\Gamma} (u_n \sigma_{nn} + u_\tau \sigma_{n\tau}) d\gamma. \quad (40)$$

Adding expressions (35), (39), (40), after simple transformations, we have

$$\int_{\Omega_F}\sum_{i=1}^{3}\rho_i u_i' u_i dx + \int_{\Omega_F}\sum_{k=1}^{3}\sum_{i=1}^{3}\rho u_k \frac{\partial u_i}{\partial x_k} u_i dx -$$
$$-\int_{\Lambda_F} p\ u_n d\gamma - \int_{\Gamma_F} p\ u_n d\gamma - \int_{\Gamma} p\ u_n d\gamma + \int_{\Omega_F} u\ \nabla p\ ds + \int_{\Omega_F} 2\mu\, e(u) : e(u)\, dx -$$
$$-\int_{\Lambda_F} (u_n p_a + u_\tau \sigma_{n\tau}) d\gamma - \int_{\Gamma} (u_n \sigma_{nn} + u_\tau \sigma_{n\tau}) d\gamma + \int_{\Gamma} u.n_F p d\gamma - \int_{\Omega_F} u.\nabla p ds +$$
$$+\frac{1}{2}\int_{\Omega_p} \frac{m\rho g}{\omega}\frac{\partial \varphi^2}{\partial t} dx + \int_{\Omega_p}\sum_{j=1}^{3} \frac{k(x,t)}{\omega}\left(\frac{\partial \varphi}{\partial x_j}\right)^2 \rho g\ dp - \int_{\Omega_p} \frac{\rho g}{\omega}\varepsilon\varphi dx -$$
$$-\int_{\Gamma} p_p \upsilon_{n_p} d\gamma + \int_{\Gamma_p} \bar{\upsilon}\ \varphi\rho g d\gamma = 0. \qquad (41)$$

Rewriting the previous expression (41) in a more convenient form, including property incompressible environment and boundary conditions (13)–(18), we obtain

$$\int_{\Omega_F}\sum_{i=1}^{3}\rho_i u_i' u_i dx + \int_{\Omega_F}\sum_{k=1}^{3}\sum_{i=1}^{3}\rho u_k \frac{\partial u_i}{\partial x_k} u_i dx + \int_{\Omega_F} 2\mu\, e(u) : e(u)\, dx -$$
$$-\int_{\Lambda_F} p\ u^0{}_n d\gamma - \int_{\Lambda_F} (u_n p_a + u_\tau \bar{\sigma}) d\gamma -$$
$$-\int_{\Gamma} (u_n \sigma_{nn} + u_\tau \sigma_{n\tau}) d\gamma + \frac{1}{2}\int_{\Omega_p} \frac{m\rho g}{\omega}\frac{\partial \varphi^2}{\partial t} dx + \int_{\Omega_p}\sum_{j=1}^{3} \frac{k(x,t)}{\omega}\left(\frac{\partial \varphi}{\partial x_j}\right)^2 \rho g\ dp -$$
$$-\int_{\Omega_p} \frac{\rho g}{\omega}\varepsilon\varphi dx - \int_{\Gamma} p_p \upsilon_{n_p} d\gamma + \int_{\Gamma_p} \bar{\upsilon}\ \varphi\rho g d\gamma = 0. \qquad (42)$$

Let's analyze the terms on joint border Γ

$$\int_{\Gamma} (u_n p_F + u_\tau \sigma_{n\tau}(u) - p_p \upsilon_{n_p}) d\gamma.$$

Given the terms the coupling (20), integral to the common border Γ is zero.
From the expression (36) given kinematic condition (15) for equation of continuity will be

$$\int_{\partial\Omega_F} u.n_F p d\gamma = \int_{\Lambda_F} u_n^0\ p d\gamma. \qquad (43)$$

Thus, the energy balance equation of compatible motion of surface and groundwater flow is written:

$$\int_{\Omega_F}\sum_{i=1}^{3}\rho_i u_i' u_i dx + \int_{\Omega_F}\sum_{k=1}^{3}\sum_{i=1}^{3}\rho u_k \frac{\partial u_i}{\partial x_k} u_i dx + \int_{\Omega_F} 2\mu\, e(u) : e(u)\, dx -$$
$$+\frac{1}{2}\int_{\Omega_p} \frac{m\rho g}{\omega}\frac{\partial \varphi^2}{\partial t} dx + \int_{\Omega_p}\sum_{j=1}^{3} \frac{k(x,t)}{\omega}\left(\frac{\partial \varphi}{\partial x_j}\right)^2 \rho g\ dp =$$
$$\sum_{i=1}^{3}\int_{\Omega_F} \rho f_i u_i ds + \int_{\Lambda_F} p\ u^0{}_n d\gamma -$$
$$-\int_{\Gamma_p} \bar{\upsilon}\ \varphi\rho g d\gamma + \int_{\Lambda_F} (u_n p_a + u_\tau \bar{\sigma}) d\gamma + \int_{\Omega_p} \frac{\rho g}{\omega}\varepsilon\varphi dx. \qquad (44)$$

Rewriting (44) through a total derivative, we have

$$\frac{1}{2}\rho\int_{\Omega_F}\frac{d}{dt}(u^2)\ ds+\int_{\Omega_F}2\mu e(u):e(u)dx-$$

$$+\frac{1}{2}\int_{\Omega_p}\frac{m\rho g}{\omega}\frac{\partial\varphi^2}{\partial t}dx+\int_{\Omega_p}\sum_{j=1}^{3}\frac{k(x,t)}{\omega}\left(\frac{\partial\varphi}{\partial x_j}\right)^2\rho g\ dp=$$

$$\sum_{i=1}^{3}\int_{\Omega_F}\rho f_i u_i ds+\int_{\Lambda_F}p\ u^0{}_n d\gamma-$$

$$-\int_{\Gamma_p}\overline{\upsilon}\ \varphi\rho g d\gamma+\int_{\Lambda_F}(u_n p_a+u_\tau\overline{\sigma})d\gamma+\int_{\Omega_p}\frac{\rho g}{\omega}\varepsilon\varphi dx. \qquad (45)$$

As we see from (45), the total energy flow depends on the energy sources that are located within the region or within its boundaries.

4. Conclusions

On the basis of conservation laws basic equations and boundary and initial conditions are derived describing the compatible motion flow of surface and ground water with unknown values of velocity and piezometric pressure. Variational problems of compatible flow are formulated and the contact conditions on the common border are obtained based on the laws of motion continuum. Energy standards of basic components of variational problem are analyzed. Full energy equation of energy balance for coupling motion of surface and groundwater flows are constructed and studied that makes it possible to investigate the properties of solutions of the problem, such as stability, regularity, existence, convergence and so on.

References

[1] Shlychkov, V. A. (2007). Numerical simulation of currents and admixture transport in a multi – arm river channel. Bull. Nov. Comp. Center, Num. Model in Atmosph., etc., 11, 79–85.

[2] Kuchment, L. S., Gelfan, A. N. (2002). Estimation of Extreme Flood Characteristics Using Physically Based Models of Runoff Generation and Stochastic Meteorological Inputs. Water International, 27 (1), 77–86. doi: 10.1080/02508060208686980

[3] Panday, S., Huyakorn, P. S. (2004). A fully coupled physically-based spatially-distributed model for evaluating surface/subsurface flow. Advances in Water Resources, 27 (4), 361–382. doi:10.1016/j.advwatres.2004.02.016

[4] Lions, J. L., Temam, R., Wang, S. (1993). Models for the coupled atmosphere and ocean. (CAO I, II). Computational Mechanics, 1 (1), 120.

[5] Discacciati, M., Quarteroni, A., Valli, A. (2007). Robin-Robin Domain Decomposition Methods for the Stokes–Darcy Coupling. SIAM Journal on Numerical Analysis, 45 (3), 1246–1268. doi: 10.1137/06065091x

[6] Cesmelioglu, A., Chidyagwai, P., Riviere, B. (2013). Continuous and discontinuous finite element methods for coupled surface-subsurface flow and transport problems. Rice University, 23.

[7] Venherskyi, P. S. (2014). Numerical investigation mathematical models coupled flow of surface and ground water from the catchment area. Mathematical and computer modeling, 10, 33–42.

[8] Venherskyi, P. S. (2014). About the problem of coupled motion of surface and ground water from the catchment area. Bulletin of Lviv University. Series Applied Mathematics and Computer Science, 22, 41–53.

[9] Venherskyi, P. S., Demkovych, O. R. (2002). Mathematical modeling of ground water in the saturated zone. 9-th National Conference Modern Problems of Applied Mathematics and Informatics, 1–36.

[10] Temam, R. (1995). Navier-Stokes equations and nonlinear functional analysis. SIAM, 148. doi: 10.1137/1.9781611970050

[11] Trushevskyi, V. M., Shynkarenko, H. A., Shcherbyna, N. M. (2014). Finite element method and artificial neural networks: theoretical aspects and application. Lviv: LNU Ivan Franko, 396.

Original Research Article: full paper

(2017), «EUREKA: Physics and Engineering»
Number 1

DEVELOPMENT OF THE SEARCH METHOD FOR NON-LINEAR SHIFT REGISTERS USING HARDWARE, IMPLEMENTED ON FIELD PROGRAMMABLE GATE ARRAYS

Nikolay Poluyanenko
Department of Information Systems and Technologies Security
V. N. Karazin Kharkiv National University
4 Svobody Sq., Kharkiv, Ukraine, 61022
rsnos@mail.ua

Abstract

The nonlinear feedback shift registers of the second order in GF(2) are considered, because based on them it can be developed a generator of stream ciphers with enhanced cryptographic strength.

Feasibility of nonlinear feedback shift register search is analyzed. These registers form a maximal length sequence, using programmable logic devices.

Performance evaluation of programmable logic devices in the generation of pseudo-random sequence by nonlinear feedback shift registers is given. Recommendations to increase this performance are given. The dependence of the maximum generation rate (clock frequency), programmable logic devices on the number of concurrent nonlinear registers is analyzed.

A comparison of the generation rate of the sequences that are generated by nonlinear feedback shift registers is done using hardware and software.

The author suggests, describes and explores the search method of nonlinear feedback shift registers, generating a sequence with a maximum period. As the main result are found non-linear 26, 27, 28 and 29 degrees polynomials.

Keywords: stream ciphers, random number generators, M-sequence, search of nonlinear shift registers, non-linear polynomials.

DOI: 10.21303/2461-4262.2017.00271

1. Introduction

There is currently rapid development of cryptanalytic systems. One of the main requirements to the main element of the cryptographic stream encryption system – a generator of pseudo-random sequences (PRSs) is an indiscernible of the sequence, complexity, speed and repetition period for PRSs [1]. Cryptographic primitives that meet these requirements are constructions on the basis of linear feedback shift registers (LFSRs).

Common cryptographic algorithms, which are built using LFSRs, are: stream cipher A5/1, used to ensure the privacy of telephone mobile communication of GSM standard [2]; stream cipher E0, used in the Bluetooth protocol [3], etc. LFSR main disadvantage is its linearity, which leads to a relatively simple cryptanalysis [4].

2. Overview of the problem and formulation of research problems

As an alternative for LFSRs to PRSs generation in the stream cipher nonlinear feedback shift registers (NLFSRs) are proposed. NLFSRs on the basis of stream ciphers are included in Achterbahn [5], Dragon [6], Grain [7], Trivium [8] and VEST [9]. In [10] it is shown that NLFSRs are more resistant to cryptanalytic attacks than LFSRs. Using L cells NLFSRs, a cryptanalyst can take up to $O\left(2^L\right)$ [11] or as given in [12], a sequence of $L\cdot(L+1)/2+L$ bits is necessary to determine the structure of L-bit NLFSR generating this sequence.

At the same time, large size NLFSR generation with a guaranteed period remains an unsolved problem [13]. Only some special cases were considered in [14]. It is known that LFSRs generate maximum length sequence (M-sequence) equal to 2^L-1 if and only if when its characteristic polynomial is primitive [15]. For NLFSRs such property is not found to this day. Small NLFSRs with a maximum period can be built with the help of simulation. Nevertheless, modern computing capacities allow to simulate NLFSRs with a size only to L<35 [16]. In [17], NLFSRs with a size to L<26 are shown. This is insufficient for cryptographic applications that require long periods, for example, 2^{128} [18].

Non-standard hardware solution for implementation of cryptographic algorithms is the use of field programmable gate arrays (FPGAs) [19]. FPGA allows to construct digital devices with high-level hardware description languages, which reduces the complexity of the development and allows the reuse the code through the use of IP-cores [20].

In [21], a search of NLFSRs that are implemented on FPGAs on the basis of analysis of de Bruijn sequences is carried out. Good statistical properties of NLFSR-generated sequences are confirmed and obtained non-linear 25 and 27 polynomials are given.

FPGAs have a high versatility and reliability, which ensures thorough testing [22]. Programmable logic is attractive due to possibility of providing performance close to ASIC technology, to achieve high throughput with high construction flexibility and low power consumption [23].

One of the important advantages of the implementation of cryptographic algorithms on FPGAs is the ability to construct a parallel and asynchronous architecture, superior to GPU and CPU microprocessor-based solutions in performance [24].

In this paper we study NLFSRs performance implemented on the FPGAs and problems of their optimization. Search method of NLFSRs generating M-sequence (M-NLFSRs) is given. This method is based on a practical synthesis of the results obtained previously. The aim of this research is to explore the possibility of NLFSR implementation of FPGA, as well as the development of an acceptable, for hardware and temporal parameters, the search algorithm for M-NLFSR.

3. M-NLFSR search method

The registers are used multiplication of only two cells, and such NLFSRs are called NLFSRs of the second order. Later, in NLFSR operation we understand NLFSR of the second order in GF(2). General NLFSR construction for the register, consisting of $L = 4$ cells, is shown in **Fig. 1**.

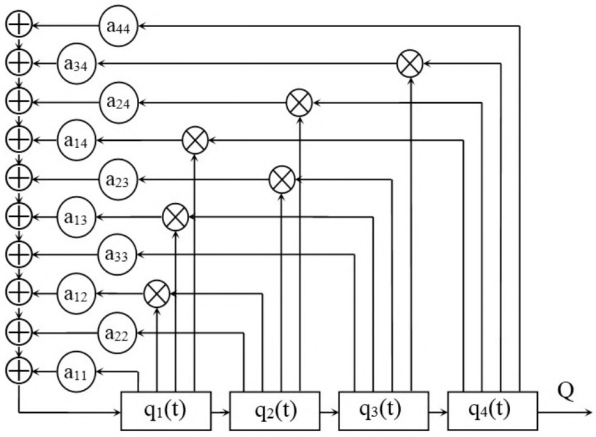

Fig. 1. General NLFSR construction

Where $a_{ij} \in \{0,1\}$ appropriate the presence or absence of feedback, $q_i(t) \in \{0,1\}$ – value of the i-th register at the time t, Q – generated sequence, bits. $\otimes$ denotes a nonlinear function of multiplication and $\oplus$ – linear function of summation.

Preliminary feedback coefficients a_{ij} are limited that equate some of the coefficients to zero. The total number of variables (initially not equal to zero) of feedback coefficient a_{ij} denoted as n_1. As has been shown in [25], the number of feedback coefficients a_{ij} for NLFSR with L size is calculated by ratio $n_L = L \cdot (L+1)/2$, therefore, n_1 can take values in the range $0 \le n_1 \le n_L$.

M-NLFSR search method consists of two stages that can be carried out simultaneously or sequentially.

Stage 1: There is a decrease in the test set by excluding NLFSRs not forming an M-sequence. The total amount of rejected polynomials is selected in the range of 90–99 % of the possible amount. The volume of rejected polynomials is limited by available memory and time resources.

Rejected set is defined by an analytical method, which is implemented in software. The analytical method consists of checking the feedback coefficients to meet certain requirements as

detailed in [25, 26, 12]. The essence of these requirements is to analyze the place, type and arrangement of non-zero coefficients of feedback a_{ij}. Mismatch of a_{ij} coefficients to specified requirements means the inability of NLFSR to form M-sequence and, therefore, its rejection.

After the first stage, we obtain the set of polynomials, acceptable (for time-consuming) to check in the second stage. Let's denote the number of such polynomials as k_0^{FPGA}.

Stage 2: Direct verification of the set of polynomials, obtained after the first stage, is carried out for the possibility of M-sequence generation by them is carried out using computer system.

As shown below, for moving the computational process from CPU on the FPGA, performance (speed) of each of NLFSRs is maintained. This fact allows to tens or hundreds of times increase the overall performance of the complex for M-NLFSR search compared to use only a PC.

4. The structure of the computer system for M-NLFSR search

Complete structure of computer system, which was used for the calculations, is shown in **Fig. 2.**

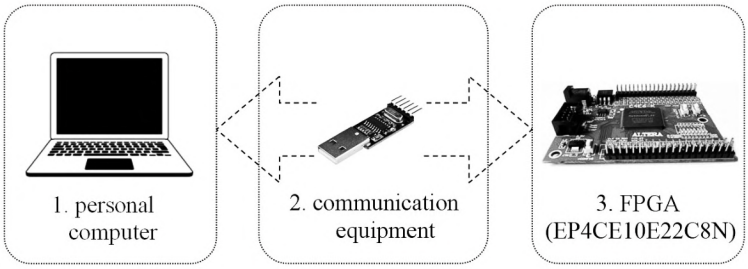

Fig. 2. The structure of the computer system for M-NLFSR search

The hardware consists of the card with integrated chip of Altera company of Cyclone IV E FPGA EP4CE10E22C8N family (China). FPGAs are made at 60 nm optimized process and includes 10 320 logic elements (LEs – Logic Elements). Project for FPGA is written in Verilog HDL, for compilation and simulation CAD CAD Altera Quartus Prime Version 16.0.0 was used.

USB-TTL converter was used as communication equipment (the maximum data transfer speed of 921 600 bps), performs the function of Universal Asynchronous Receiver/Transmitter (UART) between the FPGA and the PC. Two USB-TTL converters were used to enhance the data rate. They operate in parallel with a maximum data rate.

The software realizes: reading data from the hard disk; formation of a package to send to the FPGA; synchronous (for two USB-TTL converters) data sending to the specified COM port; receiving information through the COM port from the FPGA; decoding, visualization and storage on disk test results carried out in the FPGA.

5. FPGA-based NLFSR performance analysis

Hardware performance is a number of tested NLFSRs per time unit. Hardware performance consists of the following components:

– time for one cycle in the module that implements NLFSR operation (denoted as t_{cycle}^{FPGA}). Cycle is implementation of cyclic changes in NLFSR state in which all possible combinations are implemented for M-NLFSR, and the system returns to the initial state. Registers change their state in one clock cycle of the reference frequency, therefore amount of these clock cycles in a cycle should be 2^L;

– the number of simultaneously tested NLFSRs per cycle (denote as k_{NLFSR}^{FPGA}). The parameter depends on the number of LEs, engaged for one NLFSR and total capacity of used FPGA;

– operational clock frequency. Upon reaching a certain maximum clock frequency (f_{max}^{FPGA}) FPGA elements have no time to fully execute that leads to errors in the determination of M-RSNOS.

The increase of k_{NLFSR}^{FPGA} leads to an increase in the total number of involved LEs. As an example, the number LEs involved in FPGA to M- NLFSR search for $L = 29$ and $n_1 = 28$ depending from k_{NLFSR}^{FPGA}, are shown in **Fig. 3.**

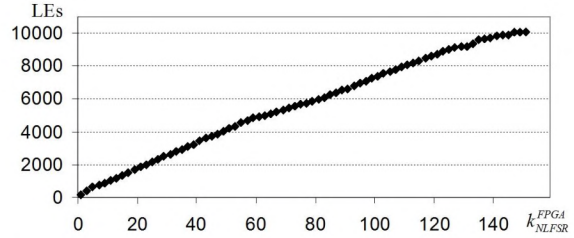

Fig. 3. Dependence of LEs involved in FPGA on k_{NLFSR}^{FPGA} for $L = 29$

Due to the increase in the number of LEs involved in FPGA, their mutual arrangement and increasing the physical distance between the interacting elements in the chip, there is a decrease of f_{max}^{FPGA}. Also f_{max}^{FPGA} significantly affect the temperature factor, which can be partly explains a small deviation observed in **Fig. 4.**

Let's consider in detail how to change the above characteristics on the number of simultaneously tested NLFSRs. **Fig. 4, *a*** shows the dependence results of observed f_{max}^{FPGA} on k_{NLFSR}^{FPGA} for NLFSRs with a size of $L = 28$ and $n_1 = 28$.

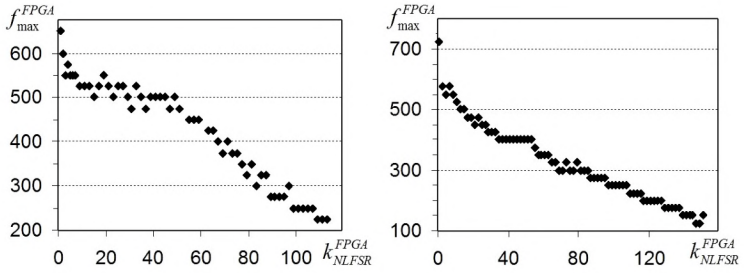

a *b*

Fig. 4. Dependence of f_{max}^{FPGA} on k_{NLFSR}^{FPGA}: *a* – for $L = 28$, *b* – for $L = 29$

Taking into account obtained results, FPGA configuration modification has been made for $L = 29$. Modification allowed to improve performance for $k_{NLFSR}^{FPGA} = 1$ to $f_{max}^{FPGA} = 725$ MHz and reduce LEs in the module. **Fig. 4, *b*** shows the results of dependence of f_{max}^{FPGA} on k_{NLFSR}^{FPGA} for NLFSRs with a size of $L = 29$ and $n_1 = 28$ .The change of the clock frequency for f_{max}^{FPGA} determination was conducted discretely, in steps of 25 MHz.

Knowing f_{max}^{FPGA}, we can determine t_{cycle}^{FPGA} for different number of simultaneously calculated NLFSRs in FPGA. Based on these data, we can calculate the time t_0^{FPGA} that is necessary to spend for the analysis of all k_0^{FPGA} polynomials in the search for the M-NLFSR in hardware. Elapsed time (in hours) will be calculated by the following relationship:

$$t_0^{FPGA} = \frac{1}{3600\,\text{sec}} \cdot \frac{k_0^{FPGA}}{k_{NLFSR}^{FPGA}} \cdot t_{cycle}^{FPGA}.$$

The dependence of the estimated time for M-NLFSR search for L=29 and restrictions imposed, in which n_1=28, $k_0^{FPGA} = 17\,619\,713$, on the number of simultaneously processed polynomials in FPGA is shown in **Fig. 5**.

As can be seen in the graph, maximum system performance can't be achieved with maximum use of all FPGA elements due to the need to reduce the clock frequency. The optimal number of simultaneously tested NLFSRs in this case is in the range from 79 to 115, after which the time for search begins to increase.

In [27], there is a generation time of 1 GB by the generator, written in assembler and optimized for different NLFSRs, including LFSRs. To compile all the examples FASM was used (flat assembler version 1.71.51). The calculations were performed on a personal computer (64 bit Windows 7 SP 1, Intel Core i5-3210M CPU 2,5GHz processor). According to the research results,

the time to generate the 1 GB ranges from 16 to 76 seconds, depending on the size and form of the polynomial.

For comparison, **Table 1** shows the time for generation of 1 GB NLFSR implemented in FPGA on different clock frequencies (f^{FPGA}).

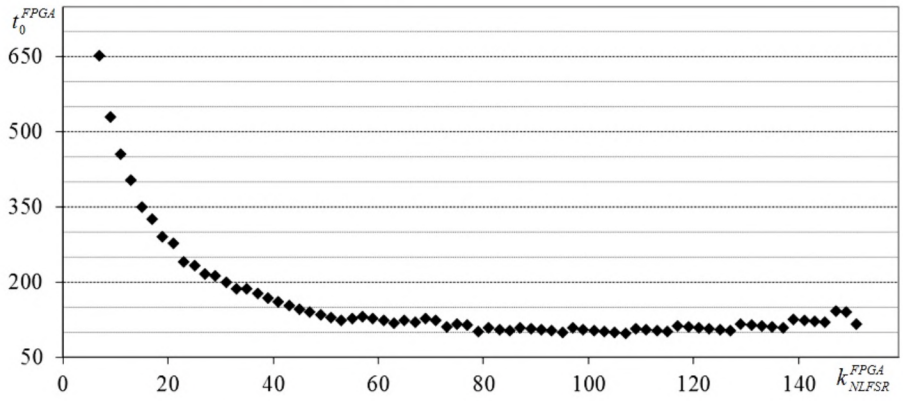

Fig. 5. Dependence of t_0^{FPGA} (in hours) on k_{NLFSR}^{FPGA} for L = 29

Table 1

Dependence of time for generation of 1 GB NLFSR on different f^{FPGA}

f^{FPGA}	t
50 MHz	172 s
100 MHz	86 s
200 MHz	43 s
400 MHz	21,5 s
600 MHz	14,3 s
700 MHz	12,3 s
725 MHz	11,8 s

As can be seen from **Table 1**, the use of the FPGA-based hardware components for PRSs generation can improve performance (two and more times) as compared to using only the CPU of a personal computer.

It is worth noting that these results are valid for used FPGA model. Using another FPGA model, it is likely to get higher system efficiency. Thus, [28] shows the results of the efficiency of hardware implementations of ciphers of GRACE-S family for various FPGA families. Unfortunately, investigated families didn't contain Cyclone IV, but tested FPGAs of Stratix IV and Stratix V family showed more than two times greater efficiency than FRGAs of Cyclone II or Cyclone V family.

6. Search results for M-NLFSRs

M-NLFSRs search with a size of L =26, 27, 28 and 29 with the above described method was carried out. Obtained polynomials, as well as time expenditures, are shown below.

L = 26:

$$x^{26}+x^{24}+x^{23}+x^{20}+x^{18}+x^{14}+x^{12}+x^{6}+x^{5}+x^{4}+x^{23}\cdot x^{25}+x^{24}\cdot x^{25}$$

$$x^{26}+x^{25}+x^{22}+x^{21}+x^{19}+x^{17}+x^{16}+x^{15}+x^{13}+x^{12}+x^{6}+x^{5}+x^{4}+x^{23}\cdot x^{25}$$

$$x^{26}+x^{24}+x^{22}+x^{21}+x^{20}+x^{19}+x^{17}+x^{16}+x^{15}+x^{14}+x^{12}+$$

$$+x^{11}+x^{8}+x^{7}+x^{4}+x^{23}\cdot x^{24}+x^{23}\cdot x^{25}+x^{24}\cdot x^{25}$$

$$x^{26}+x^{22}+x^{21}+x^{20}+x^{19}+x^{17}+x^{16}+x^{15}+x^{14}+x^{12}+x^{11}+x^{8}+x^{7}+x^{4}+x^{23}\cdot x^{24}+x^{24}\cdot x^{25}.$$

Search time – 43 hours 48 minutes.

L = 27:

$$x^{27}+x^{26}+x^{25}+x^{24}+x^{19}+x^{16}+x^{15}+x^{11}+x^{8}+x^{6}+x^{5}+x^{3}+x^{24}\cdot x^{25}+x^{24}\cdot x^{26}$$

$$x^{27}+x^{26}+x^{19}+x^{16}+x^{15}+x^{13}+x^{12}+x^{11}+x^{10}+x^{9}+$$

$$+x^{8}+x^{7}+x^{6}+x^{5}+x^{4}+x^{3}+x^{24}\cdot x^{26}+x^{25}\cdot x^{26}$$

$$x^{27}+x^{24}+x^{22}+x^{20}+x^{19}+x^{17}+x^{16}+x^{13}+x^{10}+x^{8}+x^{7}+x^{6}+x^{4}+x^{25}\cdot x^{26}$$

$$x^{27}+x^{24}+x^{23}+x^{17}+x^{14}+x^{9}+x^{8}+x^{7}+x^{5}+x^{4}+x^{3}+x^{25}\cdot x^{26}$$

Search time – 33 hours 04 minutes.

L = 28:

$$x^{28}+x^{27}+x^{25}+x^{24}+x^{22}+x^{20}+x^{19}+x^{16}+x^{14}+x^{13}+x^{10}+x^{8}+x^{5}+x^{25}\cdot x^{27}$$

$$x^{28}+x^{27}+x^{26}+x^{25}+x^{24}+x^{23}+x^{22}+x^{21}+x^{20}+x^{16}+x^{15}+x^{14}+x^{13}+x^{12}+x^{11}+x^{10}+$$

$$+x^{7}+x^{6}+x^{25}\cdot x^{26}+x^{25}\cdot x^{27}$$

$$x^{28}+x^{25}+x^{20}+x^{19}+x^{17}+x^{16}+x^{13}+x^{11}+x^{10}+x^{9}+x^{8}+x^{7}+x^{6}+x^{3}+x^{25}\cdot x^{27}+x^{26}\cdot x^{27}$$

$$x^{28}+x^{24}+x^{23}+x^{20}+x^{18}+x^{17}+x^{16}+x^{14}+x^{13}+x^{12}+x^{5}+x^{25}\cdot x^{27}$$

$$x^{28}+x^{27}+x^{26}+x^{25}+x^{15}+x^{14}+x^{11}+x^{10}+x^{25}\cdot x^{26}+x^{25}\cdot x^{27}$$

$$x^{28}+x^{25}+x^{24}+x^{21}+x^{20}+x^{18}+x^{17}+x^{16}+x^{15}+x^{14}+x^{13}+x^{12}+x^{10}+x^{9}+x^{5}+x^{3}+$$

$$+x^{25}\cdot x^{27}+x^{26}\cdot x^{27}.$$

Search time – 73 hours 25 minutes.

L = 29:

$$x^{29}+x^{28}+x^{27}+x^{26}+x^{25}+x^{24}+x^{23}+x^{20}+x^{16}+x^{12}+x^{11}+x^{6}+x^{4}+x^{26}\cdot x^{27}$$

$$x^{29}+x^{28}+x^{27}+x^{26}+x^{25}+x^{21}+x^{19}+x^{15}+x^{10}+x^{9}+x^{8}+x^{6}+x^{4}+x^{26}\cdot x^{28}$$

Search time – 133 hours 26 minutes.

The use of hardware component will significantly reduce M-NLFSRs search time. As an example, for software search at L=25 was spent 18 days, and by using hardware components for L=26 – less than two days. Estimated time for which would have made a similar search for L=26, using a software method, would constitute more than 3 months. Taking into account the modifications, introduced in the search algorithm for L=27, 28 and 29, we can expect another three-time increase in performance for L=26, while using hardware components.

Thus, using this method, we get a general performance increase for search of M-NLFSRs generating M-sequences by more than 150 times as compared with the method using only PC CPU resources. The use of more expensive and productive FPGAs will further reduce the time to search of M-NLFSRs.

7. Conclusions

The method for M-NLFSRs search using hardware-software system is given. Based on the method, as an example, the result of the search of non-linear 26, 27, 28 and 29 degrees polynomials for generation of M-sequences is given.

Use of FPGA-based hardware component can significantly improve the performance of complex for search of M-NLFSR. The time for M-NLFSR search is increased by more than 150 times as compared to using only the computing power of PC.

FPGA-based NLFSR performance capabilities are given. Recommendations on optimizing the performance of the complex to search of M-NLFSR are given.

A performance comparison of NLFSR generators performed by using the software and hardware implementation is carried out. It is shown that the hardware implementation of single FPGA-based NLFSR isn't inferior to the performance of its program analogue and in the case of a generator with several parallel NLFSRs can significantly exceed its.

Stable performance of FPGA-based NLFSR is implemented with a clock frequency (generation speed in NLFSR), equal to 725 MHz.

On the basis of the results it can be developed stream ciphers with enhanced cryptographic strength. The application of obtained non-linear polynomial allows to obtain stream ciphers, which are analogues of modern developments in this field, and the use of the described search method allows to find higher degree M-NLFSR.

References

[1] Horbenko, Yu. (2015). Pobuduvannia ta analiz system, protokoliv i zasobiv kryptohrafichnoho zakhystu informatsii. Chastyna 1: Metody pobuduvannia ta analizu, standartyzatsiia ta zastosuvannia kryptohrafichnykh system. Kharkiv: Fort, 960.

[2] Biham, E., Dunkelman, O. (2000). Cryptanalysis of the A5/1 GSM Stream Cipher. Progress in Cryptology – INDOCRYPT 2000, 43–51. doi: 10.1007/3-540-44495-5_5

[3] Shaked, Y., Wool, A. (2006). Cryptanalysis of the Bluetooth E 0 Cipher Using OBDD's. Information Security, 187–202. doi: 10.1007/11836810_14

[4] Schneier, B. (2000). A self-study course in block-cipher cryptanalysis. Cryptologia, 24 (1), 18–33. doi:10.1080/0161-110091888754

[5] Gammel, B. M., Gottfert, R., Kniffler, O. (2007). Achterbahn-128/80: Design and analysis. Workshop Record of The State of the Art of Stream Ciphers – SASC 2007, 152–165.

[6] Chen, K., Henricksen, M., Millan, W., Fuller, J., Simpson, L., Dawson, E., Lee, H., Moon, S. (2005). Dragon: A Fast Word Based Stream Cipher. Information Security and Cryptology – ICISC 2004, 33–50. doi:10.1007/11496618_5

[7] Hell, M., Johansson, T., Meier, W. (2007). Grain: a stream cipher for constrained environments. International Journal of Wireless and Mobile Computing, 2 (1), 86. doi: 10.1504/ijwmc.2007.013798

[8] Canniere, C., Preneel, B. (2006). TRIVIUM specifications. eSTREAM, ECRYPT Stream Cipher Project. Available at: http://citeseer.ist.psu.edu/viewdoc/summary?doi=10.1.1.59.9030&rank=1

[9] Gittins, B., Landman, H., O'Neil, S., Kelson, R. (2005). A presentation on VEST hardware performance, chip area measurements, power consumption estimates and benchmarking in relation to the aes, sha-256 and sha-512. IACR Cryptology ePrint Archive, 415.

[10] Canteaut, A. (2006). Open Problems Related to Algebraic Attacks on Stream Ciphers. Lecture Notes in Computer Science, 3969, 120–134. doi: 10.1007/11779360_10

[11] Dubrova, E., Teslenko, M., Tenhunen, H. (2008). On Analysis and Synthesis of (n, k)-Non-Linear Feedback Shift Registers. 2008 Design, Automation and Test in Europe, 133–137. doi: 10.1109/date.2008.4484856

[12] Kuznetsov, O., Svatovskyi, I. (2016). Analiz ta porivnialni doslidzhennia symetrychnykh kryptohrafichnykh peretvoren na postkvantovyi period. Kharkiv: KhNU im. V. N. Karazina, 119.

[13] Dubrova, E. (2013). A Scalable Method for Constructing Galois NLFSRs With Period $2^n - 1$ Using Cross-Join Pairs. IEEE Transactions on Information Theory, 59 (1), 703–709. doi: 10.1109/tit.2012.2214204

[14] Janicka-Lipska, I., Stokłosa, J. (2004). Boolean feedback functions for full-length nonlinear shift registers. Journal of Telecommunications and Informatioin Technology, 4, 28–30.

[15] Golomb, S. W. (1982). Shift Register Sequences. Aegean Park Press, 119.

[16] Dubrova, E. (2014). Generation of full cycles by a composition of NLFSRs. Designs, Codes and Cryptography, 73 (2), 469–486. doi: 10.1007/s10623-014-9947-3

[17] Dubrova, E. (2012). A list of maximum – period NLFSRs. IACR Cryptology ePrint Archive, 166.

[18] Schneier, B. (1995). Applied cryptography (2nd ed.): protocols, algorithms, and source code in C. New York: John Wiley & Sons, Inc., 758.

[19] Kulikova, A. S., Lysenko, I. V. (2012). Realization of diverse stream data encryption with keyless hash functions on the basis of programmable logic. Information processing systems, 7 (105), 22–26.

[20] Kulanov, V., Kharchenko, V., Perepelitsyn, A. (2010). Parameterized IP Infrastructures for fault-tolerant FPGA-based systems: Development, assessment, case-study. 2010 East-West Design & Test Symposium (EWDTS), 452–455. doi: 10.1109/ewdts.2010.5742075

[21] Rachwalik, T., Szmidt, J., Wicik, R., Zabłocki, J. (2012). Generation of Nonlinear Feedback Shift Registers with special – purpose hardware. In Communications and Information Systems Conference, 1–4.

[22] Perepelitsyn, A. E. (2016). Usage of parametrizable ip infrastructures for fpga-based fault-tolerant onboard systems development. Electronic and computer systems, 5 (79), 104–112.

[23] Kolesnyk, I. N., Kulanov, V. O., Perepelitsyn, A. E. (2016). Analysis of fpga technologies application as a part of cloud infrastructure. Electronic and computer systems, 6 (80), 130–135.

[24] Perepelitsyn, A., Shulga, D. (2013). FPGA technologies in medical equipment: Electrical impedance tomography. East-West Design & Test Symposium, 1–4. doi: 10.1109/ewdts.2013.6673157

[25] Potii, A. V., Poluyanenko, N. A. (2008). Analyz svojstv reghystrov sdvygha s nelynejnoj obratnoj svjazjju vtorogho porjadka, gheneryrujushhykh posledovateljnostj s maksymaljnim peryodom. Prykladnaja radyoelektronyka, 3, 282–290.

[26] Potii, A., Poluyanenko, N. (2016). The selection of forming polynomials for shift register with nonlinear feedback second order that generates the sequence with maximum period. Computer science and cybersecurity, 2 (2), 22–30. Available at: http://periodicals.karazin.ua/cscs/article/view/6209/5747

[27] Poluyanenko, N., Potii, A. (2016). Sravnenye ob'ema ansamblia M-RSLOS y M-RSNOS, skorosty heneratsyy na ykh osnove, dlia GF(2) y v rasshyrenyiakh polia GF(2^2). Radyotekhnyka, 186 (216), 153–160.

[28] Kliucharev, P. G. (2013). Proyzvodytelnost y effektyvnost apparatnoi realyzatsyy potochnikh shyfrov, osnovannikh na obobshchennikh kletochnikh avtomatakh. Nauka i obrazovanye, 10, 299–314. Available at: http://technomag.bmstu.ru/file/669391.html?__s=1

APPLICATION OF THE METHOD OF BOUNDARY INTEGRAL EQUATIONS FOR NON-STATIONARY PROBLEM OF THERMAL CONDUCTIVITY IN AXIALLY SYMMETRIC DOMAIN

Grigoriy Zrazhevsky
Department of Theoretical Mechanics
Taras Shevchenko National University of Kyiv
64 Volodymyrs'ka str., Kyiv, Ukraine, 01033
zrazhevsky@aorda.com

Vera Zrazhevska
Department of Differential Equations
National Technical University of Ukraine "Igor Sikorsky Kyiv Polytechnic Institute"
37 Peremogy ave., Kyiv, Ukraine, 03056
vera.zrazhevska@gmail.com

Abstract

The article considers the non-stationary initial-boundary problem of thermal conductivity in axially symmetric domain in Minkowski space, formulated as equivalent boundary integral equation. Using the representation of the solution in the form of a Fourier series expansion, the problem is reformulated as an infinite system of two-dimensional singular integral equations regarding expansion coefficients. The paper presents and investigates the explicit form for fundamental solutions used in the integral representation of the solution in the domain and on the border. The obtained results can be used in the construction of efficient numerical boundary element method for estimation of structures behavior under the influence of intense thermal loads in real-time.

Keywords: initial-boundary problem of thermal conductivity, boundary integral equation, axially symmetric domain, fundamental solution for axially symmetric domain.

DOI: 10.21303/2461-4262.2017.00285

1. Introduction

Large number of studies is devoted to the theory of temperature stresses and engineering methods for their calculation [1–4]. Mathematical model of thermal stresses of metal structures is reduced to calculation of non-stationary behavior of thermal fields by solving a non-stationary initial-boundary value problem of thermal conductivity, and calculation of temperature stresses by solving stationary boundary problem of elasticity [1, 2]. Basic analytical solutions for model problems for canonical domains are obtained [1–3]. At the same time, calculations and control of real structures require the development of efficient numerical methods that allow to calculate the behavior of structures under the influence of intense thermal loads in real-time. One of these methods is the boundary element method that is one of numerous implementations of the method of boundary integral equations [5–7].

The method of boundary integral equations is based on the transition from the non-stationary initial-boundary value problem of thermal conductivity to the equivalent boundary integral equation. This approach has numerous advantages over classical methods because it allows to reduce the dimension of the problem, the obtained solution is semi-analytical and therefore it can be analyzed with analytical methods. The method uses the Green function as a fundamental solution that allows to satisfy one part of the boundary conditions and the condition at infinity (in the case of infinity inclusion) automatically. The method allows to build special boundary elements, that take into account the asymptotic behavior of the solution in a neighborhood of singular points of the problem [6, 7].

Special numerical methods, that take into account some particular qualities of constructions, are more effective in comparison with universal methods. Since cylindrical structures, such as pipelines, reactor vessels, constitute a significant share of production elements, calculation of

critical temperature modes of their operation is very important. Axially symmetric domain allows to use the representation of the solution in the form of a Fourier series expansion.

In practical applications it is important to take into account a finite number of harmonics only, so this problem can be reduced to a finite system of two-dimensional (spatial domain and time) boundary singular integral equations.

2. Materials and methods

2. 1. Previous results

Let's introduce the following notations: $x = (x_1, x_2, x_3) \in R^3$, $\Omega \subset R^3$ is a space domain with the boundary surface $\Gamma = \Gamma_u \cup \Gamma_q$, t is time; $u(x,t)$ is a temperature at a point x at a time moment t; $c(x)$ is the heat capacity, $k(x)$ is the thermal conductivity; $\rho(x)$ is the matter density, $f(x,t)$ is the intensity of heat sources at a point x at a time moment t.

Let's consider the problem for the heat equation:

$$c\rho\frac{\partial u}{\partial t}(x,t) = \operatorname{div}(k \operatorname{grad} u(x,t)) + f(x,t),\ x \in \Omega,\ t > t_0 \tag{1}$$

with the boundary conditions:

$$\begin{cases} u(x,t) = \bar{u}(x,t),\ x \in \Gamma_u, t \geq t_0, \\ q(x,t) = \bar{q}(x,t),\ x \in \Gamma_{q,}\ t \geq t_0 \end{cases} \tag{2}$$

and initial condition:

$$u(x,t_0) = u_0(x),\ x \in \overline{\Omega}, \tag{3}$$

where $\overline{\Omega} = \Omega \cup \Gamma$, $q(x,t) = k\frac{\partial u}{\partial \vec{n}}$, $\vec{n}$ is an external normal to the surface.

Let's consider the initial boundary problem (1)–(3) as a boundary problem in Minkowski space (x,t), where x is a point of three-dimensional space, t is time. Obviously, we get the boundary problem for cylinder $(x \in \Omega,\ t > t_0)$ with boundary conditions: (2) on the boundary surface of the cylinder $(x \in \Gamma_u \cup \Gamma_q, t \geq t_0)$ and (3) on the cylinder base.

In [8], using the method of weighted residuals [9, 10], the integral representation of the solution is obtained and its correctness is proved, the conditions on the parameters of the passage to the limit for correct interpretation of the singular integral in four-dimensional space are formulated.

The article [8] presents the integral equivalent of the problem:

$$\chi_{(\Omega, t>t_0)}(\xi,\tau)\cdot u(\xi,\tau) + \int_{t_0}^{\tau} dt \int_{\Gamma} (u^*(\xi - x, \tau - t) q(x,t) - u(x,t) q^*(x - \xi, \tau - t))\, d\Gamma_x =$$

$$= \int_{\Omega} \rho c\, u_0(x)\, u^*(\xi - x, \tau - t_0)\, d\Omega_x - \int_{t_0}^{\tau} dt \int_{\Omega} f(x,t)\, u^*(\xi - x, \tau - t)\, d\Omega_x, \tag{4}$$

where H is the Heaviside function, u^* is a fundamental solution of the heat equation that satisfies the principle of causality and is limited at infinity for four-dimensional Minkowski space [8]:

$$u^* = -\frac{(\rho c)^{1/2}}{(4\pi k(\tau - t))^{3/2}} \exp\left(-\frac{|\xi - x|^2 \rho c}{4k(\tau - t)}\right) H(\tau - t),$$

$$\chi_{(\Omega, t>t_0)}(\xi, t) = \begin{cases} 1, (\xi, t) \in (\Omega, t > t_0) \\ 0, (\xi, t) \notin (\Omega, t > t_0) \end{cases},$$

is the area function (indicator).

Obviously, (5) is the quasi equation. It allows to determine $u(x,t)$ at any point inside the area $\left(x \in \Omega,\ t > t_0\right)$ if values of functions $u(x,t)$ and $q(x,t)$ on Γ are known. So, the problem is to determine $u(x,t)$ on Γ_q and $q(x,t)$ on Γ_u. To get a boundary integral equation in [8] the limit transition in (8) as the point of source approaches the boundary of the four-dimensional domain $\xi \to \overline{\xi} \in \Gamma$ was conducted, the interpretation of the Cauchy principal value of integral singularity $\int_{t_0}^{\tau} dt \int_{\Gamma} u(x,t) q^*(x-\overline{\xi}, \tau - t) d\Gamma_x$ was fulfilled, the conditions on the parameters of the passage to the limit for its correct interpretation were formulated.

The boundary integral equation of the problem was obtained in the form:

$$C\left(\overline{\xi}\right) u\left(\overline{\varepsilon}, \tau\right) + \int_{t_0}^{\tau} dt \int_{\Gamma} \left(u^*(\overline{\xi} - x, \tau - t)\, q(x,t) - u(x,t)\, q^*(\overline{\xi} - x, \tau - t) \right) d\Gamma_x =$$

$$= \int_{\Omega} \rho c\, u_0(x)\, u^*(\overline{\xi} - x, \tau - t_0) d\Omega_x - \int_{t_0}^{\tau} dt \int_{\Omega} f(x,t)\, u^*(\overline{\xi} - x, \tau - t) d\Omega_x,\ \overline{\xi} \in \Gamma,\ t_0 < t < \tau, \qquad (5)$$

where $C(\overline{\xi}) = \frac{1}{4\pi}(4\pi - S)$ (if $\overline{\xi}$ is regular then $C(\overline{\xi}) = \frac{1}{2}$) and the second integral in the left side is taken in the sense of principal value.

Thus, the original problem (1) - (3) was reduced to solving of the singular integral equation (5), that is, to finding $u(x,t)$ for $x \in \Gamma_q$ and $q(x,t)$ for $x \in \Gamma_u$. Then the integral representation of the solution (4) can be used to find $u(\xi,\tau)$ for $(\xi,\tau) \in (\Gamma, \tau > t_0)$. It should be emphasized that (5) is an equation in three-dimensional space $(\overline{\xi} \in \Gamma, \tau > t_0)$, and not in four-dimensional space $(\xi \in R, \tau > t_0)$ as the original problem. So, the transition to the boundary integral equation allowed to reduce the dimension of the problem [8].

2. 2. A linear boundary integral equation for the axially symmetric domain

Let the spatial domain Ω with the border Γ is axisymmetrical, but the boundary and initial conditions are not axisymmetrical. We show that in this case the boundary integral equation (5) can be reduced to an infinite countable set of singular integral equations that are two-dimensional in Minkowski space.

Let's introduce the spatial cylindrical coordinate systems $\left(r_x, \theta_x, z_x\right)$ in the space x and $\left(r_\xi, \theta_\xi, z_\xi\right)$ in the space ξ. (x is an observation point, ξ is a point of source). As Γ is the surface of rotating, all limit functions in (5) can be expanded in Fourier series:

$$f(x) = \sum_{n=0}^{\infty} \left[f_n^c\left(\overline{x}\right) \cos n\, \theta_x + f_n^s\left(\overline{x}\right) \sin n\, \theta_x \right],\ \overline{x} = \left(r_x, z_x\right) \in \overline{\Gamma}. \qquad (6)$$

$$\begin{cases} f_n^c\left(\overline{x}\right) = \frac{1}{\pi} \int_0^{2\pi} f\left(r_x, \theta_x, z_x\right) \cos n\theta_x\, d\theta_x,\ n = 1,2,... \\ f_0^c\left(\overline{x}\right) = \frac{1}{\pi} \int_0^{2\pi} f\left(r_x, \theta_x, z_x\right) d\theta_x \\ f_n^s\left(\overline{x}\right) = \frac{1}{\pi} \int_0^{2\pi} f\left(r_x, \theta_x, z_x\right) \sin n\theta_x\, d\theta_x,\ n = 1,2,... \end{cases} \qquad (7)$$

Let's substitute decompositions like (6) for functions $u(x,t)$, $q(x,t)$ to (5), multiply by $\cos k\theta_\xi$, $\sin k\theta_\xi$ and integrate over θ_ξ in the interval $[0,\ 2\pi]$. Because of the orthogonality of trigonometric functions it is easy to see that:

$$\begin{cases} \frac{1}{\pi} \int_0^{2\pi} \sum_{k=0}^{\infty} \left\{ u_k^c\left(\overline{\xi}, \tau\right) \cos k\, \theta_x + u_k^s\left(\overline{\xi}, \tau\right) \sin k\, \theta_x \right\} \cos n\theta_\xi\, d\theta_\xi = u_n^c\left(\overline{\xi}, \tau\right), \\ \frac{1}{\pi} \int_0^{2\pi} \sum_{k=0}^{\infty} \left\{ u_k^c\left(\overline{\xi}, \tau\right) \cos k\, \theta_x + u_k^s\left(\overline{\xi}, \tau\right) \sin k\, \theta_x \right\} \sin n\theta_\xi\, d\theta_\xi = u_n^s\left(\overline{\xi}, \tau\right). \end{cases} \qquad (8)$$

Let's consider the typical expressions in (5). Using the expression of the element of integration $d\Gamma_x$ in the cylindrical coordinate system $d\Gamma_x = r_x\, d\theta_x\, d\bar{\Gamma}(r_x, z_x)$ we move from the integrals over the domain to integrals over the boundary $\bar{\Gamma}$. Then we have:

$$\int_\Gamma u^*(\xi, x, \tau, t) q(x,t) d\Gamma_x = \int_0^{2\pi} d\theta_x \int_{\bar{\Gamma}} u^*(\xi, x, \tau, t) q(\bar{x}, t)\; r_x d\bar{\Gamma}(r_x, z_x) =$$

$$= \int_0^{2\pi} d\theta_x \int_{\bar{\Gamma}} u^*\left(\bar{\xi}, \theta_\xi, \bar{x}, \theta, \tau, t\right) q(\bar{x}, t)\; r_x d\bar{\Gamma}(r_x, z_x)$$

and so

$$\frac{1}{\pi}\int_0^{2\pi} \cos n\theta_\xi\, d\theta_\xi \int_\Gamma u^*(\xi, x, \tau, t) q(x,t) d\Gamma_x =$$

$$= \int_0^{2\pi} d\theta_x \int_{\bar{\Gamma}} \frac{1}{\pi}\int_0^{2\pi} \cos n\theta_\xi\; u^*\left(\bar{\xi}, \theta_\xi, \bar{x}, \theta_x, \tau, t\right) d\theta_\xi\; q\left(\bar{x}, \theta_x, t\right) r_x\, d\bar{\Gamma}(r_x, z_x). \tag{9}$$

Taking into account, that

$$u^*(\xi - x,\ \tau - t) = u^*\left(|\xi - x|,\ \tau - t\right), \tag{10}$$

$$|x - \xi|^2 = r_x^2 + r_\xi^2 - 2\, r_x r_\xi \cos(\theta_\xi - \theta_x) + \left(z_\xi - z_x\right)^2, \tag{11}$$

we have: $u^*\left(|\xi - x|,\ \tau - t\right) = u^*\left(\bar{\xi}, \bar{x}, \theta, \tau - t\right)$, where $\theta = \theta_x - \theta_\xi$. Thus, we have shown that u^* is independent separately from θ_x, θ_ξ and depends only on their difference $\theta_x - \theta_\xi$. This allows us to move from the integral over θ_x or θ_ξ to the integral over $\theta = \theta_x - \theta_\xi$.

Taking into account that $\cos n\theta_\xi = \cos n(\theta_x - \theta)$ and presented $\bar{q}\left(\bar{x}, \theta_x, t\right)$ in the form (6), we rewrite (9) as:

$$\frac{1}{\pi}\int_0^{2\pi} \cos n\theta_\xi d\theta_\xi \int_\Gamma u^*(\xi, x, \tau, t) q(x,t) d\Gamma_x =$$

$$= \int_{\bar{\Gamma}} \left[u_n^{*c}\left(\bar{\xi}, \bar{x}, \tau - t\right) q_n^c\left(\bar{x}, t\right) + u_n^{*s}\left(\bar{\xi}, \bar{x}, \tau - t\right) q_n^s\left(\bar{x}, t\right)\right] r_x d\bar{\Gamma}\left(r_x, z_x\right), \tag{12}$$

where

$$\begin{cases} u_n^{*c}\left(\bar{\xi}, \bar{x}, \tau - t\right) = \dfrac{1}{4\pi}\displaystyle\int_0^{2\pi} u^*\left(\bar{\xi}, \bar{x}, \theta, \tau - t\right)\; \cos n\theta\; d\theta, \\ u_n^{*s}\left(\bar{\xi}, \bar{x}, \tau - t\right) = \dfrac{1}{4\pi}\displaystyle\int_0^{2\pi} u^*\left(\bar{\xi}, \bar{x}, \theta, \tau - t\right) \sin n\theta\; d\theta. \end{cases} \tag{13}$$

Similarly, we obtain:

$$\frac{1}{\pi}\int_0^{2\pi} \sin n\theta_\xi d\theta_\xi \int_\Gamma u^*(\xi, x, \tau, t) q(x,t) d\Gamma_x =$$

$$= \int_{\bar{\Gamma}} \left[u_n^{*c}\left(\bar{\xi}, \bar{x}, \tau - t\right) q_n^s\left(\bar{x}, t\right) - u_n^{*s}\left(\bar{\xi}, \bar{x}, \tau - t\right) q_n^c\left(\bar{x}, t\right)\right] r_x d\bar{\Gamma}\left(r_x, z_x\right), \quad n = \overline{1, \infty}. \tag{14}$$

In view of (8), (13) and (14), (5) can be rewritten as:

$$\begin{cases} c(\bar{\xi})\, u_n^c\left(\bar{\xi},\tau\right)+\int\limits_{t_0}^{\tau} dt \int\limits_{\bar{\Gamma}} \left\{ u_n^{*c}\left(\bar{\xi},\bar{x},\tau-t\right) q_n^c\left(\bar{x},t\right)+u_n^{*s}\left(\bar{\xi},\bar{x},\tau-t\right) q_n^S(\bar{x},t)- \right. \\ \left. -u_n^c\left(\bar{x},t\right) q_n^{*c}\left(\bar{\xi},\bar{x},\tau-t\right)-u_n^s\left(\bar{x},t\right) q_n^{*s}\left(\bar{\xi},\bar{x},\tau-t\right) \right\} r_x d\bar{\Gamma}(r_x,z_x)= \\ =\int\limits_{\Omega} \rho c\, u_0(x) \frac{1}{4\pi} \int\limits_0^{2\pi} u^*\left(\bar{\xi},\theta_\xi,x,\tau-t_0\right) \cos n\theta_\xi d\theta_\xi d\Omega_x - \\ -\int\limits_{t_0}^{\tau} dt \int\limits_{\Omega} f(x,t) \frac{1}{4\pi} \int\limits_0^{2\pi} u^*\left(\bar{\xi},\theta_\xi,x,\tau-t_0\right) \cos n\theta_\xi d\Omega_x, \\ c(\bar{\xi})\, u_n^s\left(\bar{\xi},\tau\right)+\int\limits_{t_0}^{\tau} dt \int\limits_{\bar{\Gamma}} \left\{ u_n^{*c}\left(\bar{\xi},\bar{x},\tau-t\right) q_n^s\left(\bar{x},t\right)-u_n^{*s}\left(\bar{\xi},\bar{x},\tau-t\right) q_n^c(\bar{x},t)- \right. \\ \left. -u_n^s\left(\bar{x},t\right) q_n^{*c}\left(\bar{\xi},\bar{x},\tau-t\right)+u_n^c\left(\bar{x},t\right) q_n^{*s}\left(\bar{\xi},\bar{x},\tau-t\right) \right\} r_x d\bar{\Gamma}(r_x,z_x)= \\ =\int\limits_{\Omega} \rho c\, u_0(x) \frac{1}{4\pi} \int\limits_0^{2\pi} u^*\left(\bar{\xi},\theta_\xi,x,\tau-t_0\right) \sin n\theta_\xi d\theta_\xi d\Omega_x - \\ -\int\limits_{t_0}^{\tau} dt \int\limits_{\Omega} f(x,t) \frac{1}{4\pi} \int\limits_0^{2\pi} u^*\left(\bar{\xi},\theta_\xi,x,\tau-t_0\right) \sin n\theta_\xi d\Omega_x, \end{cases} \tag{15}$$

where $\bar{\xi} \in \bar{\Gamma}$, $n = \overline{0,\infty}$.

So, for an axially symmetric domain the boundary integral equation (5), that is three-dimensional in four-dimensional Minkowski space, is reduced to a system of two-dimensional singular integral equations (15). Integral equations (15) are equations of the second kind for the Neumann problem, equations of the first kind for the Dirichlet problem, mixed type for the mixed problem.

Let's note that if the boundary conditions, initial conditions and source function are also axially symmetric (in cylindrical coordinate system they are independent of θ_x), the system (15) is reduced to one two-dimensional in four-dimensional Minkowski space singular integral equation. Accordingly, if the conditions of the problem can be represented as a segment of the Fourier series with n members, the problem is reduced to a system of $2n$ two-dimensional singular integral equations.

2. 3. The fundamental solution for axially symmetric domain

Let's investigate the fundamental solution u_n^{*c}, u_n^{*s} from (15). Taking into account (10), (11), we have:

$$u_n^{*c}\left(\bar{\xi},\bar{x},\tau-t\right)=\frac{1}{\pi}\int\limits_0^{2\pi} u^*(\xi-x,\ \tau-t)\ \cos n\theta\ d\theta = -\frac{(\rho c)^{1/2}}{\pi(4\pi k(\tau-t))^{3/2}}\ H(\tau-t)\times$$
$$\times\int\limits_0^{2\pi} \exp\left\{-\frac{\rho c}{4k\ (\tau-t)}\left(r_\xi{}^2+r_x{}^2-2\ r_\xi r_x\cos\theta+(z_\xi-z_x)^2\right)\right\}\cos n\theta\ d\theta. \tag{16}$$

Due to the fact that:

$$\int\limits_0^{2\pi} e^{a\ \cos\theta} \sin n\theta\, d\theta = 0,$$

$$\int\limits_0^{2\pi} e^{a\ \cos\theta} \cos n\theta\, d\theta = 2\pi I_n(a), \tag{17}$$

where $I_n(z)$ is a modified n-th Bessel function, expressions u_n^{*s}, u_n^{*c} from (15) are the coefficients in the Fourier decomposition for fundamental solution, that can be written as:

$$\begin{cases} u_n^{*c}\left(\bar{\xi},\bar{x},\tau-t\right)=-\dfrac{(\rho c)^{1/2}\cdot 2}{(4\pi k(\tau-t))^{3/2}}\,H(\tau-t)\times\exp\left\{-\dfrac{\rho c}{4k\ (\tau-t)}\left(r_\xi{}^2+r_x{}^2+(z_\xi-z_x)^2\right)\right\}\times \\ \times I_n\left(\dfrac{\rho c\ r_x\ r_\xi}{2k(\tau-t)}\right), \\ u_n^{*s}\left(\bar{\xi},\bar{x},\tau-t\right)=0. \end{cases}$$

Define q_n^{*c} and q_n^{*s}. Because $q^*(\xi-x,\ \tau-t)=k\dfrac{\partial u^*}{\partial n_x}$, then $q^*=k\left(\dfrac{\partial u^*}{\partial r_x}n_{r_x}+\dfrac{\partial u^*}{\partial z_x}n_{z_x}\right)$. For axially symmetric domain $\hat{n}_x=\hat{r}_x\,n_{r_x}+\hat{z}n_{z_x}$ and we obtain:

$$\begin{cases} \dfrac{\partial u^*}{\partial r_x}=\dfrac{\partial u^*}{\partial|\xi-x|}\cdot\dfrac{\partial|\xi-x|}{\partial r_x}=-\dfrac{(\rho c)^{1/2}}{(4\pi k(\tau-t))^{3/2}}\dfrac{(-2)|\xi-x|\rho c}{4k(\tau-t)}H(\tau-t)\left(2r_x-2r_\xi\cos\theta\right)\times \\ \times\exp\left(-\dfrac{|\xi-x|^2\rho c}{4k\ (\tau-t)}\right), \\ \dfrac{\partial u^*}{\partial z_x}=\dfrac{\partial u^*}{\partial|\xi-x|}\cdot\dfrac{\partial|\xi-x|}{\partial z_x}=-\dfrac{(\rho c)^{1/2}}{(4\pi k(\tau-t))^{3/2}}\dfrac{(-2)|\xi-x|\rho c}{4k(\tau-t)}H(\tau-t)\ 2\left(z_\xi-z_x\right)(-1)\times \\ \times\exp\left(-\dfrac{|\xi-x|^2\rho c}{4k\ (\tau-t)}\right). \end{cases}$$

This system, using (17), can be rewritten as:

$$\begin{cases} \dfrac{\partial u^*}{\partial r_x}=\left(A_n+B_n\cos\theta+C_n\cos^2\theta\right)e^{a\ \cos\theta}, \\ \dfrac{\partial u^*}{\partial z_x}=\left(A_q+B_q\cos\theta\right)e^{a\ \cos\theta}, \end{cases}$$

where

$$A_n=-\frac{(\rho c)^{1/2}}{(4\pi k(\tau-t))^{3/2}}\frac{(-2)\rho c\left(r_\xi^2+r_x^2+\left(z_\xi-z_x\right)^2\right)}{4k(\tau-t)}H(\tau-t)\times$$
$$\times\exp\left(-\frac{\rho c}{4k\ (\tau-t)}\left(r_\xi^2+r_x^2+\left(z_\xi-z_x\right)^2\right)\right),$$

$$B_n=-\frac{(\rho c)^{1/2}}{(4\pi k(\tau-t))^{3/2}}\frac{(-2)\rho c}{4k(\tau-t)}H(\tau-t)\left(-2r_\xi\left(r_\xi^2+r_x^2+\left(z_\xi-z_x\right)^2\right)-2r_\xi r_x^2\right)\times$$
$$\times\exp\left(-\frac{\rho c}{4k\ (\tau-t)}\left(r_\xi^2+r_x^2+\left(z_\xi-z_x\right)^2\right)\right),$$

$$C_n=-\frac{(\rho c)^{1/2}}{(4\pi k(\tau-t))^{3/2}}\frac{(-2)\rho c}{4k(\tau-t)}H(\tau-t)\ 4r_\xi^2r_x\times$$
$$\times\exp\left(-\frac{\rho c}{4k\ (\tau-t)}\left(r_\xi^2+r_x^2+\left(z_\xi-z_x\right)^2\right)\right),$$

$$A_q = -\frac{(\rho c)^{1/2}}{(4\pi k(\tau - t))^{3/2}} \frac{(-2)\rho c\left(r_\xi^2 + r_x^2 + \left(z_\xi - z_x\right)^2\right)}{4k(\tau - t)} H(\tau - t)(-2)(z_\xi - z_x)\times$$
$$\times \exp\left(-\frac{\rho c}{4k\,(\tau - t)}\left(r_\xi^2 + r_x^2 + \left(z_\xi - z_x\right)^2\right)\right),$$

$$B_q = -\frac{(\rho c)^{1/2}}{(4\pi k(\tau - t))^{3/2}} \frac{(-2)\rho c(-2\, r_\xi r_x)}{4k(\tau - t)} H(\tau - t)\,(-2)(z_\xi - z_x)\times$$
$$\times \exp\left(-\frac{\rho c}{4k\,(\tau - t)}\left(r_\xi^2 + r_x^2 + \left(z_\xi - z_x\right)^2\right)\right).$$

Applying obvious trigonometric transformations and entering notation:

$$a = \frac{\rho c\, r_x r_\xi}{2k(\tau - t)},$$

we find $q_n^{*c}(\bar{\xi}, \bar{x}, \tau - t)$ and $q_n^{*s}(\bar{\xi}, \bar{x}, \tau - t)$:

$$\begin{cases} q_n^{*c}\left(\bar{\xi}, \bar{x}, \tau - t\right) = 2\pi n_r\, k_x \left\{ A_n\, I_n\left(\dfrac{\rho c\, r_x r_\xi}{2k(\tau - t)}\right) + B_n\, \dfrac{1}{2}\left(I_{n+1}(a) + I_{n-1}(a)\right) + \right. \\ \left. + \dfrac{1}{2} C_n \left(I_n(a) + \dfrac{1}{2} I_{n+2}(a) + \dfrac{1}{2} I_{n-2}(a) \right) \right\} + 2\pi n_{z_x} k \left\{ A_q\, I_n(a) + B_q\, \dfrac{1}{2}\left(I_{n+1}(a) + I_{n-1}(a)\right) \right\}, \\ q_n^{*s}\left(\bar{\xi}, \bar{x}, \tau - t\right) = 0. \end{cases}$$

Thus, we find the explicit formulas for finding functional coefficients (components) of the Fourier decomposition of fundamental solutions u^*, q^* from (15). Consequently, (15) defines a system of integral equations, solving this system we find the boundary values of functions (or u_n^s, or q_n^s). Obtaining the Fourier series of the form (6), we find the unknown boundary values. Then, using the integral representation (5), we can get the complete solution to the problem in the axially symmetric domain.

3. Conclusions

The work is devoted to investigation of non-stationary initial boundary value problem of thermal conductivity with not axially symmetric right part of the equation and boundary conditions for axially symmetric domain in Minkowski space.

Using the methods of boundary integral equations and the Fourier decomposition, the problem is reformulated as an infinite set of two-dimensional singular integral equations for coefficients of expansion. Fundamental solutions, used in the integral representation of the solution in the domain and on the border, are built in the explicit form and studied.

Reducing of the initial four-dimensional boundary problem to the set of two -dimensional equations by taking into account the axisymmetric of the domain is important for the problem of constructing of the effective numerical boundary element method for Real-Time settlements of behavior of structures.

Interpretation of initial-boundary problem as a boundary value problem in Minkowski space allows to use the results of the article for solving problems in axially symmetric domains variable over time.

The ideas and methods of this study can be applied in very similar problems in linear thermoelasticity. Such vector problems are related and imply a transition to a matrix description. According to the results of the article, such transition is possible. In addition, using the Kirchhoff transformation, the proposed approach can be generalized for problems with spatial inhomogeneous coefficient of thermal conductivity and for nonlinear problems (with power nonlinearity of thermal conductivity coefficient).

References

[1] Kartashov, E., Kudinov, V. (2012). Analytical theory of heat conduction and thermoelasticity. Librocom, 656.

[2] Lurie, A. I. (2010). Theory of Elasticity. Springer Science & Business Media, 1050. doi: 10.1007/978-3-540-26455-2

[3] Maceri, A. (2010). Theory of Elasticity, 1st Edition. Springer Science & Business Media, 716. doi: 10.1007/978-3-642-11392-5

[4] Zarubin, V., Kyvurkin, G. (2002). Mathematical models of thermal mechanics. Moscow: Fizmatlit, 168.

[5] Wrobel, L. C., Aliabadi, M. H. (2002). The Boundary Element Method, New York: John Wiley & Sons, 1066.

[6] Constanda, C., Doty, D., Hamill, W. (2016). Boundary Integral Equation Methods and Numerical Solutions. New York: Springer, 232. doi: 10.1007/978-3-319-26309-0

[7] Schanz, M., Steinbach, O. (2007). Boundary Element Analysis – Mathematical Aspects and Applications. Lecture Notes in Applied and Computational Mechanics, 352. doi: 10.1007/978-3-540-47533-0

[8] Zrazhevsky, G., Zrazhevska, V. (2016). Obtaining and investigation of the integral representation of solution and boundary integral equation for the non-stationary problem of thermal conductivity. Eureka: Physics and Engineering, 6, 53–58. doi: 10.21303/2461-4262.2016.00216

[9] Reddy, J. N. (2006). An Introduction to the Finite Element Method, 3rd Edition. McGraw Hill, 672.

[10] Chaskalovic, J. (2008). Finite Elements Methods for Engineering Sciences. Springer Verlag, 267.